The International Congress for global Science and Technology

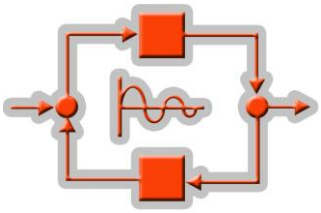

ICGST International Journal on Automatic Control & System Engineering (ACSE)

Volume (7), Issue (1)
May, 2007

www.icgst.com
www.icgst-amc.com
www.icgst-ees.com

ACSE Journal
ISSN: Print 1687-4811
ISSN Online 1687-482X
ISSN CD-ROM 1687-4838

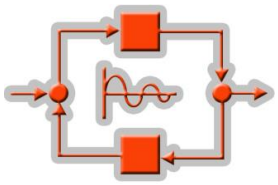

Table of Contents

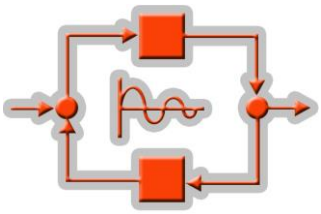

ICGST International Journal on Automatic Control & System Engineering - (ACSE)

A publication of the International Congress for global Science and Technology - (ICGST)

ICGST Editor in Chief: Dr. Ashraf Aboshosha

www.icgst.com, www.icgst-amc.com, www.icgst-ees.com

editor@icgst.com

www.icgst.com

Modeling and Control of a Hybrid Renewable Energy Production Unit

Lotfi KRICHEN
University of Sfax, National School of Engineering, Department of Electrical Engineering
BP W, 3038, Sfax, Tunisia,
lotfi.krichen@enis.rnu.tn

Abstract
This paper deals with the modeling and control of a hybrid production unit based on renewable energies comprising two sources: wind/solar and hydrogen storage system. These subsystems have different voltage-current characteristics and consequently are integrated with static converters on a DC bus by using a suitable control system. This DC bus is coupled to a load or grid through a static inverter. Each production source is provided by a regulator ensuring the Maximum Power Point Tracking (MPPT). The control strategy of the studied Hybrid Renewable Energy Source (HRES) is decomposed into two parts: a local control depending on the power structure and a global control deduced from global considerations. This strategy leads to achieve power objectives (active and reactive power targets) and system constraints.

Keywords: *Wind turbine, Photovoltaic, Fuel cell, Electrolyser, Hybrid, Control, Simulation.*

1. Introduction
The ever increasing demand for electrical power has created many challenges for the energy industry, which can affect the quality of the generated power in short and long terms [1]. In the developed countries, such as the United States or the European Union, the wind power was the fastest-growing energy in this last decade, thanks to its economy more and more attractive, its substantial environmental advantages, and the encouraging energy policies. In the same way, in the countries in the process of development, the wind power (in combination with other types of renewable energies) can play a more substantial role spectacularly to improve the quality of the human life in the immediate future [2].
The integrated Wind Energy Conversion System (WECS) and Photovoltaic (PV) array system, based on long-term seasonal energy storage as electrolytic hydrogen, is considered a promising alternative to overcome the intermittence of the Renewable Energy (RE) sources. In comparison to commonly used battery storage, hydrogen is well suited for seasonal storage applications because its inherent high mass energy density leakage from the storage tank is insignificant and it is easy to install anywhere [3-5].
In this international context expanding, search in the field of new technologies of the conversion systems of wind power and of hybrid systems requires a crucial effort. Indeed, hybrid wind/PV power generation systems have been studied extensively. Energy storage is needed in these systems due to the intermittent nature of wind and solar energy. Traditionally, deep-cycle lead acid batteries have been used as the means of energy storage. However, there are environmental concerns associated with the use of batteries; thus other alternatives are sought for this application. Fuel cells (FC) in combination with an electrolyser (EL) for hydrogen generation and hydrogen (H2) storage tanks have been considered for energy storage and implemented [6,7].
The remainder of the paper is organized as follows: Section (2) focuses on the description of the studied HRES. Section (3) emphasizes on the modeling of each component of the HRES and the FC/EL system. Section (4) describes the control strategies of the HRES. The control strategy of the studied HRES is decomposed into two parts: a local control depending on the power structure and a global control deduced from global considerations. According to the wind speed, the irradiation level and the load power, the global control part generates the adequate input references of the FC and of the EL. Section (5) presents the simulation results and section (6) gives the conclusion.

2. System description
The studied Hybrid Renewable Energy Source (HRES) consists of a 4 kW WECS and 1 kW (peak) PV array as primary energy sources. The excess energy with respect to the load requirement has been stored as electrolytic hydrogen through an electrolyser (3.6 kW) splitting water into hydrogen (H2) and oxygen (O2), a gas storage unit (4 Nm^3 of H2 and 2 Nm^3 of O2) and a PEMFC (4 kW) to generate electricity during low wind speed and sun shine periods. The studied HRES in this paper is represented in figure 1. The wind subsystem consists of a wind turbine driving a multi-pole Permanent Magnetic Synchronous Generator (PMSG) and of a AC/DC rectifier to connect this wind generator to the DC bus. The converter controls

the output voltages of the PMSG and indirectly the operating point of the wind turbine and consequently its generated power. The PV subsystem made up of several panels is connected to the DC bus via a filter and a DC/DC converter which controls the operating point of the panels and therefore the generated power. The DC bus collects the energy generated by the RE sources and supplies it through a converter DC/AC and a filter to a load or to the grid.

3. Modeling of the HRES

In this section, the model of each system component is presented as if there was no interaction between these elements. With the help of the results of this modeling, the next section will then be devoted to the building of the Energetic Macroscopic Representation (EMR).

3.1. Modeling of the WECS

The aerodynamic power at the rotor of the turbine is given by the following equation:

$$P_m = \frac{1}{2}\rho\pi R^2 \vartheta^3 C_p \quad (1)$$

where: ρ (kg.m^{-3}) is the air density, R (m) is the length of the blade, ϑ (m.s^{-1}) is the wind speed and C_p is the power coefficient. This coefficient represents the aerodynamic efficiency of the turbine and depends on specific speed λ and the pitch angle β [8].

The mechanical system is represented by the following equation:

$$J\ \frac{d\Omega}{dt} = T_m - T_{em} - f\ \Omega \quad (2)$$

the rotor speed and f (N.m.s.rad^{-1}) is a viscous friction coefficient.

The model generally used of the PMSG is the Park model. By considering only the fundamental harmonic of the flux distribution in the air-gap of the machine and by neglecting the homopolar component, the theory of the space vector gives the dynamic equations of the stator currents as follows:

$$\begin{cases} \dfrac{dI_{sd}}{dt} = \dfrac{1}{L_d}\left(V_{sd} - R_s\, I_{sd} + p\,\Omega\, L_q\, I_{sq}\right) \\ \dfrac{dI_{sq}}{dt} = \dfrac{1}{L_q}\left(V_{sq} - R_s\, I_{sq} - p\,\Omega\, L_d\, I_{sd} - p\,\Omega\,\Phi_m\right) \end{cases} \quad (3)$$

with: R_s is the phase resistance of the stator winding (Ω), L_d and L_q are the d-q stator inductances respectively (H), Φ_m is the flux of the permanent magnetic (Wb), V_{sd} and V_{sq} are the d-q components of the stator voltages respectively (V), I_{sd} and I_{sq} are the d-q components of the stator currents respectively (A) and p is the number of pairs of poles.

The electromagnetic torque is given by:

$$T_{em} = p\left(\Phi_m\, I_{sq} + \left(L_d - L_q\right) I_{sd}\, I_{sq}\right) \quad (4)$$

3.2. Modeling of the PV panel

The electric power generated by a photovoltaic panel is unstable according to the irradiation level and the temperature. The characteristic of a photovoltaic cell describing the relation between the current I_{pv} and the voltage V_{pv} is given by [9]:

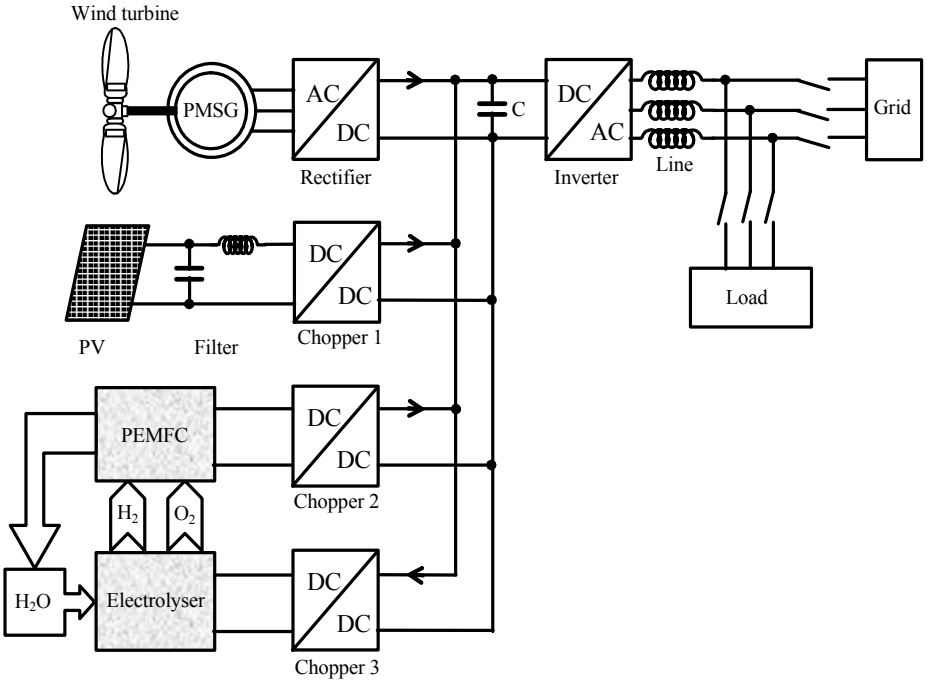

Figure 1: Configuration of the studied hybrid generation system

where J (kg.m^2) is the total inertia which appears on the shaft of the generator, T_m (N.m) is the mechanical torque, T_{em} (N.m) is the electromagnetic torque, Ω (rad.s^{-1}) is

$$I_{pv} = I_g - I_{sat}\left[exp\left(\frac{V_{pv} + I_{pv}\, R_{ss}}{V_t}\right) - 1\right] - \frac{V_{pv} + I_{pv}\, R_{ss}}{R_{sh}} \quad (5)$$

with: I_g is the generated current under a given illumination (A), I_{sat} is the current of opposite saturation of the diode (A), V_t is the thermal potential (V), R_{ss} is the equivalent series resistance of the photovoltaic panel (Ω) and R_{sh} is the equivalent parallel resistance of the photovoltaic panel (Ω).

3.3. Modeling of the hydrogen system

In terms of fuel cell steady-state performance modeling, many electrical models have been developed either from a theoretical point of view or from an empirical point of view. The model used in this article is from the empirical point of view approach. This model enables to simulate both fuel cells and electrolysers V-j curves (cell voltage versus current density) in typical conditions. This model is particularly adapted to regenerative fuel cell (RFC) simulation. It is a four degree-of-freedom model and it is convergent near zero current. It depends on the stack temperature and the oxygen partial pressure [10].

3.3.1. Electrical model

The curve of the cell potential V_{cell} versus the current density J has an inflexion point for $J = J_d$ and at this point, the slope of the tangent is noted $-\Delta$; it is the sum of activation and resistive losses. This characteristic is given by the following equation:

$$V_{cell} = E + \frac{b}{ln\left(\frac{J}{Jd}\right) - 2} + \left(\frac{b}{4J_d} - \Delta\right)J \qquad (6)$$

where: E is the open circuit voltage (for $J = 0$),

b is a parameter of the model.

The four parameters E, J_d, b and Δ have to be determined, fitting the modeling curve to the experimental data. These parameters depend on the cell temperature and on the oxygen partial pressure. The influence of the hydrogen partial pressure can be neglected as long as the hydrogen fraction on the anodic FC side is superior to 20% [11]. Due to the temperature and pressure dependence of the thermo chemical potential and the Butler Volmer equation, the influence of T and P_{O2} on the four parameters has the following form: $K_1 + K_2 T + K_3 T\, ln(P_{O2})$. Therefore, for each parameter, three constants have to be determined in order to describe the temperature and pressure dependence, so:

$$\begin{bmatrix} E \\ J_d \\ b \\ \Delta \end{bmatrix} = \begin{bmatrix} E_1 & E_2 & E_3 \\ J_{d1} & J_{d2} & J_{d3} \\ b_1 & b_2 & b_3 \\ \Delta_1 & \Delta_2 & \Delta_3 \end{bmatrix} \begin{bmatrix} 1 \\ T \\ T\, ln(P_{O2}) \end{bmatrix} \qquad (7)$$

T in K and P_{O2} in bar.

To do so, a minimum of 16 data is required: four couples (J, V_{cell}) for four pairs $\{P_{O2}, T\}$ where P_{O2} and T must be at least at two different levels. The curves of the cell potential versus the current density of the FC and the EL are shown in figure 2, respectively.

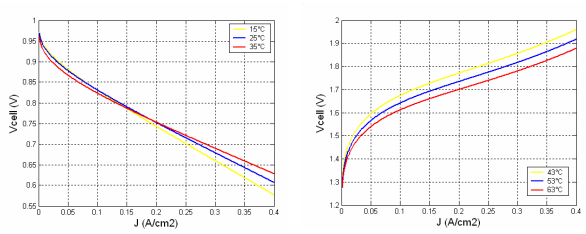

Figure 2: FC and EL V-j curves

3.3.2. Thermal model

To estimate the temperature evolution during operation, we use the following equation:

$$C_p \frac{d\theta}{dt} = P_{th} - \phi_{ext} - \phi_{ech} - \phi_{gaz} \qquad (8)$$

$\theta = T - T_a$

$P_{th} = \pm n_c (U - U_{th}) I$: thermal dissipative power

$\phi_{ext} = h\theta$: heat flow lost in the atmosphere

$\phi_{gaz} = \pm\left(C_p(H_2) F(H_2) + C_p(H_2) F(H_2)\right)\theta$: heat flow lost in gas

(+ for the electrolyser, - for the fuel cell)

where: C_p thermal capacity of the device (J.K^{-1}), T temperature (K), T_a ambient temperature (K), n_c number of cells, U cell voltage (V), U_{th} thermo-neutral cell voltage (= 1,48 V) based on the higher heating value of hydrogen, I current (A), h heat transfer coefficient (W.K^{-1}), ϕ_{ech} energy flow lost in a heat exchanger (W.K^{-1}), $C_{p(i)}$ molar heat capacity of the gas i (J.mol^{-1}.K^{-1}) and $F(i)$ molar flow of the gas i (mol.s^{-1}).

3.3.3. Pressure model

The gas management module enables to calculate gas production or consumption and the periphery pressure level during operation. To obtain the gas production or consumption, the two next equations are used:

$$F_{gaz} = \frac{n_c I}{n F}\eta_F\,(EL); F_{gaz} = \frac{n_c I}{n F}\frac{1}{\eta_F}(FC) \qquad (9)$$

with: F_{gaz} gas consumption for the FC and gas production for the EL (mol.s^{-1}), η_F faraday efficiency (%), F faraday constant (96485 C.mol^{-1}) and n number of moles of electrons transferred per mole of water (n = 2 for H_2, n = 4 for O_2).

3.4. Modeling of power electronics

The modeling of the converters is made by using the concept of instantaneous average value [12]. Indeed, this type of modeling is interesting since it adapts well to a numerical integration so it is not necessary to choose a step of integration lower than the period of operation of the converters. Moreover, it makes it possible to simulate the total dynamic behaviour of the system.

A switching function f_{ij} is defined for each power switch [12]. It represents the ideal commutation orders and takes the values 1 when the switch is closed (on) and 0 when it is opened (off):

$$f_{ij} \in \{0,1\}, \qquad (10)$$

$$with \begin{cases} i \in \{1,2,3\} \text{ no. of the leg} \\ j \in \{1,2\} \text{ no. of the switch in the leg} \end{cases}$$

As ideal power switches are considered, the switches of a same leg are in complementary states:

$$f_{i1} + f_{i2} = 1, \quad \in \{1,2,3\} \tag{11}$$

For both three-phase converters, rectifier 'rec' and inverter 'inv' of figure 1, modulation functions can be defined from the switching functions:

$$m_{rec} = \begin{bmatrix} m_{rec13} \\ m_{rec23} \end{bmatrix} = \begin{bmatrix} 1 & 0 & -1 \\ 0 & 1 & -1 \end{bmatrix} \begin{bmatrix} f_{11} \\ f_{21} \\ f_{31} \end{bmatrix}_{rec}$$
$$m_{inv} = \begin{bmatrix} m_{inv13} \\ m_{inv23} \end{bmatrix} = \begin{bmatrix} 1 & 0 & -1 \\ 0 & 1 & -1 \end{bmatrix} \begin{bmatrix} f_{11} \\ f_{21} \\ f_{31} \end{bmatrix}_{inv} \tag{12}$$

The rectifier provides the voltages $V_{s\,dq} = \begin{bmatrix} V_{sd} & V_{sq} \end{bmatrix}^T$ from the capacitor voltage U and the modulated current I_{wind}, which is the first current element of the HRES from the PMSG currents $I_{s\,dq} = \begin{bmatrix} I_{sd} & I_{sq} \end{bmatrix}^T$:

$$\begin{cases} V_{s\,dq} = m_{rec}\ U \\ I_{wind} = m_{rec}^T\ I_{s\,dq} \end{cases} \tag{13}$$

The three-phase inverter is modelled in the same way. It yields the inverter voltages $V_{inv\,dq} = \begin{bmatrix} V_{inv\,d} & V_{inv\,q} \end{bmatrix}^T$ from the capacitor voltage and the inverter modulated current I_{inv} from the line currents $I_{l\,dq} = \begin{bmatrix} I_{ld} & I_{lq} \end{bmatrix}^T$:

$$\begin{cases} V_{inv\,dq} = m_{inv}\ U \\ I_{inv} = m_{inv}^T\ I_{l\,dq} \end{cases} \tag{14}$$

The purpose of the following section is the building of the Energetic Macroscopic Representation (EMR). In an EMP graph, each component of the system is characterized by its inputs and outputs, which may be scalars or vectors. Indeed, outputs are actions, which generate reactions, inputs of the model. The mathematical product of an input and associated output must be a power. As an example, the synchronous machine, excited by permanent magnets, produces electromotive forces acting on inductive circuits, which consequently react by generating currents.

4. Control strategies of the HRES

The control strategy of the HRES can be decomposed into two parts: a local control depending on the power structure and a global control deduced from global considerations. The local part ensures an efficient energy management of each component of the system. The local control structure can be deduced from the Energetic Macroscopic Representation (EMR). The global control part is independent of the power structure. This strategy part leads to achieve power objectives (active and reactive power targets) and system constraints [13].

4.1 Local control of the HRES components

The controllers considered are of Proportional-Integral (PI) types, which adjust a reference value to an actual one.

Control of the WECS. The WECS includes the wind turbine, the PMSG and the rectifier (see figure 3). This rectifier makes it possible to control the PMSG flux and consequently the speed of the generator. Block MPPT wind provides the value $I_{sq\,ref}$ corresponding to the value of the reference electromagnetic torque. In this study, the vector control strategy applied to the PMSG, which consists in imposing a reference of the forward current $I_{sd\,ref}$ to zero, is applied [13].

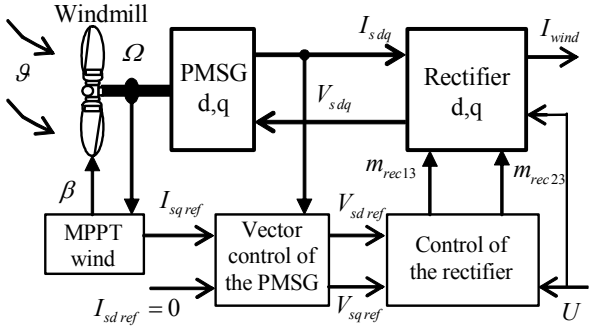

Figure 3: Energetic Macroscopic Representation of the WECS

From the wind speed ϑ, an artificial neural networks made up of radial basis functions computes the pitch angle β and the optimal aerodynamic torque T_{mref}. This computation is based on the mechanical characteristics of the wind turbine. The optimal torque gives the q-axis reference current I_{sqref}. The d- and q-axis reference currents applied to two PI regulators and two decoupling stages give the d- and q-axis reference voltages V_{sdref} and V_{sqref}. These voltages applied to two modulators provide the switching functions of the rectifier which gives the modulated current I_{wind}. The control strategy of the WECS, previously described, is illustrated in figure 4.

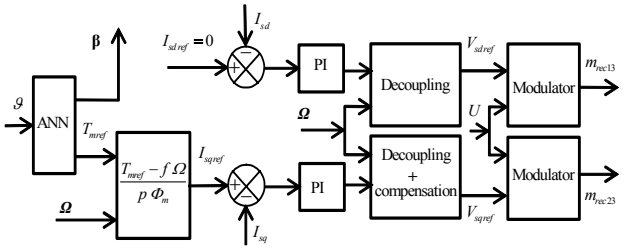

Figure 4: Control of the WECS

Control of the PV. The PV source includes in addition to the panel, a filter and a converter 'Chopper 1' (see figure 5). This DC/DC converter, of which the reference value $V_{pv\,ref}$ is calculated by MPPT solar block, allows adapting the voltage of the panel to that of the DC bus.

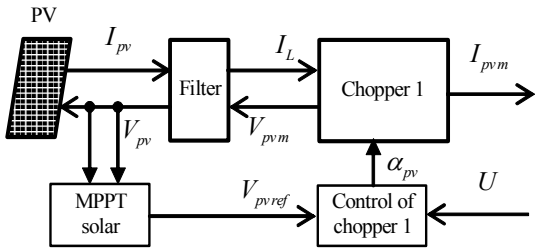

Figure 5: Energetic Macroscopic Representation of the PV

Various MPPT algorithms have been described in the literature. A good MPPT technique should produce a high efficiency at a low cost because PV systems will have to be mass-produced. In this work, the perturbation and observation technique [14,15] is used because it is simple, it requires only measurements of V_{pv} and I_{pv}, and it is capable of tracking the maximum power point.
From the PV voltage reference V_{pvref} given by the MPPT solar block, the chopper 1 adapts this voltage to that of the DC bus and provides the modulated current I_{pvm} which is the second current element of the HRES.

Control of the hydrogen system. The hydrogen source includes a PEMFC, an electrolyser and two choppers (see figure 6). These DC/DC converters adapt the voltages of the PEMFC and the electrolyser to that of the DC bus. The power management block gives the reference currents of the two converters while basing itself on the power management fixed by the global control strategy.

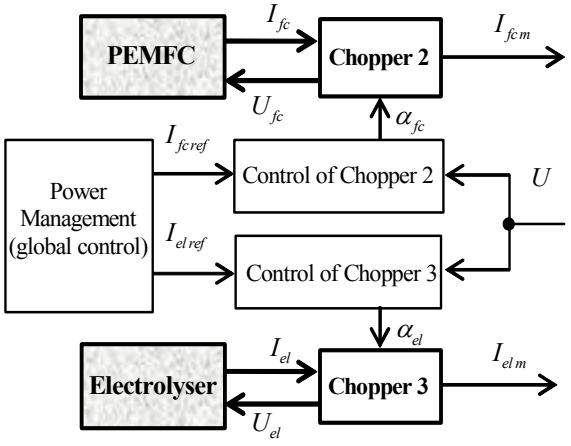

Figure 6: Energetic Macroscopic Representation of the hydrogen system

Taking into account the wind speed (wind power); the irradiance level (solar power) and the load power demand, the block power management generates the adequate values of the fuel cell current reference I_{fcref} and of the electrolyser I_{fcref} and so the on-times α_{fc} and α_{el} of the two corresponding converters.

Control of the continuous bus and of the inverter. The DC bus constitutes the central element of the entire production unit and plays the role of a decoupling interface between the various components (see figure 7). The DC bus voltage is governed by the following differential equation:

$$C\frac{dU}{dt} = I_{rem} - I_{inv} \qquad (15)$$

where: C represents the capacitance of the DC bus and I_{rem} is the total current of the HRES as shown in figure 7.

The two sources (WECS, PV) and the hydrogen system are connected to the DC bus and then to the load or to the system power via the inverter and a line (see figure 8). This converter makes it possible to control the continuous voltage and the active and reactive powers exchanged with the grid and to establish the currents at the adequate frequency $\omega_s = 100\pi\, rad.s^{-1}$.

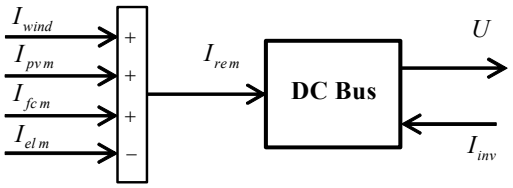

Figure 7: Energetic Macroscopic Representation of the DC bus

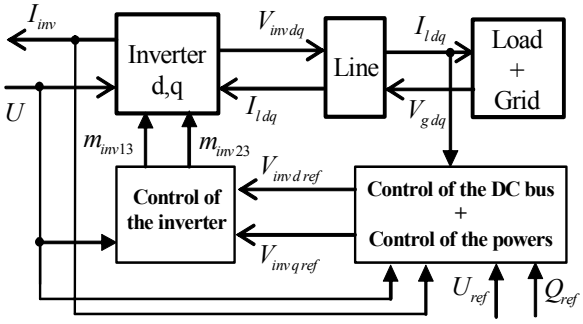

Figure 8: Energetic Macroscopic Representation of the load/grid part

In order to generate and send a current to the grid/load, the DC bus voltage 'U' has to be higher than the peak value of the voltage (phase to phase) appearing on the side of the filter. So $U > \sqrt{6}\, V_{rms}$, where V_{rms} is the rms value of the simple voltage appearing side of the filter. Since $V_{rms} = 127\ V$, we have imposed $U_{ref} = 400\ V$.
The control block permits the regulation of the DC voltage and the control of the reactive power and so the control of the inverter. We have chosen the unity power factor strategy i.e. the reactive power is set to zero ($Q_{ref} = 0$) with sinusoidal absorption. From the voltage reference U_{ref} and taking into account of the DC bus power and the copper losses in the line, we obtain the active power reference P_{ref}. The reference powers give the d- and q-axis reference currents $I_{ld\,ref}$ and $I_{lq\,ref}$. These d- and q-axis reference currents applied to two PI regulators and two decoupling stages yield the d- and q-axis reference voltages $V_{invd\,ref}$ and $V_{invq\,ref}$. These voltages applied to two modulators provide the switching functions of the inverter which gives the modulated current I_{inv}. The control strategy of the DC bus and the inverter, previously described, is illustrated in figure 9.

4.2 Global control of the HRES

The wind turbine and the PV panels are the main power sources of the plant. The electrolyser is powered as long as the available renewable power is greater than the electric load demand. When the hydrogen storage tank is full, the electrolyser is not powered. The excessive power that could be produced in this event is transmitted to the power system. The fuel cell is operated when there is a requirement for power, and hydrogen is available from storage.
The supervising system controls the overall current flow taking into account of the power supplied by the

renewable sources, the energy demands of the load and the hydrogen system following the flow chart of figure 10.

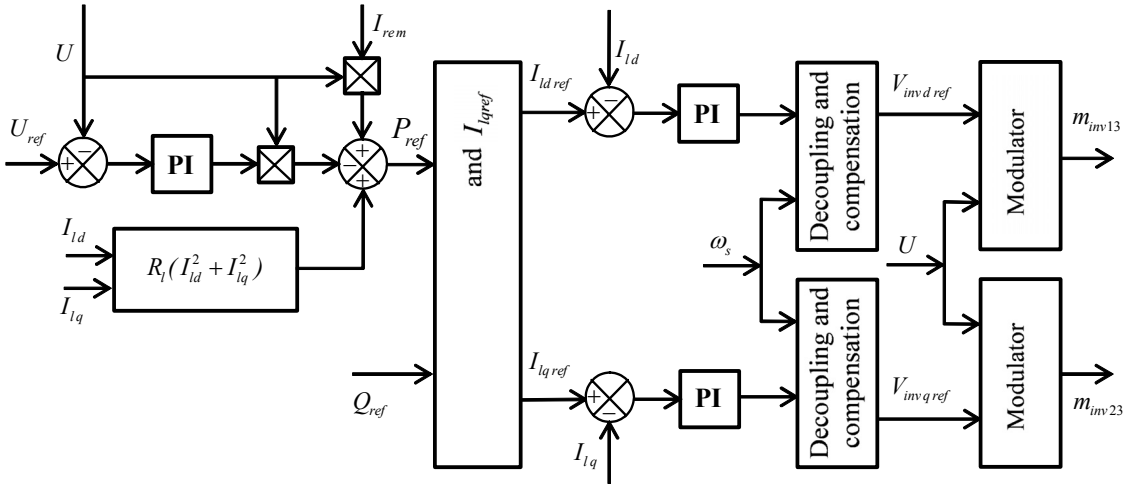

Figure 9: Control of the DC bus and the inverter

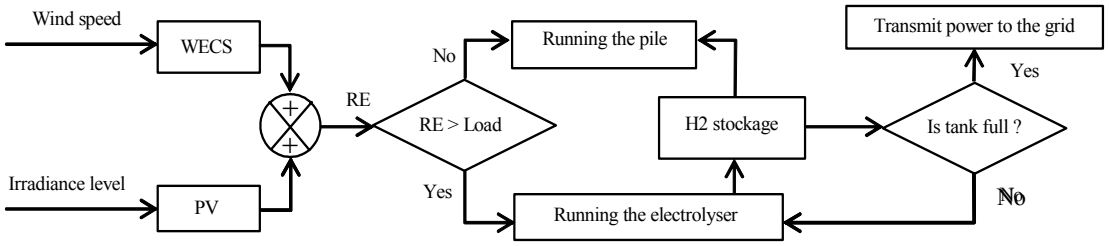

Figure 10: Flow chart of the global control strategy

5. Simulation process and results

Figure 11 shows the wind speed ranging between 8 and 13 m/s with an average value of 10 m/s. This sequence is obtained by adding a turbulent component to a slowly varying signal. Figure 12 gives the photovoltaic irradiance level of the panels whose average value is around 800 W/m².

The simulation results of the studied HRES are summarized in figures 13-25. Figures 13 and 14 present wind and photovoltaic powers respectively. It is easy to check that wind speed and irradiance level are very correlated to wind and PV powers respectively. The ANN block gives the reference mechanical torque (figure 15) according to the MPPT algorithm and the pitch angle (figure 16). For technological reasons, the regulator has to provide a lower pitch angle of 12°. In this simulation, we supposed that the load asks for a power of 3 kW between 0 and 100 s, then 5 kW between 100 and 200 s and finally 4 kW for the remainder simulation time. The curve of the load power demand is depicted in figure 17. The voltage of DC bus is represented in figure 18, which demonstrates that this voltage is perfectly constant, and thus proves the effectiveness of the established regulators. Figures 19 and 20 show the generated power and the consumed powers of the fuel cell and the electrolyser respectively. The temperature curves of the FC and the EL are depicted in figures 21 and 22 respectively. These figures prove that the two temperatures evolve in an acceptable band. Figures 23 and 24 represent the H2 and O2 consumed by the FC and produced by the EL respectively. The results of the global controller are shown in figure 25. This figure represents the reference FC and EL currents, which are very correlated to the generated FC power and the consumed EL power represented in figures 19 and 20, respectively.

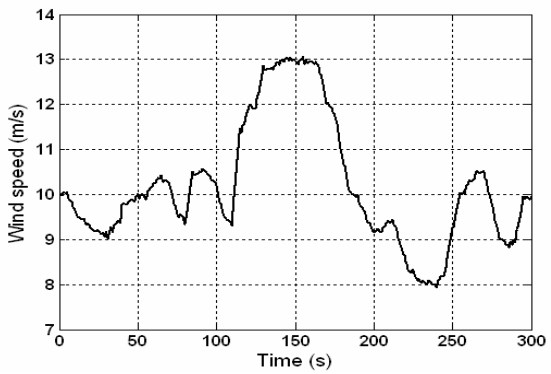

Figure 11: Wind speed

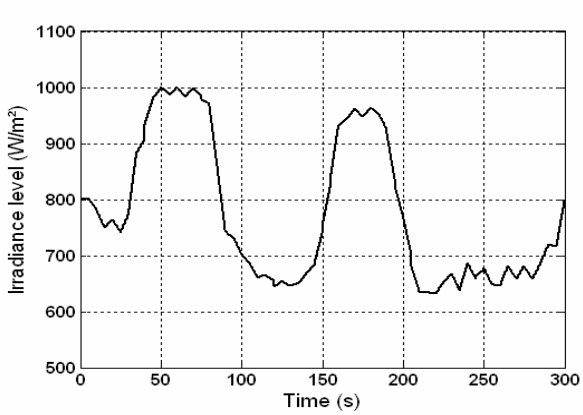

Figure 12: Irradiance level

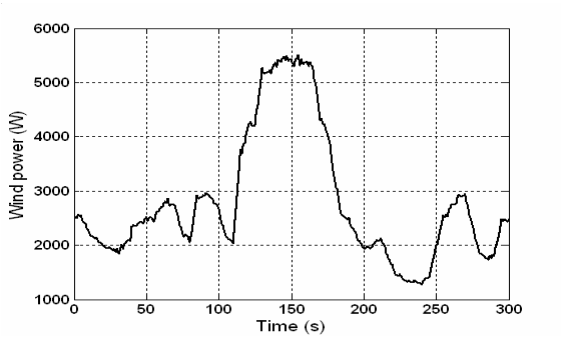

Figure 13: Wind power

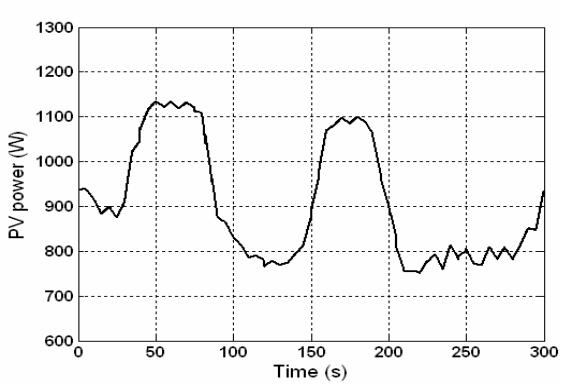

Figure 14: PV power

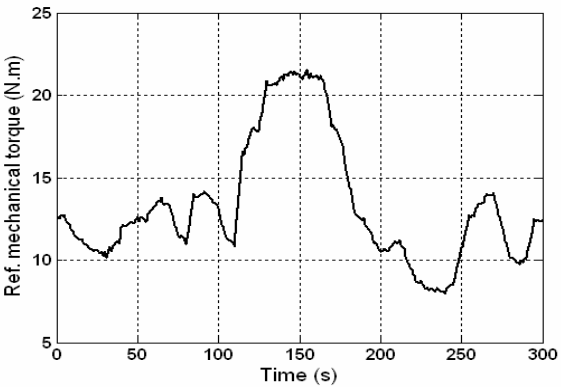

Figure 15: Reference mechanical torque

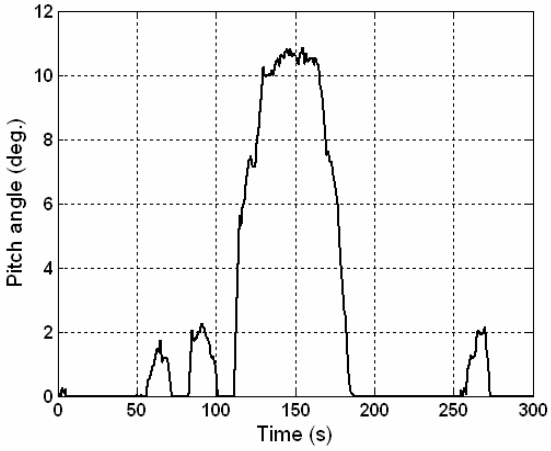

Figure 16: Pitch angle

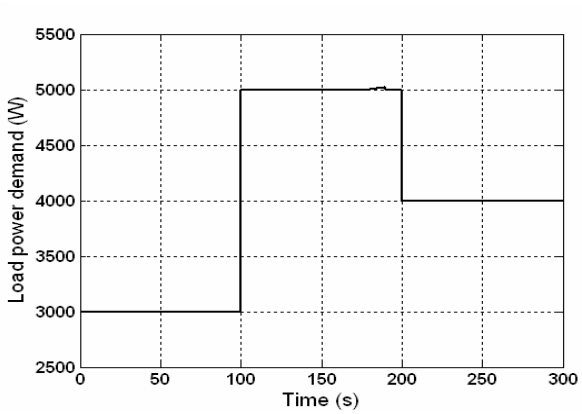

Figure 17: Load power demand

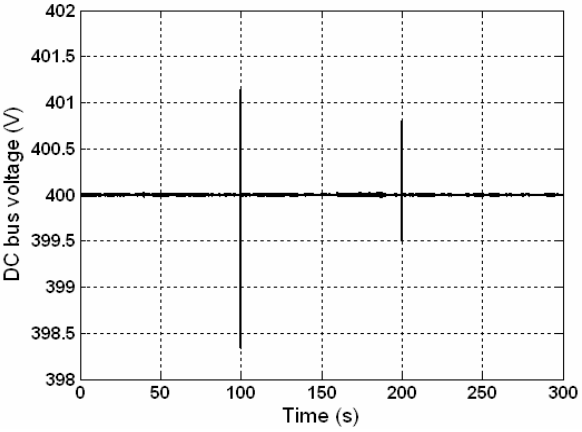

Figure 18: DC bus voltage

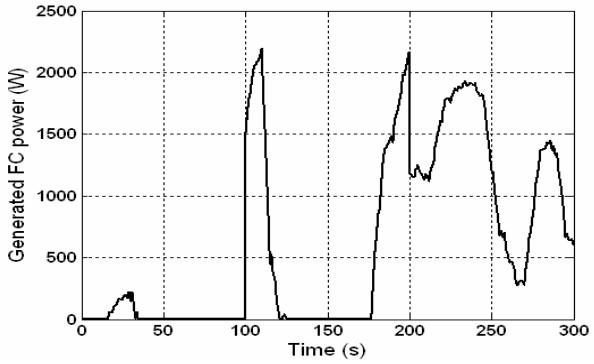

Figure 19: Generated FC power

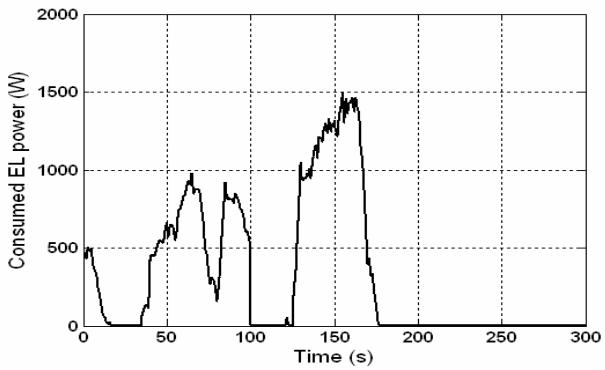

Figure 20: Consumed EL power

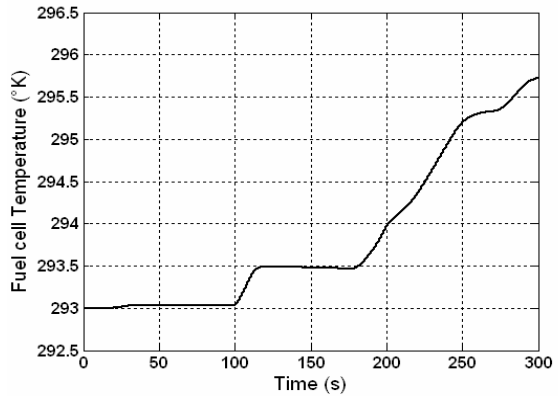

Figure 21: Fuel cell temperature

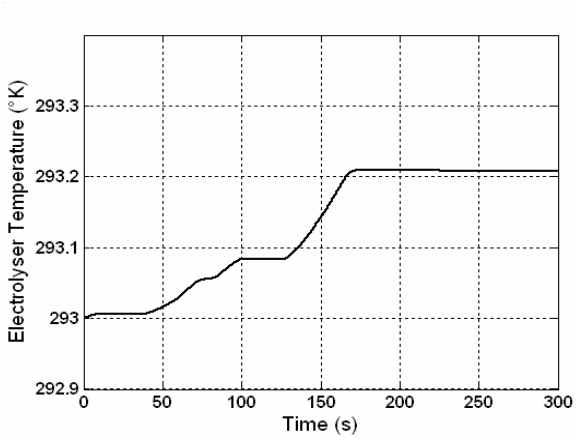

Figure 22: Electrolyser temperature

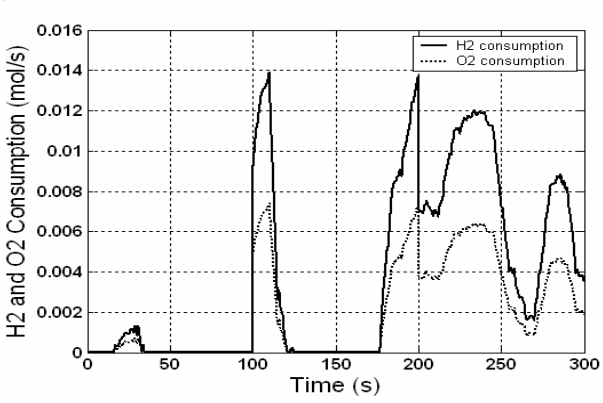

Figure 23: H2 and O2 consumption

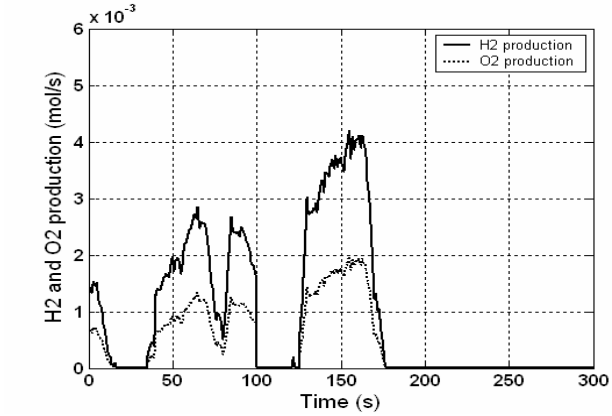

Figure 24: H2 and O2 production

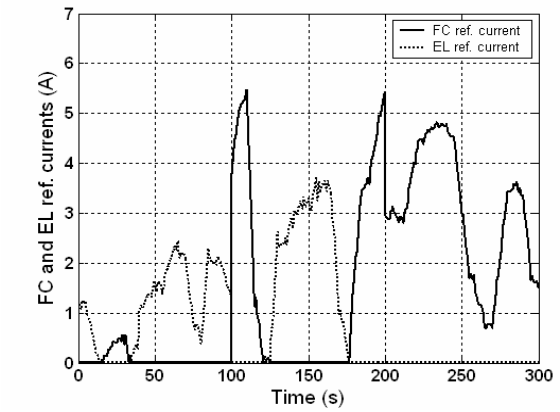

Figure 25: Results of the global controller

6. Conclusion

In this paper we treated the problem of the modeling and the supervision of a hybrid production unit containing renewable energy sources. The WECS was modelled using d-q rotor reference frame. These renewable energy sources were interfaced with the power system through an inverter and a line modelled in the power system reference frame. The control strategy of the studied Renewable Energy Hybrid Source (HRES) is decomposed into two parts, a local control depending on the power structure of each source and a global control deduced from global considerations and power objectives. The complete control device, playing the role of supervisor developed in this work, was qualified to control and coordinate the operation of the different subsets. The dynamics of the HRES with typical numerical values are plotted. The simulation results showed the effectiveness of the adopted control strategy.

7. References

[1] T. E. Hoff, H. J. Wenger and B. K. Farmer, "Distributed generation: an alternative to electric utility investments in system capacity", Energy policy, Vol. 24, No. 2, pp. 137-147, 1996.

[2] B. S. Borowy and Z. M. Salameh, "Methodology for Optimally Sizing the Combination of a Battery Bank and PV Array in a Wind/PV Hybrid System", IEEE Trans. Energy Conversion, vol. 11, no. 2, pp. 367-375, June 1996.

[3] F. Valenciaga and F. Puleston, "Supervisor Control for Stand Alone Hybrid Generation System Using Wind and Photovoltaic Energy", IEEE Trans. Energy Conversion, vol. 20, no. 2, pp. 398-405, June 2005.

[4] T. Senjyu, T. Nakaji, K. Uezato and T. Funabashi, ''A Hybrid Power System Using Alternative Energy Facilities in Isolated Island'', IEEE Trans. Energy Conversion, vol. 20, no. 2, pp. 405-411, June 2005.

[5] Kodjo Agbossou, Mohanlal Kolhe, Jean Hamelin and Tapan K. Bose, ''Performance of a Stand-Alone Renewable Energy System Based on Energy Storage as Hydrogen'', IEEE Trans. Energy Conversion, vol. 19, no. 3, pp. 633-640, September 2004.

[6] Iqbal M.T., ''Simulation of a small wind fuel cell hybrid energy system'', Renewable Energy 2003; 28(4).

[7] El-Shatter ThF, Eskandar MN, El-Hagry MT., ''Hybrid PV/fuel cell system design and simulation'', Renewable Energy 2002; 27(3).

[8] J. G. Slootweg, S. W. H. de Haan, H. Polinder and W. L. Kling, ''General Model for Representing Variable Speed Wind Turbines in Power System Dynamics Simulations'', IEEE Trans. Power Systems, vol. 18, no. 1, pp. 144-151, February 2003.

[9] S. Arul Daniel and N. Ammasai Gounden, "A Novel Hybrid Isolated Generating System Based on PV Fed Inverter-Assisted Wind-Driven Induction Generators", IEEE Trans. Energy Conversion, vol. 19, no. 2, pp. 416-422, June 2004.

[10] S. Busquet, C.E. Hubert, J. Labbé, D. Mayer, R. Metkemeijer, ''A New Approach to Empirical Electrical Modelling of a Fuel Cell, an Electrolyser or a Regenerative Fuel Cell'', Journal of Power Sources, 134, 2004, pp. 41-48.

[11] S. Busquet, R. Metkemeijer, P. Leroux, D. Mayer, "Stand-alone power system coupling a PV field and a fuel cell : Experimental results of the FC system", Proceedings of the France-Deutschland Fuel Cell Conference 2002, October 7th to 10th 2002, Forbach-Saarbrücken, pp. 85-92, 2002.

[12] A. Bouscayrol, Ph. Delarue, X. Guillaud, ''Power strategies for maximum control structure of a wind energy conversion system with a synchronous machine'', Renewable Energy, Vol. 30, pp. 2273-2288, 2005.

[13] A. Ansel, B. Robyns, ''Modelling and simulation of an autonomous variable speed micro hydropower station'', Mathematics and Computers in Simulation, Issue 71, pp. 320-332, 2006.

[14] J. Devishree, P. Anbalagan, J. Rathinavel and S. Senthil, ''An Improved Photovoltaic Power Supply System with Tracking'', ICGST, DSP Journal, Volume 6, Issue 1, September, 2006

[15] Y. Tiam Tan, D. S. Kirschen, N. Jenkins, ''A Model of PV Generation Suitable for Stability Analysis'', IEEE Trans. Power Systems, vol. 19, no. 4, pp. 748-755, December 2004.

Lotfi KRICHEN was born in Sfax, TUNISIA. He received the Engineer Diploma and the Doctorate degree in Electrical Engineering from the National School of Engineering of Sfax in 1989 and 1995, respectively. Currently, he is Assistant Professor of Electric Machines in the Electrical Engineering Department of the National School of Engineering of Sfax. His research interests are motor drives, power electronic converters, automatic control systems and renewable energy systems.

www.icgst.com

An MRAS - based full Order Luenberger Observer for Sensorless DRFOC of Induction Motors

Sbita Lassaâd and Ben Hamed Mouna
Research Unit of Modeling, Analysis and Control Systems,
National Engineering School of Gabès (ENIG)-Tunisia,
lassaad.sbita@enig.rnu.tn, benhamed2209@yahoo.fr

Abstract

A new method for the implementation of a sensorless direct flux oriented control of induction motor drives is proposed in this paper. As the induction motor is decoupled if the direct rotor flux is maintained constant and equal to the nominal flux value and the reverse rotor flux is to be fixed at zero value. It is well known that the rotor flux of the induction motor is unmeasured. To cope with this problem and the drawbacks of the sensors, a combination of two observers is used: a full order Luenberger observer to estimate the rotor flux and a model reference adaptative system (MRAS) observer for rotor speed estimation. With the help of the observed (d, q) axis components of the rotor flux, the direct rotor field orientation vector control is implemented. We show by an extensive simulation study that the proposed method for DRFOC is completely satisfactory at low speed region and in field weakening region (high speeds). It is not sensitive to disturbances and parameters mismatch. Observers and control scheme are robust to changes in load torque. The method proposed achieves good performances with an optimal and adaptative gain tuning matrix obtained from the Linear Quadratic Regulator (LQR) design principle. Digital simulation results are presented to show the improvements in performance of the proposed method and the global stability of the MRAS based speed sensorless combined to flux observer scheme with the LQR matrix gain.

Keywords: *Induction motor, Direct rotor field oriented control, Luenberger Observer, MRAS and speed sensorless.*

1 Introduction

Induction motor (IM) can produce good performance using field oriented vector control strategy. The main idea of the vector control is the control of the torque and the flux separately. In order to decouple the vectors and realize the decoupled control most control schemes require accurate flux and motor rotor speed. These informations are mainly provided by Hall sensors and sensing coils (flux measurement) and incremental encoder (rotor speed measurement). The use of these sensors implies more electronics, high cost, and lower reliability, difficulty in mounting in some cases such as motor drives in harsh environnement and high speed drives, increase in weight, increase in size and increase electrical susceptibility [1]. To overcome these problems, in recent years, the elimination of these sensors has been considered as an attractive prospect. The rotor velocity and flux are estimated from machine terminals proprieties such as stator currents or voltages as Extended Kalman Filter and Artificial Neural Network. All these methods are complex. The complexities in these algorithms impose a very high computation burden [4]. Moreover, the estimated speed error will give rise to flux error and this flux error will finally result in failures in the flux field oriented control strategy. For the field oriented control, we have two methods; the first is named indirect rotor field oriented control (IRFOC). While the second is named direct rotor flux oriented control (DRFOC). The DRFOC is based on the regulation of the d and q axis rotor flux and addition of the opposite of the decoupling terms [13]. Based on the means of the decoupling machine, we propose a method to realize the direct rotor flux oriented control without adding the decoupled terms. The principle of this idea is to regulate the flux components so that the d axis rotor flux is equal to the rated rotor flux and the q axis rotor flux to be fixed to zero. The error between the observed d-axis rotor fluxes from its reference value (the rated value) feeds the proportional plus integral (PI) controller to obtain the direct stator voltage (vds). The error between the observed q-axis rotor flux and its reference value feeds the pro-

portional plus integral (PI) controller to obtain the reverse stator voltage (vqs). The synchronous angular frequency is obtained from the output of the proportional and integral (PI) controller used in speed control loop. In this method if a decoupling error occurs the flux controllers must cancel this error. Therefore, in this paper, we propose a flux observer based on the Luenberger observer with adaptive and optimal choice of a matrix gain [19] and [20] so that the exact flux estimation is achieved. An MRAS observer [21] is used to estimate the rotor speed. Based on the observed flux and rotor speed, the direct rotor flux orientation is realized. Computer simulation results demonstrate that the proposed observation has excellent features at both steady and dynamic states and is robust to external disturbances. The efficiency of the direct oriented control method is illustrated in the simulation results in the steady and dynamic states and also at low speeds [10] and in the field weakening region. The observability and the stability of the observer are also studied and proved in this paper.
The paper is organized as follows in the second section, we give a description of induction motor model. The observability of the system is discussed in the third section. The fourth section describes the adaptative full order Luenberger rotor flux observer. The stability analysis is discussed in the fifth section. The sixth section studies the field oriented control. In the seventh section, we describe the design of a direct rotor flux oriented control. The last section deals with the simulation results and discussion. The paper is ended by a conclusion about the proposed method and perspectives.

2 Induction motor model

Assuming linear magnetic circuits, equal mutual inductances and neglecting iron losses, the dynamic equations of induction motor in the stationnary reference frame are formulated as:

$$\begin{cases} \dfrac{d}{dt}\begin{bmatrix} \vec{i}_s \\ \vec{\phi}_r \end{bmatrix} = \begin{bmatrix} A_{11} & A_{12} \\ A_{21} & A_{22} \end{bmatrix}\begin{bmatrix} \vec{i}_s \\ \vec{\phi}_r \end{bmatrix} + \begin{bmatrix} B_1 \\ B_2 \end{bmatrix}\vec{v}_s, \\ y(t) = Cx(t). \end{cases} \tag{1}$$

Where the state matrix elements are:

$$A_{11} = -\frac{1}{\sigma L_s}\left(r_s + \frac{r_r M}{L_r}\right) I,$$

$$A_{12} = \frac{r_r M}{\sigma L_s L_r} I - \frac{M}{\sigma L_s L_r}\omega J,$$

$$A_{21} = \frac{r_r M}{L_r} I, A_{22} = -\frac{r_r}{L_r} I + \omega J,$$

$$B_1 = \frac{1}{\sigma L_s} I, B_2 = 0_2,$$

$$C = \begin{bmatrix} I & 0_2 \end{bmatrix}, I = \begin{bmatrix} 1 & 0 \\ 0 & 1 \end{bmatrix}, J = \begin{bmatrix} 0 & -1 \\ -1 & 0 \end{bmatrix}$$

$$\sigma = 1 - \frac{M}{L_s L_r},$$

and

$$O_2 = \begin{bmatrix} 0 & 0 \\ 0 & 0 \end{bmatrix},$$

$\vec{i_s} = \begin{bmatrix} i_{\alpha s} & i_{\beta s} \end{bmatrix}^T$ is the stator currents vector,
$\vec{v_s} = \begin{bmatrix} v_{\alpha s} & v_{\beta s} \end{bmatrix}^T$ is the stator voltage vector,
$\vec{\phi_r} = \begin{bmatrix} \phi_{\alpha r} & \phi_{\beta r} \end{bmatrix}^T$ is the rotor flux vector,

r_s is the stator resistance, r_r is the rotor resistance, L_s is the stator self inductance, L_r is the rotor self inductance, M is the mutual inductance, σ is the leakage inductance, and ω is the rotor speed . The electromagnetic torque developed by the motor is expressed in terms of rotor flux and stator currents as:

$$T_e = p * \vec{\phi}_r \otimes \vec{i}_s, \tag{2}$$

While the load torque acts as a disturbance via the mechanical relation:

$$J\frac{d\omega}{dt} = T_e - T_L. \tag{3}$$

Where J is the moment of inertia of the rotor, p is the pole pairs and T_L is the load torque.

3 Observability study

The observability of the system can be investigated using the observability matrix defined as:

$$M_O = \begin{bmatrix} C & CA & CA^2 & CA^3 \end{bmatrix}^T \tag{4}$$

The system is observable if the rank of the observability matrix is equal to the number of states [2]. The observability is checked for various angular speeds of the rotor(from -314 rad/s to +314 rad/s) and reference frame. It is verified by computation that for each work speed value, the rank is maintained constant and equal to four as the number of states, indicating that the system is observable.

4 Adaptative full order Luenberger rotor flux observer

The adaptative full order observer for estimating the stator current and the rotor flux using the measured


currents and the measured stator voltages is described by the following set of equations:

$$\begin{cases} \dfrac{d}{dt}\begin{bmatrix} \widehat{\vec{i}}_s \\ \widehat{\vec{\phi}}_r \end{bmatrix} = \begin{bmatrix} \widehat{A}_{11} & \widehat{A}_{12} \\ A_{21} & \widehat{A}_{22} \end{bmatrix} \begin{bmatrix} \vec{i}_s \\ \vec{\phi}_r \end{bmatrix} + \\ \begin{bmatrix} B_1 \\ B_2 \end{bmatrix} \vec{v}_s + Le(t), \\ \widehat{y}(t) = C\widehat{x}(t). \end{cases} \tag{5}$$

Where , $\hat{}$, denotes the estimated values. L is the feedback gain matrix of the Luenberger observer. It is determined in order to ensure the observer stability.

The first step is to drive an equation governing the state estimation error. Subtracting the induction motor model (1) from the observed motor model given by (5), we get the differential equation governing the state estimation error. The characteristic model matrix depends on rotor speed. Therefore, the matrix $\hat{A}$ can be written as $A + \Delta A$. Replacing $\hat{A}$ with its value, we obtain:

$$\frac{de(t)}{dt} = [A - LC]\, e(t) - \Delta A\hat{x}(t), \tag{6}$$

Where ΔA is the model mismatch error. It is defined as:

$$\Delta A = A(\omega) - A(\hat{\omega}), \tag{7}$$

By subtracting the characteristic model matrix from the observed one, we obtain:

$$\Delta A = D\Delta\omega, \tag{8}$$

In which, the matrix D is defined as:

$$D = \begin{bmatrix} D_{11} & D_{12} \\ D_{21} & D_{22} \end{bmatrix}, \tag{9}$$

Where,

$$D_{11} = D_{21} = 0_2, D_{12} = \frac{M}{\sigma L_s L_r} J,$$

$$D_{22} = J,$$

and $\Delta\omega = \omega - \hat{\omega}$.

The state estimation error can be simplified as:

$$\frac{de(t)}{dt} = [A - LC]\, e(t) - W \tag{10}$$

Where W is the non linear block and is defined as:

$$W = D\Delta\omega\hat{x}(t). \tag{11}$$

As D_{11} and D_{21} are equal to zero matrix value, which denotes that ΔA is independent of $\hat{i_s}$, based on this comment, the final form of the non linear block is defined by:

$$W = F\hat{\phi}_r\Delta\omega. \tag{12}$$

Where F is defined as:

$$F = \begin{bmatrix} \frac{M}{\sigma L_s L_r} J & J \end{bmatrix}^T \tag{13}$$

Equation (10) denotes that the estimation error is a combination of a linear dynamic fed forward with a non linear element. In order to maintain the stability of the complete system, the linear element must be stable and the non linear element have to converge to zero or to a minimal energy quantity which is given by the popov's integral inequality [12]. Therefore, the matrix gain L is chosen so that the poles of the characteristic matrix A-LC is stable. The traditional way of doing this is described in [2] and [16]. It is based on the fact that the gain matrix can be analytically computed so that the observer poles are proportional to the motor poles, thus assuming the stability. For general rules, the observer poles have to be chosen 5 to 6 times faster than the motor poles [2], [11] and [15]. In this way, it is difficult to obtain accurate speed estimation due to variation of IM model characteristic matrix with the rotor speed. To cope with this problem and obtain an accurate speed estimation at both high speeds and low speeds, we propose an adaptative and optimal algorithm for computing the components of the Luenberger matrix gain. The adaptative and optimal algorithm is based on the well known LQR design principle in order to design varying matrix gain so that fast convergence and accurate speed and flux estimation can be realized. The LQR design principle is stated as follow:

$$\mathrm{I_m} = \frac{1}{2}\int_0^\infty \left(\mathrm{X}^T Q\mathrm{X} + U^T RU\right)\, dt, \tag{14}$$

Where Q is positive semi definite and R is positive definite. The optimal linear state feedback gain K is:

$$K = -R^{-1}B^T P. \tag{15}$$

Which minimize the performance of the index I_m. Here P is the solution of the algebric RICCATI equation defined as follows:

$$PA + A^T P - PBR^{-1}B^T P + Q = 0. \tag{16}$$

If we choose $L = -R^{-1}B^T P$ as a feedback gain of Luenberger observer, we ensure that the matrix A-LC is stable.

5 Stability analysis

5.1 Stability of the linear element

The linear element is represented by the matrix (A-LC). Its stability condition is guaranteed by the negativity of this matrix.

lemma:
A matrix H is definite negative if the determinant of their K^{th} principal minors have the same sign of $(-1)^k$.

Remark:
The K^{th} principal minor of a square matrix(nxn) is a matrix (kxk) obtained by eliminating the lasted (n-k) lines and columns of the matrix.

The determinants of the fourth principal minor are numerically computed for different operating angular speeds and reference frame.
Fig. 1, 2, 3 and 4 show the evolution of the determinants of the different principal minors in the stationary frame.
From these results, it is clear that the determinant of each K^{th} principal minor have the same sign of $(-1)^k$, indicating that the matrix (A-LC) is strictly definite negative. Therefore, we conclude that using $L = -R^{-1}B^TP$ as a feedback gain of Luenberger observer ensure that the matrix (A-LC) is stable.
The root loci of the full Luenberger observer in one hand and on the other hand the induction motor are represented in Fig. 5 and 6 respectively.
These results show that the use of the new form of matrix gain ensure the rapidity of the observer poles. The rapidity rate is fixed by R and Q matrix index ponderation.

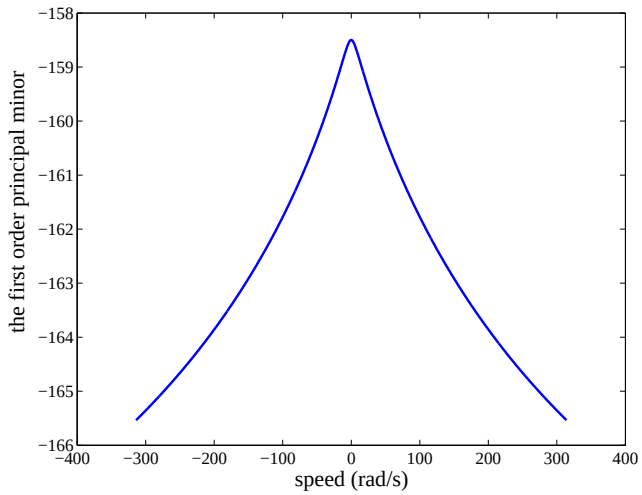

Figure 1: The first order principle minor

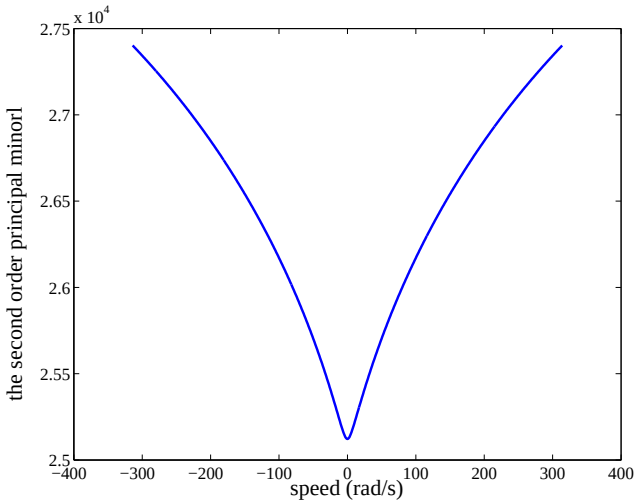

Figure 2: The second order principle minor

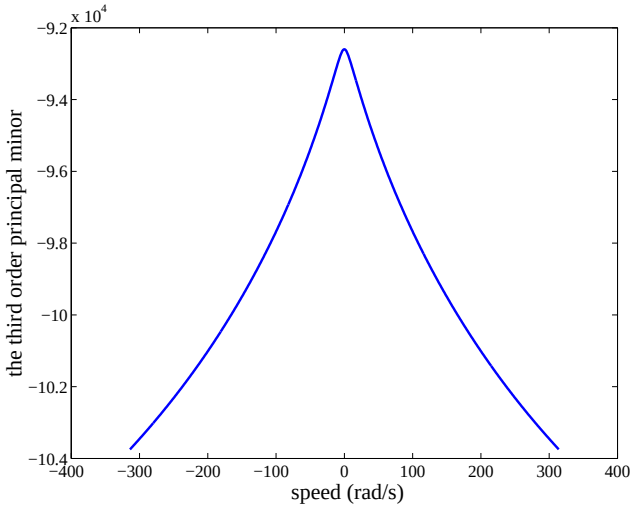

Figure 3: The third order principle minor

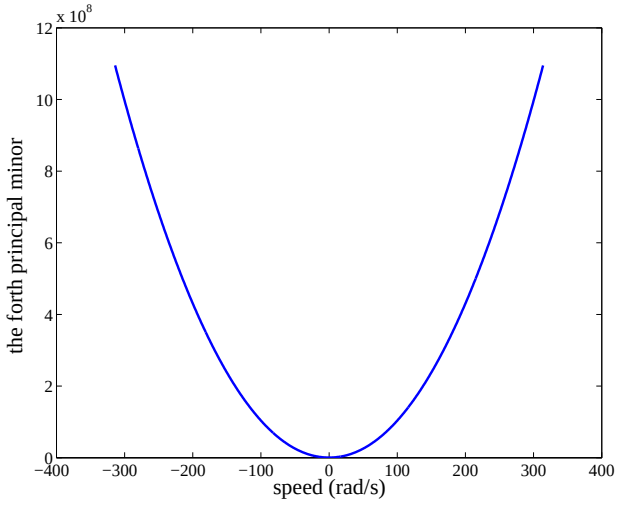

Figure 4: The fourth order principle minor

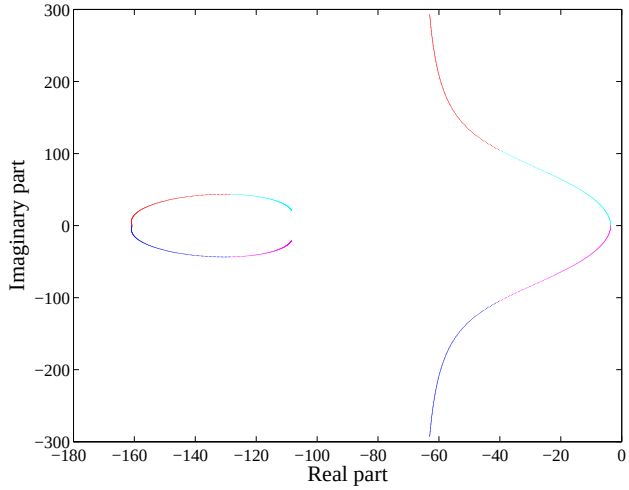

Figure 5: Full observer root loci for variable rotor speeds

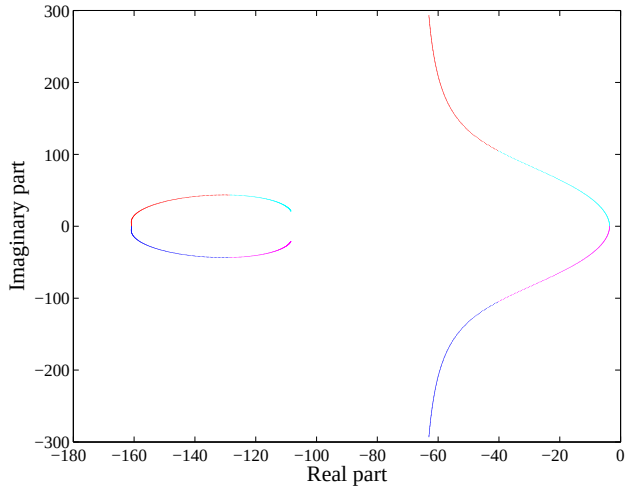

Figure 6: IM root loci for variable rotor speeds

5.2 MRAS rotor speed observer

The MRAS representation is given in Fig. 7. According to MRAS method, we consider the motor as reference model and the observer as an adjustable model. The error between the states $\vec{i}_s$ and $\hat{\vec{i}}_s$ is used to regulate the adaptative mechanism to adjust estimated speed $\hat{\omega}$. To ensure the global stability of the observer, the non linear feedback block must converge to zero or to a minimal quantity of energy. Therefore, the system will be known as hyperstable. As defined in [3], the system is hyperstable if the forward path transfer matrix is strictly positive real, and the input , output of non linear feedback block satisfy popov's inequality defined as:

$$\int_0^t \Delta y \Delta z dt \geqslant -\gamma, \tag{17}$$

Where: γ is a finite positive constant, Δy is the output of linear block and Δz is the output of non linear block.
Consider the left hand size of the inequality (17), substituting for Δy and Δz, we get:

$$\int_0^t e^T W dt \geqslant -\gamma, \tag{18}$$

By replacing W with its value, we obtain:

$$\int_0^t e^T F \hat{\phi}_r \Delta\omega dt \geqslant -\gamma, \tag{19}$$

Schauder propose the following adaptative mechanism [17]:

$$\hat{\omega} = Q_1(e) + \int_0^t Q_2(e) dt, \tag{20}$$

(20) in (19) gives

$$\int_0^t e^T F \hat{\phi}_r \left[\omega - Q_1(e) - \int_0^t Q_2(e) dt \right] \geqslant -\gamma, \tag{21}$$

The solution of this inequality is given by the following expression:

$$\int_0^t h \left[\frac{df(t)}{dt} \right] f(t) dt \geqslant -\frac{1}{2} h f(0), \tag{22}$$

Where h is finite positive constant. Using (22) to resolve the popov inequality, we obtain:

$$\begin{cases} Q1 = k_p * \vec{e} \otimes \hat{\vec{\phi}}_r, \\ Q2 = k_i * \vec{e} \otimes \hat{\vec{\phi}}_r, \end{cases} \tag{23}$$

(23) in (20) yields

$$\hat{\omega} = k_p * \vec{e} \otimes \hat{\vec{\phi}}_r + k_i * \int \vec{e} \otimes \hat{\vec{\phi}}_r dt. \tag{24}$$

Where K_i, K_p are the integral and proportional constants. Here K_i and K_p are considered as the weights multiplying the vectored product between current error and estimated rotor flux and its integral respectively. Therefore, the tracking performance of the speed estimation and the sensivity to noise are depending on the proportional and integral gains. The integral gain K_i is chosen high for fast tracking of speed. While, a low proportional K_p gain is needed to attenuate high frequency signals denoted noises [5]

and [6].

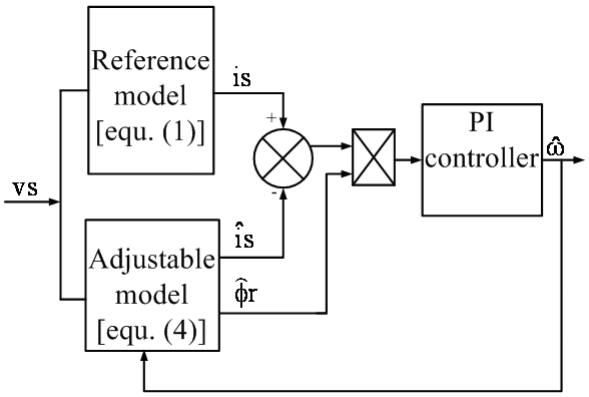

Figure 7: MRAS representation for rotor speed estimation

6 Field oriented control

One particular approach for the control of induction motor is the field oriented control (FOC) induced by Blaschke [18]. This control strategy is based on the orientation of the flux on the d axis [9] and [14], which can be expressed by considering:

$$\phi_r^{(d,q)} = [\phi_r, 0]^T \tag{25}$$

For the flux oriented control, we have two approaches. The first is known as indirect flux oriented control. While, the second is named as direct flux oriented control. For the IRFOC, the rotor flux vector is aligned with d axis and setting the rotor flux to be constant and equal to the rated rotor flux. Based on these conditions, we establish the d and q axis voltage. While for the DRFOC, the d and q axis rotor flux must be known and they will be regulated so that the d axis rotor flux will be equal to the rated rotor flux and the q axis rotor flux will be equal to zero. The d and q axis rotor flux can be provided by the use of sensors or observers. Due to the drawbacks of the use of sensors, the d and q axis rotor flux are provided by the use of the Luenberger observer with an adaptative matrix gain.

7 Design of direct rotor flux oriented control

The direct rotor flux oriented control strategy consists on the regulation of the d and q axis rotor flux so that the rotor flux is aligned with the d axis [Fig. 8] Based on the dynamic induction motor model and the rotor winding linkages, we establish:

$$\phi_{dr} = G(s)v_{ds} + e_{vds} \tag{26}$$

$$\phi_{qr} = H(s)v_{qs} + e_{vqs} \tag{27}$$

Where:

$$G(s) = \frac{ML_r}{1 + (L_s r_s \tau_r + L_s\sigma + M)\, s + L_s r_s \sigma s^2},$$

$$H(s) = \frac{ML_r}{1 + (L_s r_s \tau_r + L_s\sigma + M)\, s + L_s r_s \sigma s^2},$$

$$e_{vds} = \frac{a\phi_{qr} + b}{L_r\,(r_s + L_s\sigma s)\,(\tau_r s + 1) + Ms},$$

$$e_{vqs} = \frac{\omega_r L_r \tau_r\,(r_s + L_s\sigma s) + L_r M L_s \sigma \omega_s i_{ds} + M\phi_{dr}}{L_r\,(r_s + L_s\sigma s)\,(\tau_r s + 1) + Ms}.$$

Where τ_r, s, ω_r and ω are the rotor time constant, the Laplace operator, the slip speed and synchronous speed respectively,

$$a = \omega_r L_r \tau_r\,(r_s + L_s\sigma s)\,(1 + \tau_r s) - \omega_s,$$

and

$$b = -\omega_s M L_r L_s \sigma i_{qs}.$$

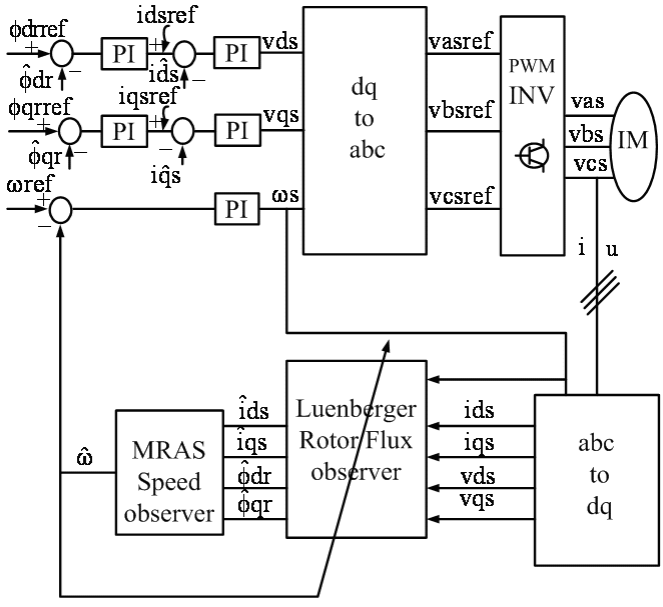

Figure 8: Bloc diagram of the speed sensorless direct rotor field oriented control (DRFOC)

It can be seen from (26) and (27) that it is possible to control the d axis and q axis voltage separately if the coupled terms are equalled to zero. Here, these terms are considered as disturbances. Therefore, these

disturbances are canceled by the use of a PI controllers d for d and q axis rotor flux. The block diagram of PI controllers for d axis, q axis rotor flux and speed rotor is given in Fig. 8. Thus, the dynamics of the d axis and q axis voltage are now represented by simple linear second order differential equations. Therefore, it is possible to effectively regulate the flux with a PI controller. To assume perfect decoupled machine, the dynamics of the d axis and q axis must be equivalent in order to obtain the d axis flux equal to the rated rotor flux and the q axis flux equals to zero at the same time. The strategy adapted to specify the PI controller parameter is at first time to compensate the system zero on open loop. After that, we calculate the closed loop, we obtain a transfer function of the second order system. By fixing the desired closed loop dynamic, we find the appropriate parameters of the PI controllers [16]. In order to protect the system, an inner current loop was added. To validate the strategy, the proposed algorithm has been implemented in the Matlab environnement.

8 Simulation results

The dynamic behavior of the system was investigated by using computer simulations with Matlab/ Simulink software. We have tested the proposed method at variable speed, in the field weakening region and at zero speed command with load applied.
The results obtained in the forward operation at variable step target speeds are represented in Fig. 9 to 12. It can be seen that the d axis rotor flux converges very quickly to the target, the q axis rotor flux is equal to zero, indicating that the decoupling is established in a very short time. Compared to the indirect rotor flux oriented control, we can not command the time of the decoupling machine. For the DRFOC, the decoupling time is controlled by the rotor d and q axis flux controllers.
To investigate the efficiency of decoupling controllers and speed control system, a zero reference speed is studied. Fig. 13 to 16 show the simulation results with a zero reference speed by adding the load torque of 8 Nm at t=7s. It is shown in Fig. 13 that the d axis rotor flux converges to the rated rotor flux (1.1 webers) and the q axis rotor flux has a zero value. By adding of the load torque, the d and q axis stator flux deviate from their reference values and due to the existence of controllers, they converge quickly to their target values.
Fig. 17 to 20 show the trapezoidal response in forward and reverse operation. In this test, both the field weakening operation and load torque disturbance are considered. It is noted that the ideal decoupling is established at a very short time. Hence, high speeds require rather large input voltages. In practice, the voltage must be kept within the inverter ceiling limits so that the flux is decreased from the rated as the speed increases above rated one. This method of reducing the flux at high speeds is called "field weakening" [8].
In different tests, as the load is applied, the d and q axis rotor flux deviate from their value and due to the controllers the deviation error is attenuated in time.
From all these results, it is clearly proved that the speed sensorless IM drives proposed method for the direct rotor field oriented control gives good results under load disturbances. However, the quality of this method is related to the controller which must be robust.

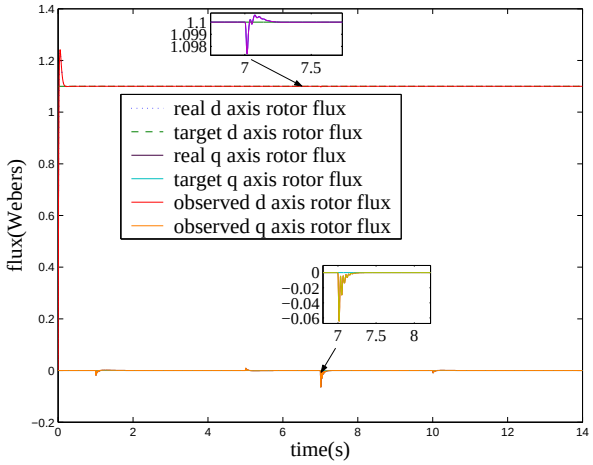

Figure 9: Real, observed and target d and q axis rotor flux at variable motor speed

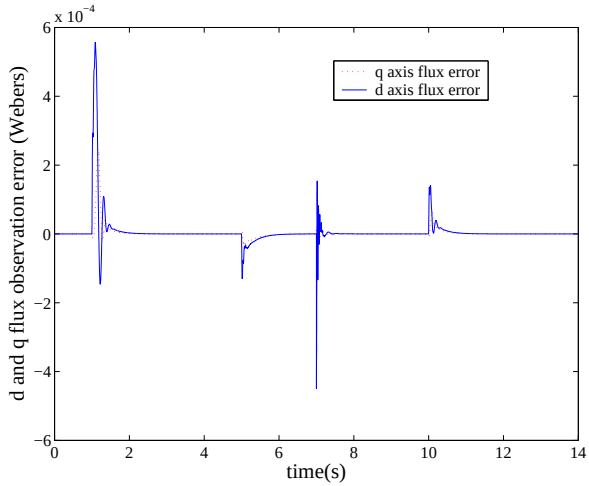

Figure 10: d and q axis rotor flux observation error at variable rotor speed

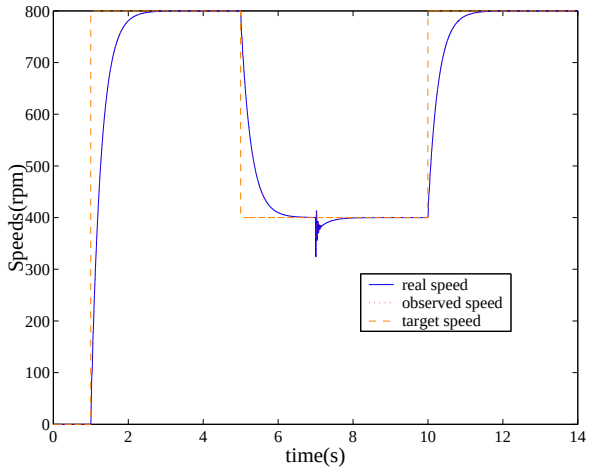

Figure 11: Real, observed and target rotor speed at variable speed operation

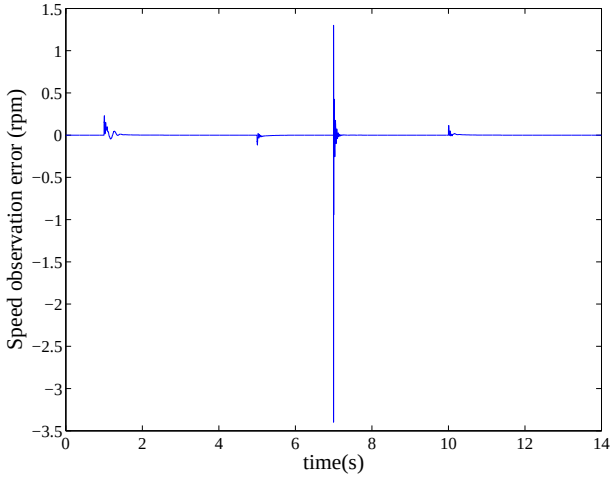

Figure 12: Rotor speed observation error at variable speed operation

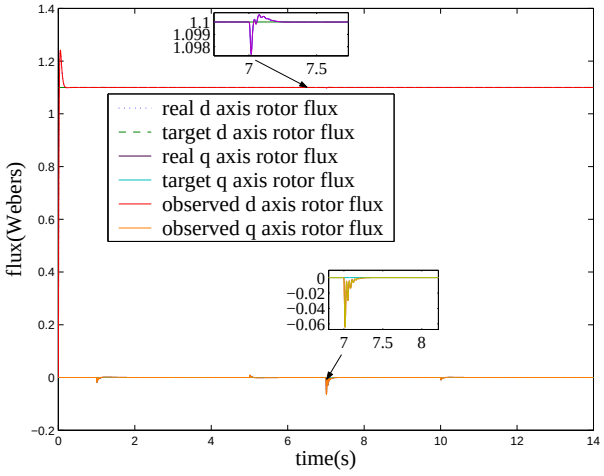

Figure 13: Real, observed and target d and q axis rotor flux at zero speed command

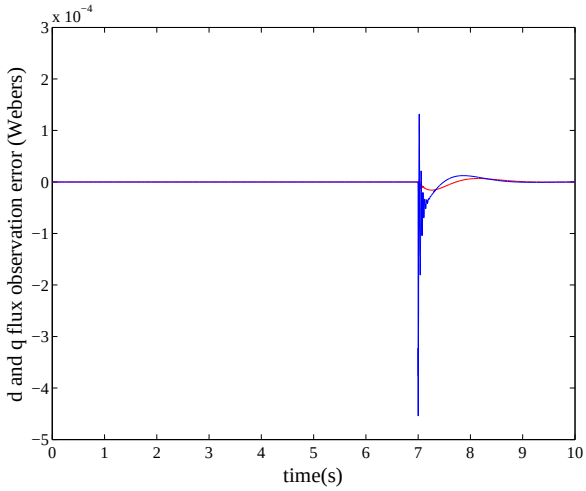

Figure 14: d and q axis rotor flux observation error at zero speed command

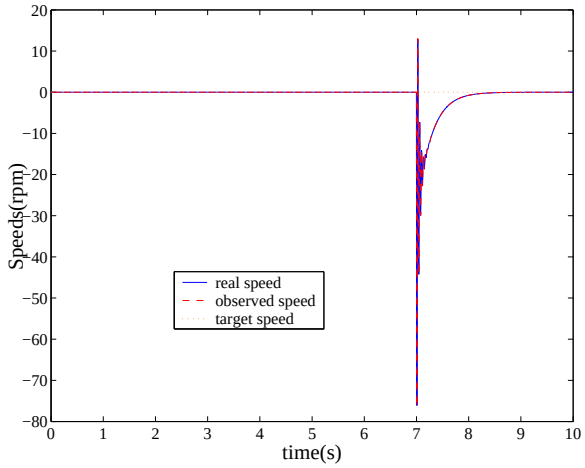

Figure 15: Real, observed and target rotor speed at zero speed command

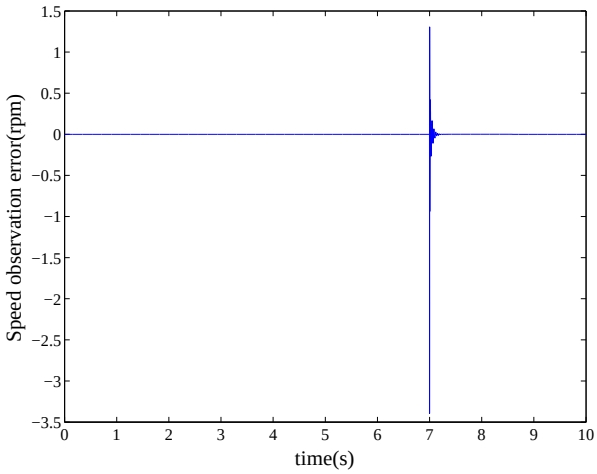

Figure 16: Rotor speed observation error at zero speed command

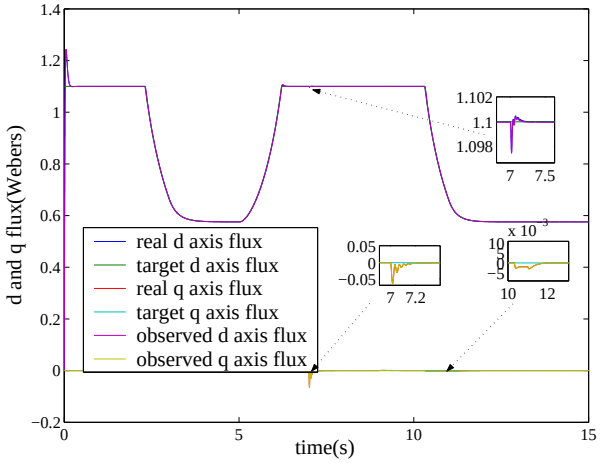

Figure 17: Real, observed and target d and q axis rotor flux at the field weakening region and reverse speed operation

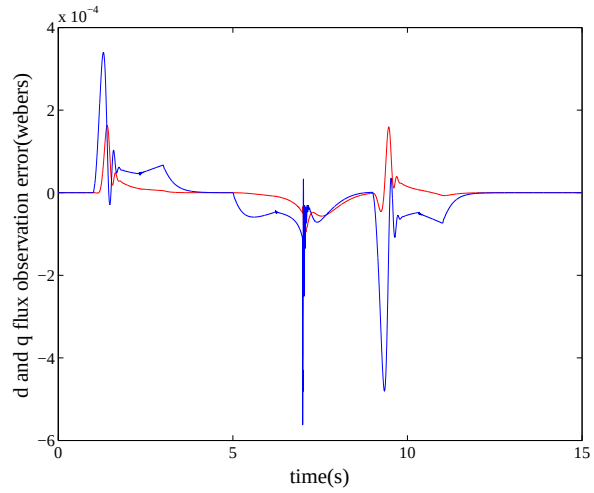

Figure 18: d and q axis rotor flux observation error at the field weakening region and reverse speed operation

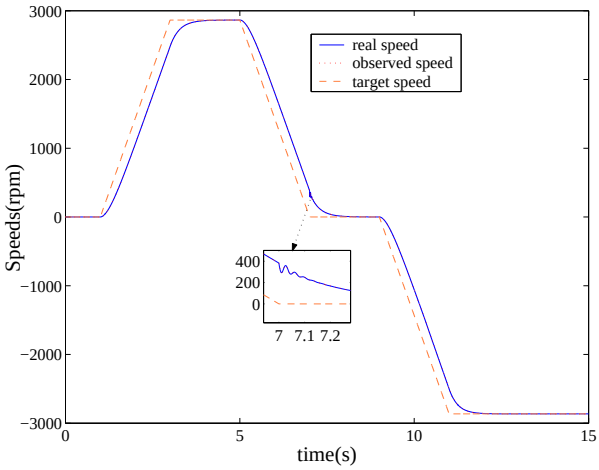

Figure 19: Real, observed and target rotor speed at the field weakening region and reverse speed operation

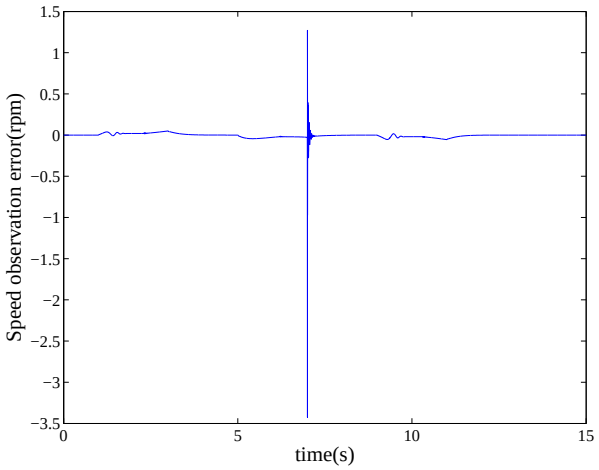

Figure 20: Rotor speed observation error at the field weakening region and reverse speed operation

9 Conclusion

A new method for direct rotor field oriented control, in low speed, zero speed and in field weakening region, has been presented and verified by using extensive simulation work. The novelty and advantage of this method consists in decoupling used technique and observer matrix gain computation. The use of the controllers force the d-axis rotor flux to be constant and equal to the rated value and the q-axis rotor flux to be fixed at zero value. If the decoupling error occurs, it is canceled by the controller which justifies the efficiency of this method compared with the indirect rotor field oriented control where the decoupling of the machine is not controlled. The quality of this method is related to two conditions; firstly, the accuracy and robustness of the observers and secondly the controllers which must be robust. Moreover, a stability analysis study is performed and justified for the proposed speed sensorless induction motor drives.
Practical implementation of the proposed method , at low and high speeds regions, are the subject of future followup research work.

References

[1] M. Boussak and K. Jarray. A high performance Sensorless indirect stator flux orientation control of induction motor drive. *IEEE Transactions on Power Electronics*, 53(1):41–49, 2006.

[2] Carlos Canudas de Witt. *optimisation, discrétisation et observateurs machine asynchrone*. France, 2002.

[3] H. M. Kojabali, L. chang and R. Doraismi. A MRAS based adaptative pseudo reduced order flux observer for sensorless induction motor

drives. *IEEE Transactions on Power Electronics*, 20(4):930–937, 2005.

[4] L. Sbita and M. Ben Hamed. Fuzzy Controller and ANN Speed Estimation For Induction Motor Drives. In procceding of the IEEE-SSD'07 on CD conference.

[5] S. Suwankawin and S. Sangwongwanich. Design strategy of an adaptative full-order observer for speed sensorless induction motor drives - tracking performance and stabilisation. *IEEE Transactions on Power Electronics*, 53(1):96–119, 2006.

[6] C. Lascu and al. Comparative Study of adaptative and inherently sensorless observers for variable speed induction motor drives. *IEEE Transactions on Power Electronics*, 53(1):57–65, 2006.

[7] K. B. Lee and F. Blaabjerg. Reduced order extended Luenberger observer based sensorless vector control driven by Matrix converter with non linearity compensation. *IEEE Transactions on Power Electronics*, 53(1):66–75, 2006.

[8] Ben Salem. Y and L. Sbita. A Non Linear State Feedback Control for Induction Motors. In procceding of the IEEE-ICIT06 on CD conference.

[9] C. S. Staines. Sensorless control of induction machines at zero and low frequency using zero sequence currents. *IEEE Transactions on Power Electronics*, 53(1):195–206, 2006.

[10] M. Edelbaher and K. Jezenik. low speed sensorless control of induction machine. *IEEE Transactions on Power Electronics*, 53(1):120–129, 2006.

[11] M. Ben Hamed and L. Sbita. Speed Sensorless Indirect Stator Field Oriented Control of Induction Motor Based On Luenberger Observer. In procceding of the IEEE-ISIE06 on CD conference.

[12] P. Vaclavek and P. Blaha. Lyaponov Function based flux and speed observer for induction motor drives. *IEEE Transactions on Power Electronics*, 53(1):138–145, 2006.

[13] I. Boldea and S. A. Nasar. Electric Drives. Taylor and Francis Group, : 16–33, 2005.

[14] M. J. Duran and al. induction motor Sensorless vector control with on line parameter estimation and over current protection. *IEEE Transactions on Power Electronics*, 53(1):154–160, 2006.

[15] M. Ben Hamed and L. Sbita. Direct Stator Field Oriented Control of Speed Sensorless Induction Motor. In procceding of the IEEE-ICIT06 on CD conference.

[16] M. Ben Hamed. *Master Thesis Flux and speed observers for induction motor drives.* Master thesis (ATI:07-06), Tunisia-Gabes University, 2006.

[17] C. Schauder, Adaptative Speed Identification for Vector Control of Induction Motor Without Rotationnal Transducteur. Conf. Rec. IAS. Annu. meeting. pp. 439–499,1989.

[18] F. Blaschke. The principle of the field orientation as applied to the new transvector closed -loop control system for rotating - field machines. Siemens Rev., 34:217–220, 1972.

[19] N. B. Almutari and M. F. Hassan. New algorithm for continous linear quadratic control problem with inequality constraints. ICGST - ACSE., 5(1), 2005.

[20] O. Boubaker. Robust observers for linear systems with unknown inputs: a review. ICGST - ACSE., 2, 2005.

[21] R. M. Guerra and R. Aguilar. Risk population estimation for HIV transmission using a reduced order uncertainty observer and a Luenberger's observer. ICGST - ACSE., 2, 2005.

Lassaâd Sbita obtained the doctorate thesis on July 1997 in Electrical engineering from ESSTT of Tunis, Tunisia. He works as an associate Professor at the electrical-automatic genuis department of the Natioanl Engineering School of Gabès, Tunsia. He is manager of the research group on electric machine drives in the research Unit MACS-ENIG. His fields of interest include power electronics, machine drives, automatic control, modeling, observation and identication.

Mouna Ben Hamed obtained the Master degree on September 2006 in automatic and intelligent techniques from National engineering School of Gabès. She is a member of the research Unit MACS-ENIG. She is actually preparing the PhD in the field of sensorless induction motor drives. She works actually as assistant professor at the National Engineering School of Gabès-University of Gabès -Tunisia.

www.icgst.com

Autonomous Intelligent Agent-Based Tracking Systems, Recent Developments

Y.M.A. Khalifa[1], E. Okoene[1], and M.B. Al-Mourad[2]
[1] *Department of Electrical & Computer Engineering, State University of New York at New Paltz,* New Paltz, NY 12561, USA
[2] *School of Computing & Information technology, University of Wolverhampton,* WV1 1SB, UK

Abstract

In this paper, we present recent developments in ground surveillance and target tracking systems. Such systems posses various characteristics which include having the ability to strategically integrate information from several sources so as to make accurate decisions, optimizing the location of sensors to achieve complete coverage of the desired area and efficiently utilizing the resources of the system. Various techniques (including Evolutionary Algorithm) have been used to accomplish this. In addition, such systems posses intelligent agents, which are autonomous devices that have various sensors, and have the capability of processing and communicating information with other agents either directly or through a central processing system.

Keywords— Autonomous Agents, Surveillance Systems, Evolutionary Algorithm, Distributed Network

1. Introduction

The design and development of surveillance systems is increasing, especially in military applications where there is a need for fast and accurate decision-making under a variety of complex situations. The main objective of these systems is to provide accurate detection and precise tracking of moving targets by integrating information from several sensors. In addition to that, these systems should also be capable of 1) optimizing the location of sensors in order to achieve complete coverage of the desired area; 2) efficient use of the system's resources (e.g. maintenance of sensor's battery life for a longer life-span); and 3) reliable real-time communication in the midst of harsh environmental conditions and/or changes in the system [1]. As a result of such a dynamic environment a lot of research has been done into the development of autonomous systems, capable of achieving the goals of surveillance (such as target detection, location and tracking etc) in the midst of constantly changing conditions. In addition, such systems have intelligent agents, which are autonomous devices comprised of various sensors (such as acoustic, infrared) and have the capability of processing and communicating information with other agents and with a central processing system. This paper presents a summary of research that has been undertaken with the intent of conquering the above-mentioned obstacles. The rest of this paper is organized as follows: Section 2 gives an overall description of agents; passive and active. Different coverage area optimization techniques are presented in section 3. In section 4, the power optimization techniques utilized in such sensor networks are described. Section 5 expounds on the communication aspect of the distributed collaboration scheme and section 6 gives a summary and a conclusion.

2. Agents

Although the concept of a sensor network is not new (DARPA initiated the Distributed Sensor Networks program in 1980), recent advances in microprocessor fabrication has lead to a dramatic reduction in the size and power consumed by such devices. Battery and sensing technology together with radio hardware have also followed a similar minaturisation trend. The aggregation of these advances has lead to the development of networked, millimeter-scale, sensing devices capable of complex processing tasks. Collectively these form a Wireless Sensor Network (WSN), thus heralding new era for ubiquitous sensing technology. Large scale deployments of these networks have been used in many diverse fields such as wildlife habitat monitoring [2], traffic monitoring [3] and lighting control [4].

Due to the limited power supply of these devices, it is imperative that the operation of each node factor into account when making any decision to perform an action. For example, consider the case where a nodes power has depleted to a point where it is capable of only a handful of transmissions. The network should be able to adapt to this fact and this node should only transmit if it deems it critical to do so. This decision must be taken on a per-node-basis as off node deliberation would necessitate further transmissions.

Intelligent and proactive behavior such as this is characteristic of an intelligent software agent. Agents form the basis for distributed, artificially intelligent

applications [5], and their applicability to WSNs is the central theme of this paper. Making an informed decision by incorporating various perceptions or beliefs about an environment is at the very heart of an agents deliberative cycle. Goal oriented reasoning can allow the agent to commit to the course action that best realizes its goals, in this case the agents goal is to maximize the network life span. Its perceptions are the sensory modality or modalities it is capable of sensing and the remaining battery power. By reasoning about the effect of a transmission, the agent can see if that action best suits its goals, which in this sample instance is unlikely to be the case.

Generally speaking there are two types of agents: passive and active. Passive agents are agents designed to solve well-defined problems by responding to situations with predefined actions; in other words, for every situation they face, they have well defined procedures of how to respond to these situations. There are different ways agents react to situations. A few examples include making reference to a lookup table of situation-action pairs or implementing a combinational logic circuit. The designer of the agent (or some Artificial Intelligent process embedded into the agent) usually determines these actions for the majority of situations that could occur. As a result, such systems require very little effort in computation but have very large memory. Passive (or reactive agents) operate well in environments that do not change very much. On the other hand, these agents have very fast response-time, since their response has already been predetermined. Some examples of these types of agents include patient diagnosis agents and certain kinds of data-mining agents [6] and [7].

Intelligent agents are information-based systems that perceive their environment, via interfacing with their physical world using sensors, or a collection of other agents, or other complex environments. Intelligent agents also have the capability to interpret perceptions, draw inferences, solve problems and determine actions. They can also act upon that environment to realize a set of goals or tasks for which they are designed. Intelligent agents interact with a human or some other agent via some kind of agent-communication language [8]. If needed, these agents are able to adapt to their environment in order to realize their goals. These agents have the capacity to learn new things (from past experiences and current precepts), which enables them to evolve into smarter machines and make more accurate decisions. There are 3 primary types of intelligent agents: reasoning, learning and evolving agents [9]. Reasoning agents have the ability to make inferences by following a chain of predefined rules, and can be proactive in their use of reasoning. On the other hand, learning agents are not only able to follow a set of rules, but also improve their responses by learning from their experiences. One means is by programming them to weight their decisions. Lastly, agents that evolve with each successive generation are termed evolving agents. Here, knowledge acquired or learned can be passed from agent to its offspring. The most common of these three are the learning agents.

A theoretical example that shows the difference between intelligent and passive agents is a mail-sorting system of a manufacturing company. The passive agent system would be designed to place each department's mail in their mailboxes, while mail not directly linked with any department would be placed in the "unknown" mailbox, to be sorted out by a person. On the other hand, the intelligent agent would be designed not only to distribute the mail, but also to figure out the destination of the ambiguous mail. Ambiguous mail is mail that could have vague or inaccurate origin, name of the person to whom it is sent, destination, etc. In addition, as the intelligent agent system learns the destination of the ambiguous mail, it stores this newly acquired knowledge. Common techniques used for learning in intelligent agents are Neural Networks, Bayesian Rules, Credit Assignments and Classifier Rules. Through learning, these agents are better able to adapt to their environments. Adaptation is behavior of an agent in response to unexpected events or dynamic environments. Examples of unexpected events include the unscheduled failure of an agent, an agent's computational platform, or underlying information sources. Examples of dynamic environments include the occurrence of events that are expected but it is not known when, events whose importance fluctuates widely (e.g., price information on a stock), the appearance of new information sources and agents, and finally underlying environmental uncertainty (e.g., not knowing beforehand precisely how long it will take to answer a particular query). [10]

Adaptation is achieved through first establishing a proper symbolic representation of the environment. These symbolic representations are produced by the timely interpretation of the environment through feedback from perception processes. The work presented by Diehl et al. [11] is an example that illustrates part of this; it presents the initial steps taken towards the ultimate goal of developing a distributed surveillance system that produces a timely interpretation of the environment through feedback from perception processes. The main component of the system presented by Diehl et al. [11] is the CyberARIES, which is an agent-based software architecture responsible for the coordination of sensing, processing and communication among the agents, and the development of efficient perception algorithms for detection and classification. The CyberARIES architecture consists of two main parts: the agent and the distribution layer. The agent is able to communicate with other agents (through its source and sink), which is controlled by an agent run loop, Figure 1. The distribution layer is the communications infrastructure that manages the flow of stimuli amongst agents and within the system. It also determines which agents should assist another agent during perception.

The efficient perception algorithm consists of a motion detection algorithm that quickly acquires a model of the environment while being insensitive to jitter caused by vibration. First, constructing a background model that continuously changes and subtracting this image from each frame to obtain the foreground image, which in turn is used to segment each target, achieves the motion detection. The background model is constructed using an Auto Regressive (AR) filter applied to the current frame and a time-lagged frame. In addition, the motion detection algorithm classified moving objects


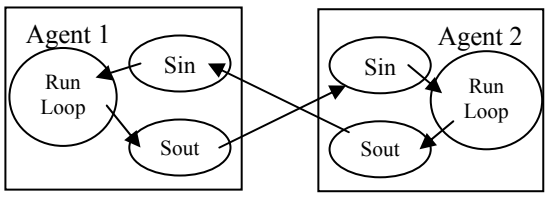

Figure 1. Communication between agents, by Diehl et al. (1999)

either as people (single or multiple), vehicles or unknown objects. This classification was carried out using the difference image, rather than the threshold difference image, since the former provided a more stable representation of the object image without influence from the background.

Another example of an agent system that implements symbolic representation is presented by J. Orwell et al. [12]. It consists of an architecture that implements a scene-understanding algorithm in the visual arts domain. This architecture consists of multiple cameras and an agent framework (where each camera has its own agent). These agents are responsible for tracking the events in their field of view, which is accomplished by performing the following tasks:

- a planar homograph is maintained between a three dimensional (3D) image plane and the ground plane;
- a model of the appearance of the scene is learned and continuously updated;
- an Object Agent is invoked for each stable tracked event;
- and lastly, 3D positional and color data supplied by the scene model are integrated within the tracker, which is then transferred to the object agent.

The main objective of the tracker is to associate moving objects between frames by first classifying pixels as either moving or not moving. Next, these moving regions are then recovered and interpreted. Finally, a temporal continuity of the moving regions is matched. In addition, the task of the object agent is to describe the appearance, motion and activity of the event within the ground plane. The object agent utilizes the 3D color and positional data (being the pixel data and computed location) of the event to accomplish this. This results in an approximation of the trajectory and color of the 3D event, and a classification of this event based on a set of pre-stored activities. Periodically, each invoked object agent communicates with the other (by sharing trajectory and color data). If two object agents have similar data (indicating that their cameras are viewing the same event), both agents are combined to form one agent; this new agent then inherits the camera data link of both cameras and its (the new object agent's) trajectory and color data are updated from both sources.

Piaggio et al. [13] present a unique way of representing the world in terms of the radial distance between objects in the world and the agent. Here, real-time sensor data acquisition and representation of the world and its usage for real-time navigation is proposed. Figure 2 is a block representation of the system's architecture. The Perceiver and the Motion Controller are interrupt-driven processes that connect the robot to the real world through a virtual interface. The former receives its information through ultrasonic sensors located around the robot's body, while the motion controller is responsible for the robot's motion, through the robot's actuators.

The three message-driven processes, the Map Handler, the *Artificial Potential Field* (APF) Handler and the Navigator, operate simultaneously under a more relaxed time constraint and are, to a large extent, machine independent; the first two develop and update an internal representation of the world, while the third alters the parameters that control the robot's motion, based on this internal representation.

For a more efficient APF representation, two map representations are formed. The first is the ecocentric representation (mentioned earlier) while the second is the robocentric representation. As a clarification from the authors, the latter shows the radial distances of objects from the robot that were generated during navigation. The APF is a graph built from this robocentric representation; it (the APF) characterizes obstacles as regions of high-energy and it works directly with the navigator to coordinate the robots motion.

The authors' view is as shown in Figure 2. There are two main processes: interrupt driven (software or hardware) and message driven (software). The former does not require any special communication scheme, while the latter operates when certain conditions are met, which depend on a message broadcasting protocol. In addition, the message driven processes send messages that are grouped according to their content, in order to indicate that an action/computation has occurred or is required by the sender, or to indicate the type of message it will receive.

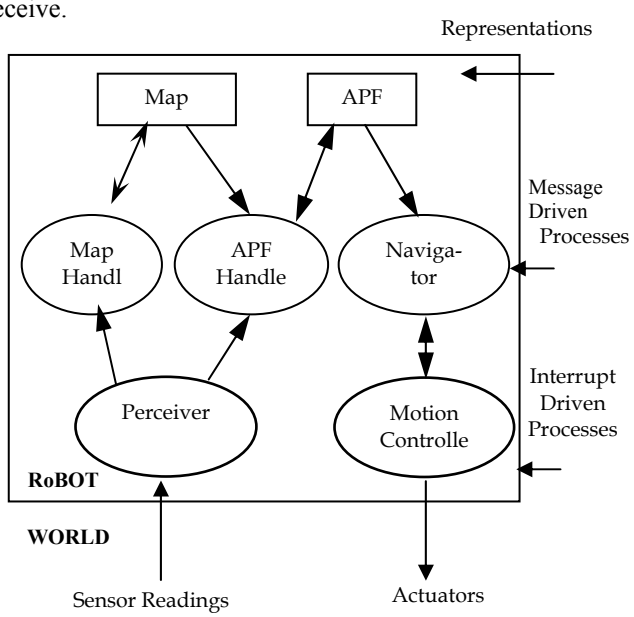

Figure 2. Piaggo et al. (1996) System's Architecture.

As a further clarification by the authors, an advantage of this second function is the conservation of the CPU's resources, i.e. processes are suspended until the required message is received.

Gesù et al. [14] present a system which illustrates the means of adaptation through perception and symbolic representation. They present the design of a Distributed Architecture System for *Autonomous Robot Navigation* (ARN) utilizing *Genetic Algorithm* (GA). The architecture presented is based on three modules that are

implemented on separate and interacting agents (the target recognizer, the obstacle evaluator and the planner). In addition, an adaptive form of GA is used to identify mechanisms for reaching the target and for manipulating the two directions of the robot. Data about the environment is collected through a video camera placed on the head of the robot, and two infrared sensors on the bottom of the robot. Information from the video is used to recognize the target, while evaluation of distances from obstacles is carried out with information received through the sensors. The first two agents within the ARN system (the *Target Recognizer* and the *Obstacle Evaluator*) are dedicated to the evaluation of the sensors information, while the third agent (the *planner*) plans the robot's movements according to an optimization strategy. Moreover, additional modules are used (in conjunction with the three main modules) to handle *Input/Output* (I/O) and evaluate the robot's movements (see Figure 3).

The author suggests that more attention should be paid to the evolution of data by mentioning that the system's evolution is based on an *Active Information Fusion* (AIF) loop that consists of five modules (*Observe, Evaluation, Optimization, Choose-Next*, and *Action* - Figure 4) that could be implemented in parallel. Their responsibilities are stated below:

- Observe: acquires and preprocesses sensorial data;
- Evaluation: computes the robot's next choice of action based on the observed parameters and its current state. The evaluation makes use of the Optimization module (which implements Genetic Algorithm);
- Choose-Next: selects the new movement (or Action) of the robot on the basis of the Evaluation module.

Once the *Action* has been executed, further sensor-explorations are undertaken.

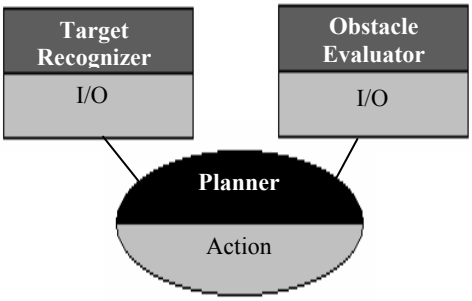

Figure 3. The Agents of the Distributed Architecture System for Autonomous Robot Navigation.

According to the authors, the planning agent is responsible for driving the robot toward the target. Its aim is to "… *find the minimum number of steps [required] to reach the target in position (x_T, y_T) starting from the position (x_0, y_0) and avoiding obstacles in the room* …". Assuming there is one rectangular obstacle present, Figure 5, then the navigation problem can be formulated as a dynamic programming problem (Equations 4 through 7), where the variables in the equations represent the coordinates of the robots (x_i, y_i), the coordinates of the top-left corner of the obstacle (x_{ob}, y_{ob}), the

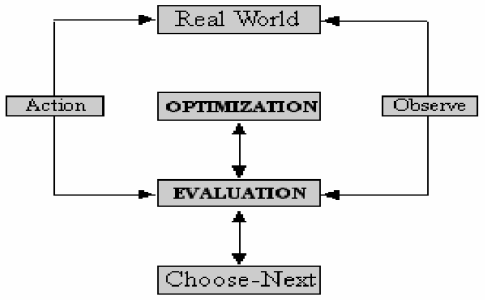

Figure 4. The Active Information Fusion Loop of the Distributed Architecture System for Autonomous Robot Navigation.

coordinates of the target (x_T, y_T) and the angle between the direction of the robot displacement and the vector robot-target (θ), Figure 5. Sx, Sy and S_θ describe the dynamic evolution of the system and δ measures the length of the path made by the robot to reach the target in step units. Although the robot has no knowledge of the coordinate system, it is able to navigate through the evaluation of distances from the obstacles and the direction of the target with respect to its displacement direction.

$$x_i = S_x(\theta_{i-1}, x_{i-1}, y_{i-1}, x_{ob}, y_{ob}, x_F, y_T; \alpha, \beta) \quad (1)$$

$$y_i = S_y(\theta_{i-1}, x_{i-1}, y_{i-1}, x_{ob}, y_{ob}, x_F, y_T; \alpha, \beta) \quad (2)$$

$$\theta_i = S_\theta(\theta_{i-1}, x_{i-1}, y_{i-1}, x_{ob}, y_{ob}, x_F, y_T; \alpha, \beta) \quad (3)$$

$$\min(\delta(x_0, y_0, x_T, y_T)) \quad (4)$$

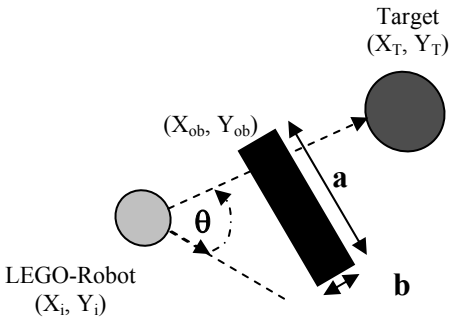

Figure 5. The Robot-Target Assessment.

The planner (responsible for providing θ and the speed of the robot) incorporates the GA that was designed to approximate a solution to the navigation problem mentioned previously. This GA:

- selects a starting population of 200 genomes (e.g. "1010101111010111"; each genome represents the displacement directions, α, in the interval [-π,π] (see Figure 6). They are mapped in 16-bits word using the function: $R(\alpha) = \left[\frac{(\alpha + \pi)(2^{15} - 1)}{2\pi} \right]$ (5)
- performs a uniform-probability single-point crossover operation on randomly chosen genomes;
- performs a one-bit mutation, with probability rate of 0.01;
- determines the fitness ($F_{h,k}$) for each pair of chromosomes; and
- selects a new population using the tournament technique), and terminated if

the global fitness, F, satisfies the convergence criteria.

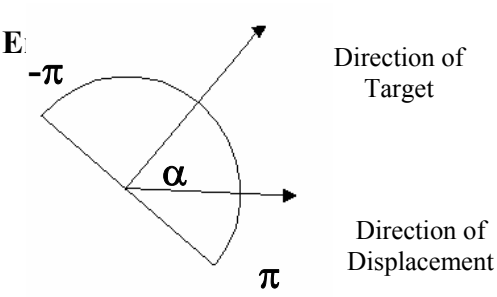

Figure 6. The direction of the displacement (with respect to the target).

The fitness function is defined based on a formulation that considers obstacles and target as electric objects, which generate electrostatic fields (the target attracts and obstacles repel):

$F_{itness} = (\alpha * F_{target}) - (\beta * F_{obstacles})$, with $\alpha + \beta = 1$ (6)

- $F_{target} = K * (\pi - \theta)$, is a linear decreasing function of θ,
- K is a positive constant experimentally determined,
- $F_{obstacles} = \sum_{i=1}^{2} \left(\frac{C_i}{R_i^2} \right)$, is a function of the measurements from the range detectors, R_i,
- C_i's is a constant that depends on the directions of the infrared sensors, which are computed during the calibration phase.

Another multi-target tracking system is presented [15]. In this system, a video is used to track the movement of people as they enter and leave a bus. In order to track a moving/stopped target, each frame produced by the video camera is divided into hexagonal cells, with the aim of assigning a group of cells to one target. Each pixel in a frame is assigned to a cell. If the intensity of a pixel is greater than a certain threshold, it is considered to be on and each cell is considered active if the number of "on" pixels in the cell is above 40%. Once a group of cells are formed (which are either in direct or indirect contact with one another) they are considered to be an estimation of the position of the target, only if they satisfy certain rules – this group of cells is termed a blob. In addition, the author mentions that if two blobs are close to one another (where they actually touch each other), the entire group of cells undergoes a series of tests in order to identify the group as two separate blobs, and as such, two separate targets.

3. Coverage Area Optimization

Another area of autonomous surveillance agents that is very critical is the optimization of the location of sensors in order to maximize the area covered by these sensors, while accurately tracking targets. A great deal of research has been conducted into achieving this goal with the help of Evolutionary Algorithms e.g. GA and Neural Networks; one example is presented by Buczak [16]. In this work, the author suggests that new ways for the collection and treatment of sensor information should be applied. The author introduces a novel method, which utilizes GA to determine the optimal combination of sensors (with minimal network power consumption and best location accuracy) that can detect and/or locate targets. It was discovered that one sensor triplet is needed per target, and sensors used for different targets can be shared. Within this system, a network of randomly distributed unattended ground sensors perform *Self-Organization* (SO) based on the *Mission Statement* (MS). The commander (or the central control system) issues the MS, which defines the goal of the surveillance, the geographical area and target types. The SO results in the translation of the MS into a *Network Objective* (NO) that defines what sensors should be used to perform the current objective at each point in time, and as events happen in the environment, the SO adapts the NO. The NO Adaptation (NOA) and Optimization modules (modules of the NO) are responsible for carrying out these functions. More specifically, the NOA module is responsible for the automatic generation of the optimization problem based on the MS and the events that happen in the environment, and starting the tracking with the sensors chosen by the Optimization module.

The author also suggests that more attention should be allocated with GA data and processes. Since GA is used to obtain an optimum solution, each solution (or chromosome) is an *m*-tuple of sensors that can be used to track a given target. Assuming we have *k* targets, where n sensors can detect each target, then the number of tuples per target is given by equation (7) and the search space is given by equation (8)

$$\#M-Tuples = C_m^n = \frac{n!}{(n-m)!\cdot m!} \quad (7)$$

$$SearchSpace = \left(NumberOfMTuples \right)^k \quad (8)$$

Each chromosome contains the identification of the sensors (or genes) that are chosen to be active at a given moment (i.e. to track the target). The number of genes per chromosome varies with the NO. For the fitness function, it depends on the location accuracy and the network power consumption. It has the following form:

$$Fitness = -(w_1 \cdot \sum_{i=1}^{k} E_i + w_2 \cdot \sum_{j=1}^{l} P_j) \quad (9)$$

where E_i (i=1,2,…,n) is the estimated position error for the *i*-th target, P_j (j=1,2,…, m) is the power consumption of the *j*-th sensor, *k* is the number of targets, *l* is the total number of selected sensors and w_1/w_2 are two weight constants. The implementation of the GA was carried through the GeneHunter™ Dynamic Link Library of basic GA functions, which was linked to the authors C/C++ program. In addition, the authors used an elitist GA with a constant probability of one-point crossover set at 0.9 (per gene) and a constant probability of mutation set at 0.01 (per bit). With the number of individuals in the population constant, the GA was run until there was no improvement in the best individual of the population.

Another unique area of research that utilizes GA to optimize coverage area [16] focuses on merging trackers that track the same object, in order to reduce redundancy as well as increase the accuracy of tracking. In other words, trackers (which consist of 2 or 3 sensors that can track an object) are created, merged, separated and


removed so that each target is properly tracked and redundant trackers are avoided. A few sensors are placed along the perimeter of the area under surveillance, and they are turned and left on. When one of these perimeter sensors detects an object, a tracker and its database are created (which is based on the amount of sensors that can and do detect the object). In addition, each tracker has to be updated with the help of a GA (i.e., sensors are replaced if they are unable to detect the target), while trackers with sensors that are tracking the same target are merged/fused (i.e., their database). Figure 7 shows a basic example of fusing two trackers' database:

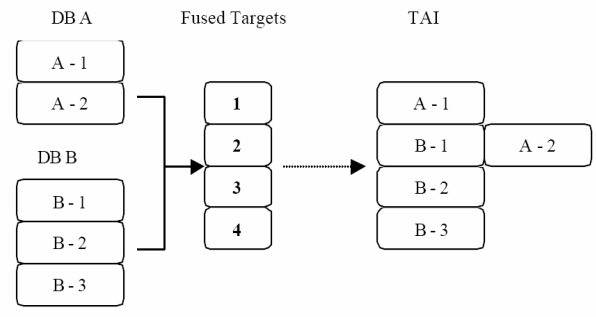

Figure 7. Basic example of fusing two trackers.

In the example shown in Figure 7, the database of Tracker A (DB A) and the database of Tracker B (DB B) are fused. Within database A, two targets are registered and associated with two tracks (A-1 and A-2) while three targets are registered and associated by three tracks (B-1, B-2 and B-3) in database B. After the fusion process, only four (instead of five) targets are obtained. After comparisons, it was concluded that tracks A-2 and B-1 are the same.

[17] propose a *Dynamic Coverage Maintenance* (DCM) scheme that exploits the limited mobility of sensor nodes. Here, the main objective is to compensate the loss of coverage with minimum expenditure of energy. Four (4) DCM schemes are proposed which can be executed on individual sensor nodes having the knowledge of just the local neighborhood topology. These schemes determine which neighbors to migrate and to what distance, such that the energy expended is minimized and the coverage obtained for a given number of live nodes is maximized. The schemes and their responsibilities are described as follows: a) the *Maximum Energy Based* (MEB) scheme moves the node with maximum available energy; b) the *MinMax Distance* (MMD) scheme moves that neighbor which needs to cover minimum distance to achieve maximum compensation for the dead node's coverage; c) the *Minimum Distance/Energy* (MDE) scheme considers the ratio between distance to be moved and energy available, and chooses the node with minimum ratio; and lastly, d) the *Minimum Distance Lazy* (MDL) scheme moves the least distance possible so that the coverage is maintained, unlike the first three which try to move as close to the dead node's position as possible without affecting their existing coverage. The decision and movement is completely autonomous in the network and involves movement of one-hop neighbors of a dead sensor node. An extension to these algorithms is also proposed called Cascaded DCM, which extends the migrations to multiple hops, if the net migration distance is less than a single-hop migration.

Additionally, Megerian et al. [18] consider another angle of sensor coverage area. They present best and worst-case formulations for isotropic sensor coverage in wireless sensor networks. As well, they proposed an optimal polynomial time algorithm that uses graph theoretic and computational geometry constructs for solving for best and worst-case coverage. The results they achieved from their experiments show potential at being applied in applications of the theoretic coverage formulations and algorithms specifically for solving for additional sensor deployment heuristics to improve coverage, worst-case coverage (Maximal Breach), best-case coverage (Maximal Support) and stochastic field coverage.

4. Power Optimization Techniques

Another unique area of interest within the study of surveillance systems is the investigation into techniques that optimize power resources. In [14], the authors present a system that implements a technique taking into consideration the power resources of the system. This system utilizes a wireless surveillance network and an algorithm that determines if a local node should be made active for the next snapshot/scan. Each node contains an autonomous node manager, which determines whether the node should be made active or not based on two factors: 1) the locations of the active nodes that were present in the last snapshot, and 2) the ability of the node to reduce the Root Mean Squared position error of the target, under low power constraints.

In [19], Buczak presents another surveillance system, along with the use of a network of sensors, to automatically generate the optimization problem, which depends on the events happening in the environment, and utilize a GA generated specifically for the problem to find the quasi-optimal combination of sensors (i.e. sensors with minimized power consumption and accurate tracking) that can detect and/or locate targets.

Burne, in [20] also presents a surveillance system designed to replace today's military-used *unattended ground sensors* (UGSs), which have a rather large size (> 1 ft^3) and are relatively expensive. The author states that the system will posses smaller and less costly sensors that will work cooperatively together as a network, under the supervision of an algorithm, in order to maximize its tracking accuracy and minimize its power utilization.

So far, a general description of various schemes/architectures that utilize intelligent agents in the area of surveillance have been presented. Each has some form of organization where there is either a central processing system that processes information gathered by the agents and in-turn communicates its conclusions to these agents or the agents themselves possess the information-processing capability and communicate amongst themselves. The communication scheme adopted by the surveillance system depends on the objective of the entire system. The next section presents a definition of the different communication schemes implemented within surveillance systems and gives examples of schemes/architectures that implement each.


With the advent of ad hoc networks of geographically distributed sensors in remote site environments (e.g. sensors dropped from aircraft for personnel/vehicle surveillance), there is a focus on increasing the lifetimes of sensor nodes through power generation, power conservation, and power management. Current research is in designing small *Microelectromechanical Systems* (MEMS) *Radio Frequency* RF components for transceivers, including capacitors, inductors, etc. The limiting factor now is in fabricating micro-sized inductors. Another thrust is in designing MEMS power generators using technologies including solar, vibration (electromagnetic and electrostatic), thermal, etc.

RF-ID (RF identification) devices are transponder microcircuits having an L-C tank circuit that stores power from received interrogation signals, and then uses that power to transmit a response. Passive tags have no onboard power source and limited onboard data storage, while active tags have a battery and up to 1Mb of data storage. RF-ID operates in a low frequency range of 100kHz-1.5MHz or a high frequency range of 900 MHz-2.4GHz, which has an operating range up to 30m. RF-ID tags are very inexpensive, and are used in manufacturing and sales inventory control, container shipping control, etc. RF-ID tags are installed on water meters in some cities, allowing a metering vehicle to simply drive by and remotely read the current readings. They are also be used in automobiles for automatic toll collection.

Meanwhile, software power management techniques can greatly decrease the power consumed by RF sensor nodes. TDMA is especially useful for power conservation, since a node can power down or 'sleep' between its assigned time slots, waking up in time to receive and transmit messages. The required transmission power increases as the square of the distance between source and destination. Therefore, multiple short message transmission hops require less power than one long hop. In fact, if the distance between source and destination is R, the power required for single-hop transmission is proportional to R^2. If nodes between source and destination are taken advantage of to transmit n short hops instead, the power required by each node is proportional to R^2/n^2. This is a strong argument in favor of distributed networks with multiple nodes, i.e. nets of the mesh variety.

A current topic of research is *active power control,* whereby each node cooperates with all other nodes in selecting its individual transmission power level [21]. This is a decentralized feedback control problem. Congestion is increased if any node uses too much power, but each node must select a large enough transmission range that the network remains connected. For n nodes randomly distributed in a disk, the network is asymptotically connected with probability one if the transmission range r of all nodes is selected.

5. Communication Schemes

The control of the activities of autonomous agents within a surveillance system is characterized into three schemes: the hierarchical scheme, the centralized scheme, and the distributed scheme. In the hierarchical scheme, there are several groups of agents and each group has one agent that controls the actions of the others. The centralized scheme is different; it has a single agent that coordinates the actions of the remaining agents. Within the distributed scheme, each agent independently controls itself. In addition, there are systems that utilize a combination of these three schemes.

5.1. Hierarchical Scheme

One system that implements this scheme is presented by Liu et al. [22]. The work presented here focuses on the optimal selection of perimeter sensors that will initially detect targets as they enter the region under surveillance. Once the target is detected, a Self Organization Module will select a set of sensors (at most 3 sensors that are capable of detecting the object), which will track the movement of this target.

B. Horling et al. [23] present another target tracking system that implements the hierarchical collaboration scheme. Here, the environment is divided into a series of sectors (which are non-overlapping, identically-sized rectangles), the sensor agents are distributed amongst these sectors and within each sector, a sensor agent is chosen to be the sector manager – Figure 8. In addition, the remaining sensor agents (within each sector) are divided to assume the following roles: sensor data production; target detection and location; target tracking and sensor's data processing. Once each sensor agent has determined the sector to which it belongs, it informs its sector manager of its capabilities and the sector manager negotiates with the sensor agent in order to organize the scanning of the region. Each sensor agent determines when its assigned tasks get performed and it can chose between which assignments it will undertake if received from more than one sector manager – Figure 9. Once an object has been detected, the sector manager picks one of the sensor agents as the track manager, who in turn selects a group of sensor agents to track the movement of the object – Figure 10. The data gathered from these sensors are then sent to another sensor agent who determines the current location of the object and develops the objects track, which is in turn used to estimate the direction in which the agent would move. This information is then given back to the track manager, and the whole process repeats itself – Figure 11. From the above-mentioned process of target detection, location and tracking, the hierarchical scheme is realized through two main steps: the first is through the distribution of the entire body of sensors into the divided sectors with the appointment of one sensor from each group as a sector manager, and the second is through the selection of a track manager (within each sector) following the detection of a target.

S. Lazar et al. [24] present a unique method of mobile agent communication and location. Within their scheme, all mobile agents (small software objects capable of moving around a network and executing tasks) are considered to be the leaves of the tree-like hierarchy structure, and they are placed on an agent server (or agent runtime environment). In addition, each node within this network is considered a Domain Gateway Server (DGS - see Figure 12), and it holds the address of its parent node (except the root node) and the path registration entry for every agent within its group. This entry consists of the


agent's unique identifier and a pointer to the next location where the agent was transferred (unless otherwise stated).

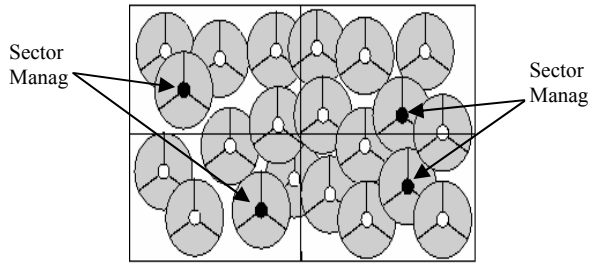

Figure 8. Division of the region under surveillance into sectors.

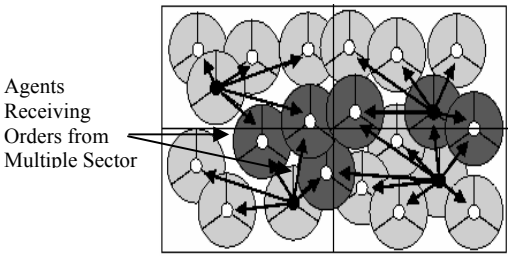

Figure 9. Negotiation between sector managers and the sensors within each sector.

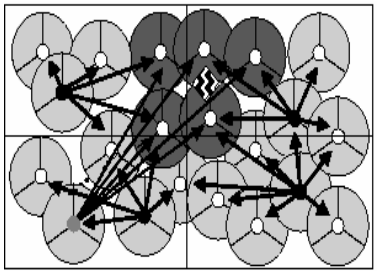

Figure 10. The track manager chooses sensors that will track the movement of the object.

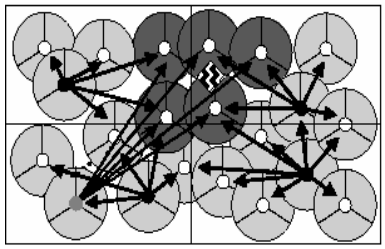

Figure 11. The location and track of the object are determined by the data received.

5.2. Centralized Scheme

As mentioned earlier, the centralized scheme consists of a Central Processing System that controls/coordinates the activities of the surveillance system. The work presented by B. Jung et al. [25] incorporates (to a large extent) the centralized scheme. This system undertakes the tracking of targets within a large structured, complex environment, e.g., an office environment containing numerous small rooms. There are two levels of control within this system. The first is the coarse level, where a Central Processing System distributes the agents into the regions that contain the targets (i.e., the entire environment is divided into simple regions by using landmarks as demarcaters). This distribution is based on the regions need of agents and the distance between the region being considered and the agents. The second level of control is amongst the agents themselves, i.e. in terms of tracking the targets. Here, each agent maintains a topological map of the region (which it receives from the Central Processing System) and any necessary information needed for tracking).

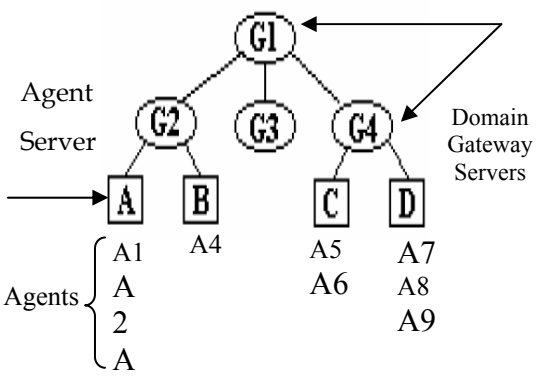

Figure 12. The Domain Tree Network.

Feller et al. [26] present another centralized system, which utilizes infrared sensors and high-resolution cameras to detect, locate, track and identify targets. This system consists of 22 binary infrared detectors that are commercially available over the Internet (for object tracking), a Merlin NIR Infrared Camera by Indigo Systems Corporation (for object identification), a PC104 Modular Computer with a Pentium Processor (as the central control node) and a display for the results. The Modular Computer and the Infrared Camera interact through a Netgear FVM318 802.11b Enhanced Wireless VPN Firewall Router, while data sent through the infrared detectors' built-in transmitters is received by the serial port antennae of the Modular Computer. Within this system, a two-dimensional pixel map represents the environment under surveillance. When an object is detected, the pixel's intensity, which corresponds to the field of view of the sensor that detected the object, is incremented. As such, pixels with higher intensities have a greater probability of specifying the location of the target and, in turn, are used to specify the angle that the infrared camera should turn.

5.3. Distributed Scheme

Soh et al. [27] present an agent system that utilizes the distributed scheme for agent communication or collaboration. The agents within this system each have time-bounded, limited resources allocated to them (with no centralized information shared), they are fully autonomous, and there is no hierarchical organization among them (which increases their autonomy). As a result, these agents have to 1) utilize their available resources to track targets (individually or as an alliance) that appears within their coverage area, and 2) share these resources and information pertinent to target tracking with other agents during negotiation sessions. The 3 main resources that make-up this system are: 9.3GHz Doppler *Moving Target Indication* MTI sensors, which communicate using 900MHz wireless RF transmitters over 8 channels (at any time-scan, one of three 120° swath sectors is available to each sensor); a network of CPU platforms, upon which sensor-controlling agents

reside; and the "tracker" - the software that calculates a probable location and velocity of the target.

The agents within this system are reflective (they are conscious of the availability of their resources and the effect of their actions on these resources) and perform negotiation through a bottom-up approach of solution creation. In addition, they execute *Case-Based Reasoning* (CBR) thus allowing their negotiation to adapt to the changing environment.

Hegazy et al. [28] present another system whose agents operate within a distributed scheme. The system contains mobile agents that must detect and track the movement of targets that enter the surveillance region (each target is assigned a value that determines its importance). Whenever an agent detects a target, it must interact (through broadcasting) with its neighboring agents to find out if the detected target is currently or was under surveillance; it then makes a decision on whether or not to track this object, based on the response it gets.

Another system designed and presented by Bererton et al. in [29] implements a distributed collaboration scheme. The robots within this system (called CMU Milli-bots) are constructed at the 5-10cm scale so as to allow them accessibility to tight areas. In addition each robot is equipped with customized modules based on the robots tasks (there are three modules: sensing, processing and mobility). As such, one robot might be equipped with a mobility module suited for coarse terrain, while another could be equipped with one suited for flat terrain. If desired, this would allow the system to partially incorporate the hierarchical collaboration scheme (where one robot can be equipped with a more powerful processor module that supervises the operations of a group of sensors). One very unique feature about this system is the ability of each robot to sense/detect objects in a variety of ways: in other words, each sensor can be mounted with multiple types of sensors such as an infrared proximity sensor, a sonar or a video camera. This is useful when an object positioned at a certain angle cannot be detected by a particular sensor (such as a sonar), but can be detected by another type of sensor (such as an infrared sensor). In addition, although information from a sonar sensor, for example, can be used to generate a 2D description of the environment, it is not sufficient enough to identify or distinguish between objects. So another sensor would need to be used at the same time.

Similarly, research has been conducted in the area of space exploration: more specifically, exploring small bodies like asteroids and meteors. As explained by Udomkesmalee et al. [30], exploring such bodies will require small, low-cost spacecraft with autonomous landing capabilities, and due to the uncertainty of the surface of these bodies, remotely controlling this spacecraft from the earth will be impractical and ineffective. As a result, such spacecraft must contain autonomous agents, which will be responsible for landing the spacecraft safely. The autonomous design proposed by the authors utilizes The Gabor Filters [17] to identify planetary features, calculates the location of theses and then determines the right place to land the spacecraft (based on these locations).

Distributed scheme consist of agents that possess the ability to operate independently. As a result, such agents should have a reliable communication scheme that will enable them to interact with other agents within their network. This section presents various schemes that have been developed.

Kay et al. [31] give a very good example. Their system, which is called the ATL (Advanced Technology Laboratories) Postmaster System, is placed on every machine that an agent could visit and it coordinates the collaboration and information dissemination between the agent and the computer. This system was designed with the intent of reducing the costs acquired by the agents (such as duplicate requests sent to a particular server and duplicate data transmitted across low-bandwidth lines). There are three main features about the ATL Postmaster system, explained below:

ATL Postmaster systems are able to automatically deliver data to the agent's system (i.e., the system that placed the request) as specified by the agents, either periodically (updated or not) or as the updated versions are available;

Since agents check-in with the Postmaster before and after working at a machine, the Postmaster is able to modify the agent's itinerary, such as redirecting the agent to another machine where the information needed by the current agent is already cached (cheaper services) or piggyback data on the agent if headed in the right direction (cheaper communication).

A Postmaster can act as a middleman in the sense of storing information to be used by other agents or relaying information to other Postmasters from agents.

In addition, the Postmaster system is written in the Java language and is designed in a general way such that it could be applied to a variety of agents.

In [32], Johnson presents another algorithm that discovers and maintains a communication route between two mobile agents; such an algorithm is designed to be used within an ad hoc network, e.g., amongst a collection of research scientists who have gathered in a hotel ballroom and wish to communicate with each other through PDAs (Personal Digital Assistant). If the source and receiving agents are within transmission range of each other, then discovering/setting up a route is a matter of transmitting requests and acknowledgments. On the other hand, if the receiving agent is not within transmitting range, then the source agent will broadcast this request to its neighboring agents. As each agent receives this request, it tags on its address to the request and then broadcasts it to its neighboring agents, until the receiving agent receives the request. The inclusion of the address serves two purposes: a) the route is specified, and b) the request is prevented from being broadcast twice by any agent. Upon receiving the request package, the target agent will return this route information back to the sender, using a similar method of broadcasting and address appending. In terms of route maintenance, an intermediate agent (or router) may request a confirmation from the next hop; if this is not received within a certain period of time, it can be assumed by the agent that the hop is faulty or has moved outside the transmission range. This agent can either inform the source agent about the situation (in order for the source agent to discover


another route) or the intermediate agent can discover another route that will originate from itself.

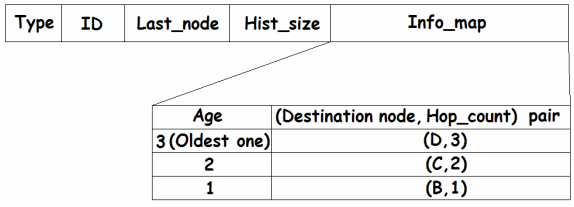

Figure 13. Structure of a Routing Agent in MAR.

Another type of communication protocol implemented within a distributed scheme is introduced by Zhou et al. [33]. This protocol (known as MAR – Mobile Agent Routing) employs mobile agents - packets that travel the network and collect routing information - in order to make this information available to every node within the network. More specifically, when these packets visit nodes, they update the node's routing table with information about other nodes and retrieve information from this table, which was left by other packets. The structure of each packet is shown in Figure 13 and a description of each part of the packet is given as follows:
Type: differentiates the mobile agents from other packets,
ID: differentiates each agent from the other;
Last_node: stores the most recent node visited;
Hist_size: defines the size of Info_map;
Info_map: stores all gathered routing information; and
Age: records the sequence of nodes visited.
With the information stored within the routing table, each node would be able to determine what route to take in order to get data to a certain destination. In addition, Chen and Gerla [34] and [35] present another routing scheme with a design that has the routing accuracy of the Link State scheme [32] and the dissemination method of the *Distributed Bellman-Ford* (DBF) scheme [31]. This new scheme, called Global State Routing, consists of an ad-hoc network that is modeled as an undirected graph G = (V, E), with V as a set of nodes and E as the undirected links connecting each node within V. A list and three tables are maintained for each node i – a neighbor list A_i, a *Topology Table* TT_i, a next hop table $NEXT_i$ and a distance table D_i. In addition, TT_i contains entries for each destination node j; $TT_i.LS(j)$, the link state information reported by node j, and $TT_i.SEQ(j)$, the timestamp indicating the time node j generated the link state information. Lastly, a weight function ($E \rightarrow Z_0^+$) is used to determine the distance of a link. Each node i considers its neighbors to be the nodes whose routing message packets are placed in its inbox queue. It updates its routing information (with the packets received) by comparing the sequence number of the packets received with those locally stored. It then rebuilds its routing table with this new information. This up-to-date information is then disseminated only to the neighboring nodes of node i, rather than flooding the entire network.
Leu et al. [22] investigate mobile agent communication issues and propose a distributed sendbox approach based on a Session Initiation Protocol (SIP) as the signaling protocol, which offers two modes: a) a direct mode used when the receiving agent is stationary, and b) a forward mode used when the receiving agent is moving. Both modes are illustrated in Figures 14 and 15.

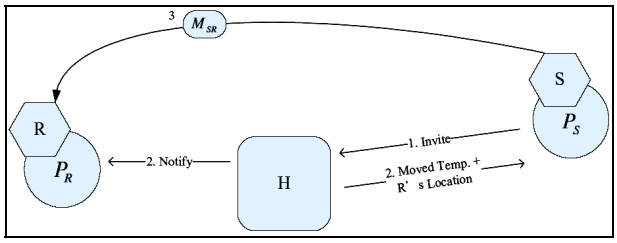

Figure 14. Direct Mode of the Distributed Sendbox. Here, the location of the receiving agent (R) is identified (via a central station – H).

In addition, a prototype was developed and the results of the experiments conducted followed their prediction, and at the same time illustrated the variation of communication time and utilization rates under different receiver's moving frequencies.

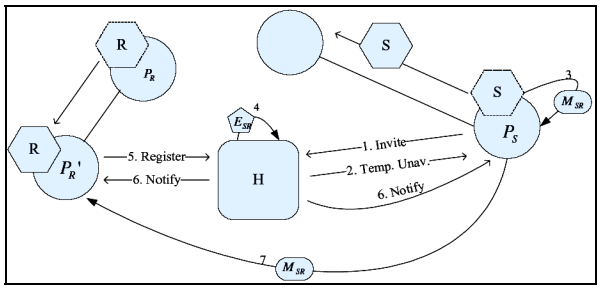

Figure 15. Forward Mode of the Distributed Sendbox Scheme. Here, the sending agent (S) buffers the message intended for the receiving agent (R) that is currently in motion.

The selection of centralized vs. distributed architecture depends upon a number of factors, including the number of restraint devices, controller throughput requirements, package size, system cost and assembly considerations. In relatively simple mechanizations involving a small number of restraint devices and limited sensing and processing requirements, the centralized architecture may offer cost and assembly advantages. In relatively complex mechanizations involving a large number of restraint devices and sophisticated sensing and processing requirements, the distributed architecture may offer packaging and processing advantages.

6. Conclusion

Recent developments in surveillance systems have been presented in this paper. Such systems have the following capabilities (but are not limited to them): (1) strategically integrate information from several sources to make accurate surveillance decisions; (2) optimize the location of sensors to achieve complete coverage of the desired area; (3) efficiently use the resources of the system, and (4) reliably communicate in real-time in the midst of harsh environmental conditions and/or changes in the system. Various methods and techniques (including Evolutionary Algorithm) have been utilized to accomplish the above-mentioned capabilities of surveillance systems through the use of intelligent agents (which usually are autonomous devices that posses sensory and processing components). In addition, various

information communicating/processing techniques have been presented, with the main focus on a distributed communication scheme.

7. REFERENCES

[1] Owen, M. W., Klamer, D. M. and Dean, B. (2001) "*Evolutionary Control of an Autonomous Field*", white paper by the SPAWAR System Center San Diego and Oricon Corporation.

[2] Mainwaring A., Polastre J., Szewczyk R., Culler D., and Anderson J. (2002) "Wireless Sensor Networks for Habitat Monitoring", In *International Workshop on Wireless Sensor Networks and Applications*.

[3] Coleri S., Cheung S. Y., and Varaiya P. (2004) "Sensor Networks for Monitoring Traffic", In *Allerton Conference on Communication, Control and Computing*, 2004.

[4] Sandhu J., Agogino A. (2004) "Wireless Sensor Networks for Commercial Lighting Control: Decision Making with Multi-agent Systems", In *AAAI Workshop on Sensor Networks.*

[5] UCC SugarCube Website. http://www.nmrc.ie/research/mai-group.

[6] Nareyek, A., (2001) "*Reactive Agents*", EXCALIBUR: Adaptive Constraint-Based Agents in Artificial Agents, http://www.ai-center.com, 19 May 2001.

[7] Lakshmikumar, A., "*Reactive Agents*", http://zen.ece.ohiou.edu/~robocup, 17 February 2001.

[8] Tecuci, G. (1998) "*Building Intelligent Agents: An Apprenticeship Multistrategy Learning Theory, Methology, Tool and Case Studies*", Academic Press, San Diego, CA.

[9] Odell, J., (2002) "*Agents and Beyond: A Flock is not a Bird*", Distributed Computing, April.

[10] Giampapa J., Paoluc M., Sycara K., (2000) "Agent interoperation across multi agent system boundaries", *4th International Conference on Autonomous Agents*, June.

[11] Diehl, C. P., Saptharishi, M., Hampshire II, J. B. and Khosla, P. K. (1999) "Collaborative Surveillance using both Fixed and Mobile Unattended Ground Sensor Platforms", *AeroSense '99: SPIE's 13th Annual International Symposium on Aerospace/Defense Sensing Simulation and Controls, Orlando, FL*.

[12] Orwell, J., Massey, S., Remagnino, P., Greenhill, D. and Jones, G. A. (1999) "A Multi-Agent Framework for Visual Surveillance", *IAPR International Conference on Image Analysis and Processing, Venice*, 1104-1107.

[13] Piaggio, M. and Zaccaria, R. (1996) "Autonomous Navigation Based on a Dynamic World Representation", *2nd IEEE International Conference on Engineering of Complex Computer Systems, Montreal, Canada,* 152.

[14] Gesù, V. D., Lenzitti, B., Bosco, G. L. and Tegolo, D. (2000) "A Distributed Architecture for Autonomous Navigation of Robots", *Proceedings of the 5th IEEE International Workshop on Computer Architectures for Machine Perception*.

[15] Mabey, G. W. and Gunther, J. (2003) "A Robust Motion-Estimation Algorithm for Multiple-Target Tracking at close Proximity Based on Hexagonal Partitioning", *Proceedings of the IEEE Conference on Advanced Video and Signal Based Surveillance, Miami, Florida*, 107 – 112.

[16] Buczak, A. L., Jin, Y., Darabi, H. and Jafari, M. A. (1999) "Genetic Algorithm Based Sensor Network Optimization for Target Tracking", *Intelligent Engineering Systems through Artificial Neural Networks, ASME Press, New York*, 9, 349-354.

[17] Sekhar, A. Manoj, B.S. Siva, C. Murthy, R., (2005) **"**Dynamic Coverage Maintenance Algorithms for Sensor Networks with Limited Mobility", 3rd *IEEE International Conference on Pervasive Computing and Communications*, 51- 60.

[18] Megerian, S., Koushanfar, F., Potkonjak, M., Srivastava, M.B., (2005) "Worst and Best-Case Coverage in Sensor Networks," *IEEE Transactions on Mobile Computing*, vol. 4, no. 1, 84-92.

[19] Buczak, A. L., Wang, H. H., Darabi, H. and Jafari, M. A. (2001) "Genetic algorithm convergence study for sensor network optimization", Information Sciences, 133, (3-4), 267-282.

[20] Burne, R., Buczak, A., Jin, Y., Jamalabad, V., Kadar, I. and Eadan, E. (1999) "A Self-organizing, Cooperative Sensor network for Remote Surveillance: Current Results", *SPIE Proceedings, Unattended Ground Sensor Technologies and Applications*, 3713, 238-248.

[21] Ganeriwal, S., Kumar, R., Srivastava, M., (2001) "Timing-sync protocol for sensor networks", Conference On Embedded Networked Sensor Systems, 138-149**.**

[22] Liu, J., Jafari, M. A. and Buczak, A. L., (2004) "Merging Redundant Sensors in Precision Tracking", http://coewww.rutgers.edu/ie/research/working_paper.html

[23] Horling, B., Vincent, R., Mailler, R., Shen, J., Becker, R. Rawlins, K. and Lesser, V. (2001) "SPT: Distributed Sensor Network for Real-Time Tracking", *The 5th International Conference on Autonomous Agents, Montreal, Canada*.

[24] Lazar, S. Weerakoon, I. and Sidhu, D. (1998) "A Scalable Location Tracking and Message Delivery Scheme for Mobile Agents", *Proceedings of the 7th Workshop on Enabling Technologies: Infrastructure for Collaborative Enterprises*, 243-249.

[25] Jung, B. and Sukhatme, G. S. (2002) "A Region-based Approach for Cooperating Multi-Target Tracking in a Structured Environment", *2002 IEEE/RSJ International Conference on Intelligent Robots and Systems, EPFL, Switzerland,* 2764-2769.

[26] Feller, S. D. Zheng, Y. Cull, E. and Brady, D. J. (2002) "Tracking and Imaging Humans on Heterogeneous Infrared sensor Array for Law Enforcements Applications", *Proceedings of SPIE AeroSense, Orlando, Florida*, 4708, 212 – 221.

[27] Soh, L. and Tsatsoulis, C. (2001) "Reflective Negotiating Agents for Real-Time Multi-sensor Target Tracking", *International Journal Conference on Artificial Intelligence, Seattle, Washington*, 1121-1127.

[28] Hegazy, T. and Vachtsevanos, G. (2004) "Dynamic Agent Deployment for Tracking Moving Targets", *12th Mediterranean Conference on Control and Automation (MED'04), Kusadasi, Aydin, Turkey*.

[29] Bererton, C., Navarro-Serment, L. Grabowski, R. Paredis, C. and Khosla, P. (2000) "Millibots: Small Distributed Robots for Surveillance and Mapping", *Proceedings of the Government Microcircuit Applications Conference 2000, Orlando, Florida.*

[30] Udomkesmalee, S., Lin, C., Politopoulos, A., Hu, G. and Huntsberger, T. (2003) "Autonomous Target Tracking for Asteroid Landing", *The Fourth International Conference on Control and Automation, Montreal, Canada.*

[31] Kay, J., Etzl, J., Rao, G. and Thies, J. (1998) "The ATL Postmaster: A System for Agent Collaboration and Information Dissemination", *Proceedings of the Second International Conference on Autonomous Agents, Minneapolis, Minnesota,* 338-342, 1998.

[32] Johnson, D. B. (1994) "Routing in Ad Hoc Networks of Mobile Hosts", *Proceedings of the IEEE Workshop on Mobile Computing Systems and Applications*.

[33] Zhou, Y. and Zincir-Heywood, A. N. (2004) "Intelligent Agents for Routing on Mobile Ad-Hoc Networks", *Proceedings of the Second Annual Conference on Communication Networks and Services Research, Fredericton, N.B., Canada*, 249-254.

[34] Chen, T. and Gerla, M. (1998) "Global State Routing: A New Routing Scheme for Ad-Hoc Wireless Networks", *Proceedings of IEEE International Conference on Communications, Atlanta, Georgia*, 171-175.

[35] Chen, T. and Gerla, M. (1998) "The New Routing Algorithm for the ARPANET", *IEEE Transactions International Conference on Communications, Atlanta, Georgia*, 171-175.

Yaser M.A. Khalifa received his BSc degree from Alexandria University, Egypt, and his PhD from Cardiff University of Wales, UK, in 1992 and 1997 respectively. He is currently with the Dept. of Electrical and Computer Engineering at the State University of New York (SUNY) at New Paltz, USA.

Ehi Okoene received his BSc and MSc. Degrees in Electrical Engineering from the State University of New York at New Paltz, in 2002 and 2004 respectively.

Mohamed Basel Al-Mourad received his BSc in Informatics Engineering, from Aleppo University, Syria, and his PhD from Cardiff University of Wales, UK. Dr. Al-Mourad is currently with the Department of Information Systems at Wolverhampton University, UK.

www.icgst.com

State and Fault Parameter Estimation Applied To Three-Tank Bench Mark Relying On Augmented State Kalman Filter

S.Abraham Lincon[1] D.Sivakumar[1] J.Prakash[2]
[1.] *Department of Electronics and Instrumentation Engg, Annamalai University, Annamalai Nagar,,INDIA*
[2.] *Department of Instrumentation Engg, MIT Campus, AnnaUniversity, Chennai, INDIA.*
linsun_2k5@yahoo.co.in, dsk2k5@gmail.com

Abstract
Fault detection and diagnosis (FDD) can be described as early determination (detection) and localization (diagnosis) of faulty elements in a dynamic system. In this paper, a model based approach to detect and diagnose abrupt and slowly varying faults in a three-tank benchmark system is developed. The Fault detection and diagnosis scheme is formulated as a state estimation problem by considering the fault parameter as an additional state. It is then solved as a simultaneous state and fault parameter estimation using Augmented State Kalman Filter (ASKF) and Two Stage Kalman Filter (TSKF). Extensive simulation studies performed on three tank bench mark system reveal that the FDD scheme is capable of generating reasonably accurate state and fault parameter estimates in the presence of process and measurement noises. This holds good for different types of faults. Further the performance of ASKF is compared with that of TSKF.

Keywords: *Augmented State Kalman Filter(ASKF),Two Stage Kalman Filter (TSKF),Fault Detection and Diagnosis (FDD),Three-Tank System.*

1. Introduction
Fault detection and diagnosis for dynamic systems has gained more attention in the recent years mainly due to an increasing demand for better performance as well as higher safety and reliability standards (Isermann, [1] Basseville, [2] Frank, [3] Gertler,[4] Patton,[5]). Faults can occur either in the main processing equipments (leak in tanks, variation in process parameters like heat transfer coefficient etc.) or in the auxiliary equipments (bias/drift in sensors, actuators, controller outputs, stuck actuators and sensors). Faults such as stuck sensors and stuck actuators are classified as hard faults. In principle such faults occur less frequently and it is comparatively easy to detect using low and high alarm thresholds. On the other hand small biases in sensors, actuators and controller outputs are considered as soft faults and are not that much easy to detect.
This paper is focused on detection and diagnosis of soft faults only. FDD methods can be broadly classified into model based methods and model free methods. Model free methods do not use mathematical model of the process, whereas model based methods make use of mathematical model of the process either in state space or in input-output form. The model based methods can be further classified as state estimation approach, and parameter estimation approach. State estimation provide reliable information on process state variables, they are classified in to linear state estimation, nonlinear state estimation and parameter estimation. Luenberger observer [6] is used for state estimation of deterministic linear dynamic systems. Extended Luenberger observer is the straight forward extension of Luenberger observer to nonlinear system. The parameter estimation method has significant engineering importance, because in many real world problems accurate values of physical system parameters are not known a priori for use in tasks such as control, monitoring or fault diagnosis. In fault diagnosis its application is to detect the onset of fault and to estimate the parameter drifts and/or abrupt changes in system parameters. Parameter estimation problem can be formulated as state estimation problem by considering the fault parameter of interest as additional state.
Normally, the FDD task could be realized in two steps: (i) Residual generation (ii) Residual evaluation. Residual generation is the construction of signals that are accentuated by the changes in the parameters (faults). Residual evaluation is the decision and isolation of the occurrence of the changes in parameters (faults). In an ideal case, a residual generated will be zero if no faults are present, different from zero when fault is present Observer based approaches to fault detection are model dependent. Depending on the nature of the models used in the observer, they are classified.
Luenberger observer (Luenberger [6]) uses the linear state space model of the system and it is used for state estimation of deterministic linear dynamic systems. A Fuzzy observer (Efran Alcorta [7]) uses the Takagi-Sugeno Fuzzy model of the system. A Neural observer (T.Marcu [8]) uses the ANN model of the system and a bilinear observer (L.EL.Bahir [9]) uses the bilinear system model. A non-linear observer uses the original non-linear equation of the system. Three Kalman Filters are run in parallel to estimate the angular velocity in

Gyroless Spacecraft [10].

In Kalman filter approach, state estimates are obtained using two distinct steps, a one step ahead prediction is obtained based on the latest state estimate and in the second step the state estimate is refined by linearly combining the state prediction obtained in the first step with a new output measurement.

Traditional Kalman filter has been widely used only for state estimation of linear stochastic systems. In order to generate state estimates fault parameter estimates in the presence of fault and plant model mismatch, the state vector has been augmented with fault parameter as an additional state, accordingly the system matrices are augmented resulting which is an Augmented State Kalman Filter (ASKF) and solved as simultaneous state and fault parameter estimation problem. However this approach can lead to unacceptably large computational burden and numerical inaccuracy. To overcome the above difficulties, Friedland,[11], has shown that optimum state estimates can be expressed as output of the bias free filter based on non existence of the bias, corrected with output of the bias filter. This algorithm is called Two Stage Kalman Filter (TSKF). R.J. Patton,[5] has regarded three tank water process as a valuable experimental setup for investigating multivariable feed back control as well as fault diagnosis. For identifying components, sensor and actuator faults in three tank bench mark system various fault diagnosis schemes such as Neural observer[8], Generalized Likelihood Ratio based FDI[9], Fuzzy observer [7], Multiple model based approach[12], Non-linear observer[13] have been demonstrated.

The existing FDD schemes are capable of handling only single fault (either component or sensor or actuator). If multiple faults occur simultaneously these methods cannot work satisfactorily. Further they are working in the principle of residual generation and residual evaluation. Residual generation is finding the difference between process and model output. Residual evaluation is comparing the residual with threshold, and threshold is the difference between process output in the presence of noise and model output when no fault is present. Hence the existing methods cannot estimate the fault when their magnitude is less than noise present in the system. The proposed methods are capable of estimating the faults even their magnitude is very small as compared to the noise present in the system and the number of faults that can be estimated is equal to the number of estimated states. The paper is organized as follows: The fault detection and diagnosis scheme is described in section 2, the detailed simulation results are presented in section 3 and section 4 provides the conclusion drawn from the simulation results.

2. Fault Detection and Diagnosis Scheme

Let us assume that the process is described by the following linear time invariant state space model as,

$$X(k+1) = \Phi X(k) + \Gamma_u U(k) + \Gamma_w W(k) \quad (1)$$

$$Y(k) = CX(k) + V(k) \quad (2)$$

Where $X(k) \in R^n$ state vector, $U(k) \in R^m$ the known deterministic inputs and $y(k) \in R^r$ the measured outputs. W(k) and V(k) represents state and measurement noises. It is further assumed that W(k) and V(k) are zero mean normally distributed and mutually uncorrelated white noise sequences with covariances,

$$E[W_i(k) W_j(k)^T] = Q \delta_{ij}$$

$$E[V_i(k) V_j(k)^T] = R \delta_{ij} \quad \text{with } Q \geq 0; R \geq 0$$

Where δ_{ij} is the Kronecker delta and E denotes the expectation operator. The linear time-invariant matrices Φ, Γ_u, Γ_w and C are obtained from the first principles model of the process after performing linearization and discretization operations. In the absence of fault, the process evolves as given in equations (1) and (2).

A fault f(k) due to step change in process parameter, or actuator bias is modeled using the following state evolution equation,

$$X(k+1) = \Phi X(k) + \Gamma_u U(k) + \Gamma_w W(k) + \Gamma_f e_{f,i} f(k) \quad (3)$$

Where Γ_f represents coupling matrix and $e_{f,i}$ is a unit vector indicating the index of the variable. The matrix Γ_f for different faults are obtained from first principle models.

A fault due to sensor bias(Γ_s) is modeled by modifying the measurement equation (2)

$$Y(k) = CX(k) + V(k) + \Gamma_s e_{f,i} f(k) \quad (4)$$

In the presence of fault the process evolves according to equations (3) and (4). It is also assumed that the process evolves according to an augmented state space model after combining equations (3) and (4) as follows:

$$X(k+1) = \Phi X(k) + \Gamma_u U(k) + \Gamma_w W(k) + \Gamma_f f(k) \quad (5)$$

$$f(k+1) = f(k) \quad (6)$$

$$Y(k) = CX(k) + V(k) + \Gamma_s f(k) \quad (7)$$

Defining an augmented state vector as

$$X_a(k) = \begin{bmatrix} X(k) \\ f(k) \end{bmatrix}$$

Equations (5), (6), and (7) can be rewritten as

$$X_a(k+1) = \Phi_a X_a(k) + \Gamma_{ua} U(k) + \Gamma_{wa} W_a(k) \quad (8)$$

$$Y(k) = C_a X_a(k) + V(k) \quad (9)$$

From these equations,

$$\Phi_a = \begin{bmatrix} \Phi & \Gamma_f \\ 0 & I \end{bmatrix} \qquad \Gamma_{ua} = \begin{bmatrix} \Gamma_U \\ 0 \end{bmatrix}$$

$$\Gamma_{wa} = \begin{bmatrix} \Gamma_w \\ 0 \end{bmatrix} \qquad C_a = [C \quad \Gamma_s]$$

The initial states X(0) and f(0) are Gaussian random variables with

$$E\{X(0)\} = \bar{X}(0), \; E\{f(0)\} = \bar{f}(0),$$

$$E\{(X(0) - \bar{X}(0))(X(0) - \bar{X}(0))^T\} = P^x(0)$$

$E\{(f(0) - \bar{f}(0))(f(0) - \bar{f}(0))^T\} = P^f(0) > 0$

The specific values of Γ_f and Γ_s in the augmented state space model for each type of fault under consideration are as follows:

(i).For Sensor bias:

$\Gamma_f = 0$ & $\Gamma_s = I$ and

(ii).For Actuator bias:

$\Gamma_f = \Gamma_u e_{ui}$ & $\Gamma_s = 0$

2.1 Augmented State Kalman Filter

The maximum likelihood estimates of the augmented states are generated using Augmented State Kalman Filter.

One step ahead prediction of state estimates and fault parameter estimation $\hat{X}_a(k+1/k)$ is given by

$$\hat{X}_a(k+1/k) = \Phi_a \hat{X}_a(k/k) + \Gamma_{ua} U(k) \quad (10)$$

One step ahead measurement prediction $\hat{Y}(k+1/k)$ is given by

$$\hat{Y}(k+1/k) = C_a \hat{X}_a(k+1/k) \quad (11)$$

One step ahead prediction of error covariance $P_a(k+1/k)$ is given by

$$\begin{bmatrix} P^X \\ P^f \end{bmatrix} = P_a(k+1/k) = \Phi_a P_a(k/k) \Phi_a^T + \Gamma_{wa} Q_a \Gamma_{wa}^T \quad (12)$$

The Kalman gain $K_a(k+1)$ is given by

$$K_a(k+1) = \Phi_a P_a(k+1/k) C_a^T [C_a P_a(k+1/k) C_a^T + R]^{-1} \quad (13)$$

The updated state estimates and parameter estimator $\hat{X}_a(k+1/k+1)$ are given by

$$\hat{X}_a(k+1/k+1) = \hat{X}_a(k+1/k) + K_a(k+1)[Y(k+1) - \hat{Y}(k+1/k)] \quad (14)$$

Error covariance update $P_a(k+1/k+1)$ is given by

$$P_a(k+1/k+1) = [I - K_a(k+1) C_a] P_a(k+1/k) \quad (15)$$

Where $P_a(0/0) = Q_a = \begin{bmatrix} P^X(0) & 0 \\ 0 & P^f(0) \end{bmatrix}$

2.2 Two Stage Kalman Filter

The algorithm for estimating the state X in the presence of bias f is explained as follows:

State Estimator

One step ahead bias free state estimate $\hat{X}(k+1/k)$ is given by

$$\hat{X}(k+1/k) = \Phi X^1(k/k) + \Gamma_u U(k) \quad (16)$$

One step ahead measurement $\hat{Y}(k+1/k)$ is given by

$$\hat{Y}(k+1/k) = C \hat{X}(k+1/k) \quad (17)$$

Estimate of a priori state covariance $P^X(k+1)$ is given by

$$P^X(k+1) = \Phi T^x(k) \Phi^T + \Gamma_w Q \Gamma_w^T \quad (18)$$

The estimate of state Kalman gain $K^x(k+1)$ is given by

$$K^x(k+1) = P^X(k+1) C^T [C P^X(k+1) C^T + R]^{-1} \quad (19)$$

The update of a posteriori state covariance matrix $T^X(k+1)$ is given by

$$T^X(k+1) = [I - K^x(k+1)C] P^X(k+1) \quad (20)$$

The estimate of residual r(k+1) is given by

$$r(k+1) = Y(k+1) - \hat{Y}(k+1/k) \quad (21)$$

Compute the bias Free State estimate $X^1(k+1/k+1)$

$$X^1(k+1/k+1) = \hat{X}(k+1/k) + K^x(k+1) r(k+1) \quad (22)$$

Bias estimator

Bias transformation matrix $U^x(k+1)$ is calculated as

$$U^x(k+1) = \Phi V(k) + \Gamma_f \quad (23)$$

The sensor bias transformation matrix S(k+1) is calculated as

$$S(k+1) = C U^x(k+1) + \Gamma_s \quad (24)$$

Compute V(k+1) matrix from the relation

$$V(k+1) = U^x(k+1) - K^x(k+1) S(k+1) \quad (25)$$

The bias covariance M(k+2) is calculated as

$$M(k+2) = M(k+1) - M(k+1) S^T(k+1) [C P^X(k+1) C^T + R + S(k+1) M(k+1) S^T(k+1)]^{-1} S(k+1) M(k+1) \quad (26)$$

The Kalman gain for bias $K^f(k+1)$

$$K^f(k+1) = M(k+2) [V^T(k+1) C^T + \Gamma_s^T] R^{-1} \quad (27)$$

The estimate of Bias parameter $\hat{F}(k+1/k+1)$ is given by

$$\hat{F}(k+1/k+1) = [I - K^f(k+1) S(k+1)] \hat{F}(k/k) + K^f(k+1) r(k+1) \quad (28)$$

Estimate of Bias correction factor $\delta(k+1)$ is given by

$$\delta(k+1) = V(k+1) \hat{F}(k+1) \quad (29)$$

The Estimate of State is $\hat{X}(k+1/k+1)$ is given by

$$\hat{X}(k+1/k+1) = X^1(k+1/k+1) + \delta(k+1) \quad (30)$$

The initial parameters of the filter are given by

$$P(0) = M(0) = Q \qquad U^x(0/0) = 0$$

3.1 Description of Three-tank benchmark system

The mathematical model of a three-tank benchmark problem is considered for simulation studies for validating the performance of TSKF and ASKF. The three-tank system shown in figure.1 composed of three identical tanks with identical area of cross section. The tanks are coupled by two inter connecting pipes; the normal outflow is located at tank 3. The measured variables are levels of first tank (h1), second tank (h2) and third tank (h3) respectively. Inflow of first tank (fin1) and third tank (fin3) are chosen as known inputs. The material balance for the three tank system yields the following equations.

$$\frac{dh1}{dt} = \frac{fin1}{A_T} - \frac{C1Sp\sqrt{2g(h1 - h2)}}{A_T} \quad (31)$$

$$\frac{dh2}{dt} = \frac{C1Sp\sqrt{2g(h1-h2)}}{A_T} - \frac{C2Sp\sqrt{2g(h2-h3)}}{A_T} \quad (32)$$

$$\frac{dh3}{dt} = \frac{fin3}{A_T} + \frac{C2Sp\sqrt{2g(h2-h3)}}{A_T} - \frac{C3Sp\sqrt{2gh3}}{A_T} \quad (33)$$

where $C1, C2, C3 \rightarrow$ constant flow coefficient
$Sp \rightarrow$ cross section of the connecting pipe
$g \rightarrow$ acceleration due to gravity (9.81 m/sec^2)
$A1=A2=A3=A_T \rightarrow$ Area of the tank

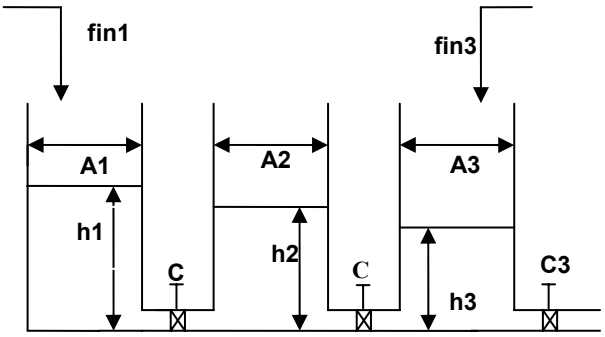

Figure1a. Schematic of Three -Tank Bench Mark System

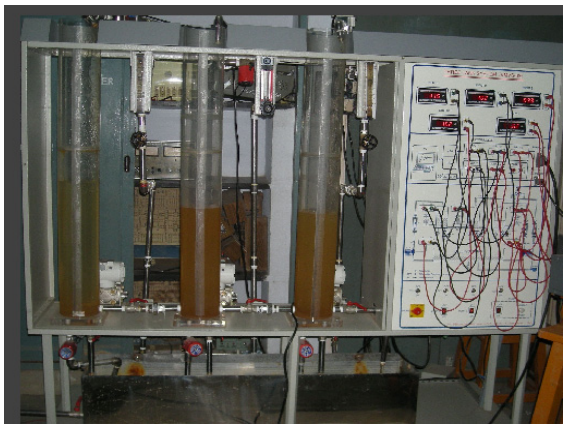

Figure1b. Three -Tank Bench Mark System

Table 1. Steady State Operating Data of the Three-Tank System

h1, h2, h3 (m)	0.5, 0.45, 0.4
fin1 and fin3 (ml/sec)	50
Area of the tank A_T (A1, A2, A3) (m^2)	0.0154
Constant Outflow Coefficients (C1, C2 ,C3)	1.0 ,0.8 ,1.0
Cross section of connecting pipe(Sp) (m^2)	5×10^{-5}

The system matrices corresponding to linear time invariant model (equations 1 and 2) are obtained by linearizing and discretizing the non linear differential equations (31, 32 and 33) around the nominal values shown in table 1 with sampling time $t_s = 15$ seconds then the system matrices become

$$\Phi = \begin{bmatrix} 0.68245 & 0.26315 & 0.051015 \\ 0.26315 & 0.51314 & 0.20226 \\ 0.051015 & 0.20226 & 0.61293 \end{bmatrix}$$

$$\Gamma_U = \begin{bmatrix} 797.11 & 19.284 \\ 156.74 & 122.16 \\ 19.284 & 762.11 \end{bmatrix} \qquad C = \begin{bmatrix} 1 & 0 & 0 \\ 0 & 1 & 0 \\ 0 & 0 & 1 \end{bmatrix}$$

3.2 Validation of FDD scheme on the three-tank system

The ASKF and TSKF based FDD schemes have been validated on the model of a three-tank benchmark system with identical noise covariance, initial state parameters for the following cases.

$$Q = \begin{bmatrix} (0.25e-6)^2 & 0 & 0 \\ 0 & 0 & 0 \\ 0 & 0 & (0.25e-6)^2 \end{bmatrix}$$

$$R = \begin{bmatrix} (8.36e-4)^2 & 0 & 0 \\ 0 & (7.08e-4)^2 & 0 \\ 0 & 0 & (5.09e-4)^2 \end{bmatrix}$$

$$\tilde{X}(0) = \begin{bmatrix} 0 \\ 0 \\ 0 \end{bmatrix} \qquad P(0) = Q$$

$$P_a(0/0) = Q_a = \begin{bmatrix} Q & 0 \\ 0 & 0 \end{bmatrix} \qquad \hat{X}_a(0/0) = \begin{bmatrix} 0 \\ 0 \\ 0 \\ 0 \end{bmatrix}$$

T = V = Zeros (3, 3) and M = Q

The measurement noise (1σ) is selected as 0.25% of normal height of the tanks. Process noise (1σ) is selected as 0.75% of nominal inflow to tanks 1 and 3 respectively.

3.3 Simulation Procedure

Simulation runs are performed using ASKF and TSKF algorithms for state and fault parameter estimation on the model of three-tank system linearized about the operating point 0.5m, 0.45m, 0.4m for tank1, tank2 and tank3 respectively. The performance of ASKF and TSKF are analyzed after deliberately introducing the fault for the following situations.

Case 1: The slowly varying actuator fault is applied as a ramp having zero initial value up to 500 sampling instants. The maximum of 0.75e-6 ml/sec (5σ) is reached at 1000th sampling instant after which it remains constant upto 5000th sampling instant.

Case 2: Multiple abrupt simultaneous sensor faults are step like faults having zero initial value up to 500 sampling instants and rise to a magnitude of 2.5e-2m (5σ) and 1.5e-2m (5σ) in sensor1 and sensor3 respectively. They remain constant up to 5000th sampling instant.

Case 3: Multiple abrupt sequential sensor faults are also step like faults having zero initial value and rise to a magnitude of 2.5e-2m(5σ) and 1.5e-2m(5σ) at 500th and 1000th sampling instants in sensor1 and sensor3 respectively. They remain constant up to 5000th sampling instant.

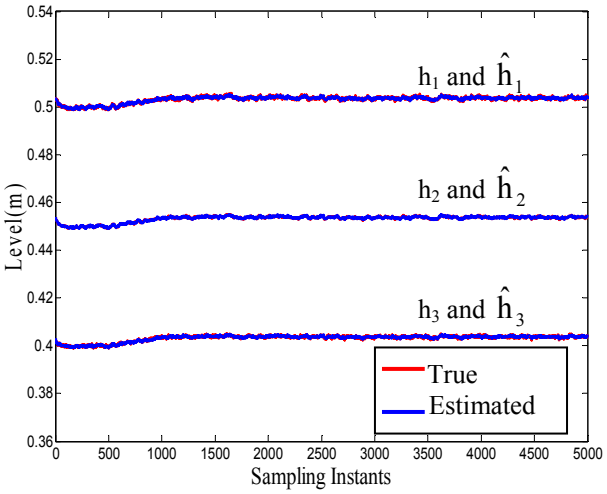

Figure 2a. Evolution of true and estimated levels in the presence of slowly varying actuator fault – ASKF.

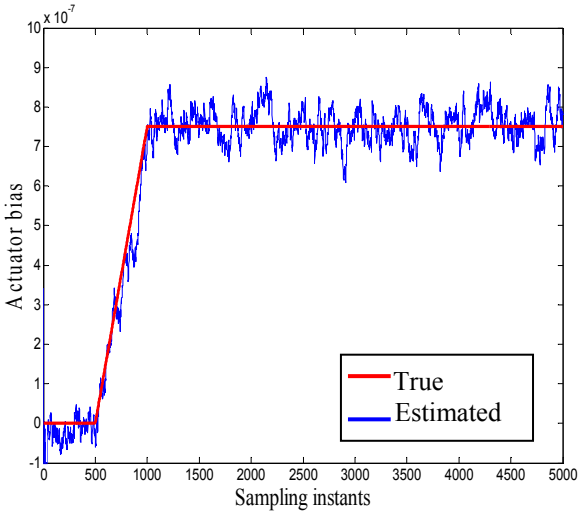

Figure 2b. Evolution of true and estimated slowly varying actuator fault (bias) – ASKF.

Figure 2a shows the evolution of true (h_1, h_2, h_3) and estimated ($\hat{h}_1$, $\hat{h}_2$, $\hat{h}_3$) heights of the tanks 1, 2 and 3 in the presence of slowly varying actuator bias. From the plots it is evident that the estimated states are reasonably accurate and they are unbiased. Figure 2b shows the evolution of true and estimated slowly varying fault in actuator3. From the Figure it is evident that the actuator bias estimate is reasonably accurate.

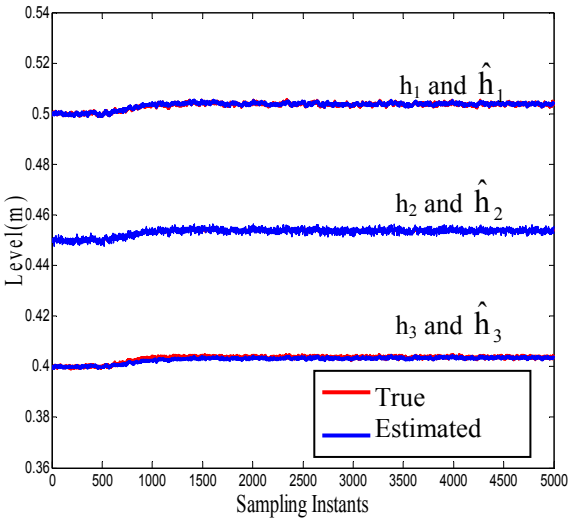

Figure 3a. Evolution of true and estimated levels for slowly varying actuator fault – TSKF.

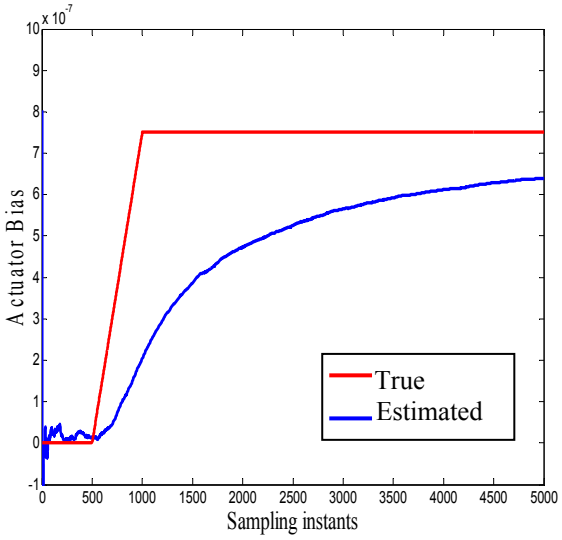

Figure 3b. Evolution of true and estimated slowly varying actuator fault (bias) – TSKF.

Figure 3a shows the evolution of true (h_1, h_2, h_3) and estimated ($\hat{h}_1$, $\hat{h}_2$, $\hat{h}_3$) heights of the tanks 1, 2 and 3 in the presence of slowly varying actuator bias, and the estimated states are reasonably accurate and they are unbiased. Figure 3b shows the evolution of true and estimated slowly varying fault in actuator3. The actuator fault is not properly estimated by the TSKF algorithm. Even up to 5000 sampling instants the true and estimated values are not converging and the estimate is biased.

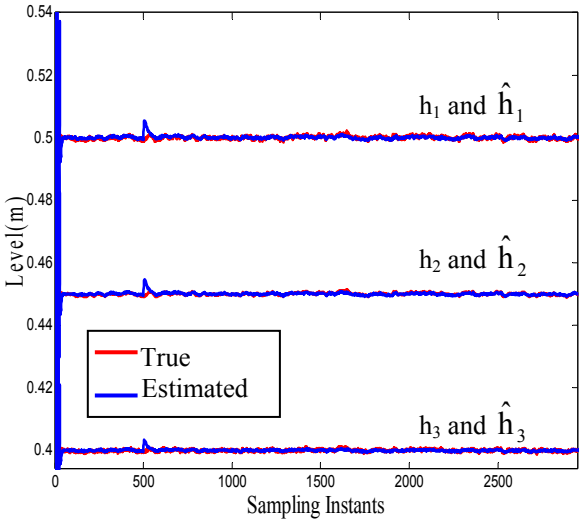

Figure 4a. Evolution of true and estimated levels in the presence of abrupt simultaneous sensor fault - ASKF.

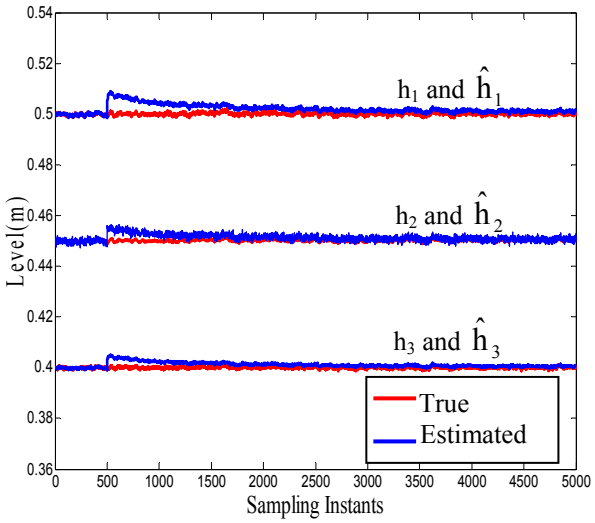

Figure 5a. Evolution of true and estimated levels in the presence of abrupt simultaneous sensor fault – TSKF.

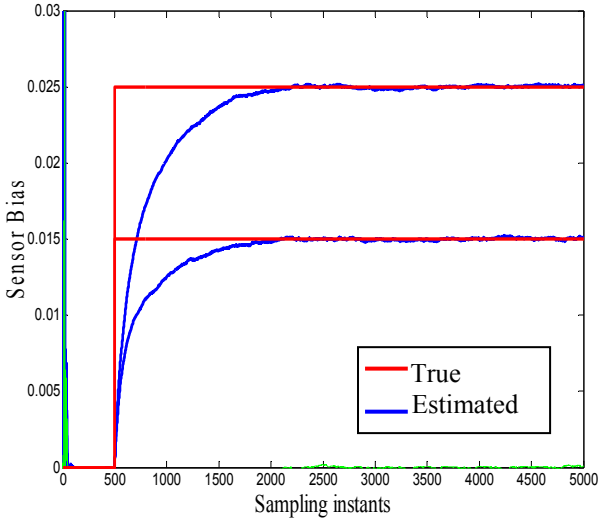

Figure 4b. Evolution of true and estimated abrupt Simultaneous sensor faults (bias) – ASKF.

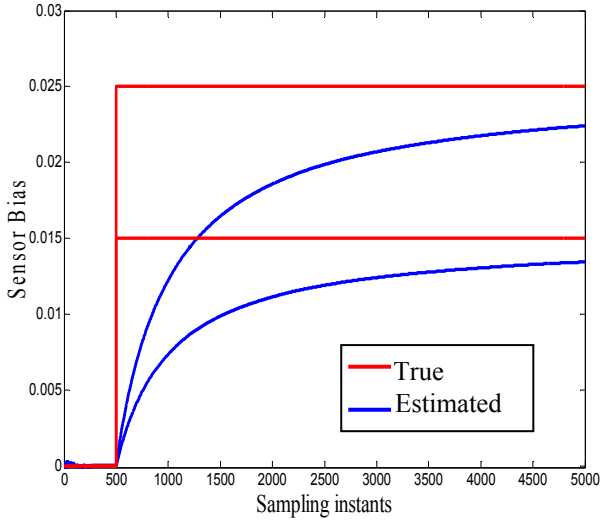

Figure 5b- Evolution of true and estimated abrupt Simultaneous sensor faults (bias) – TSKF.

Figure 4a presents the evolution of true (h_1, h_2, h_3) and estimated ($\hat{h}_1$, $\hat{h}_2$, $\hat{h}_3$) heights of the tanks 1, 2 and 3 in the presence of simultaneous abrupt faults in sensors 1 and 3. From the Figure it is to be observed that the estimated states are reasonably accurate and they are unbiased. The evolution of true and estimated simultaneous abrupt faults in sensors 1 and 3 indicated in Figure 4b. The figure depicts that the sensor biases are estimated accurately by the algorithm within 1500 sampling instances.

Figure 5a provides the evolution of true (h_1, h_2, h_3) and estimated ($\hat{h}_1$, $\hat{h}_2$, $\hat{h}_3$) heights of the tanks 1, 2 and 3 in the presence of simultaneous abrupt faults in sensors 1 and 3. The estimated states are reasonably accurate and they are unbiased. The evolution of true and estimated simultaneous abrupt faults in sensors 1 and 3 are shown in Figure 5b and the TSKF algorithm cannot estimate the fault magnitudes accurately. They are biased with offsets $0.2436e^{-2}$ and $0.1528e^{-2}$ even at 5000^{th} sampling instant.

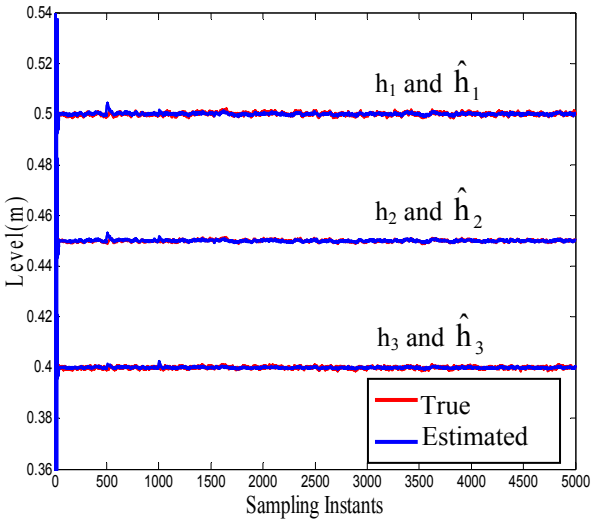

Figure 6a. Evolution of true and estimated levels in the presence of abrupt sequential sensor faults – ASKF.

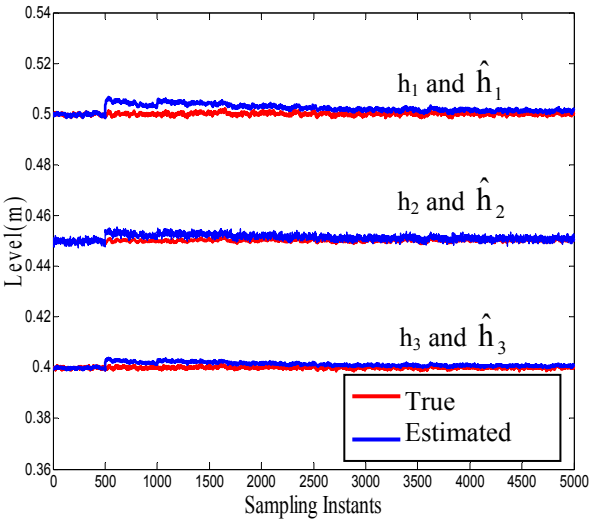

Figure 7a. Evolution of true and estimated levels in the presence of abrupt sequential sensor fault – TSKF.

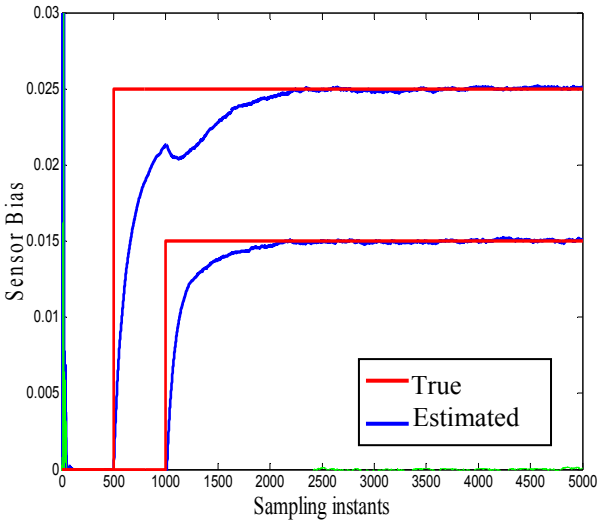

Figure 6b. Evolution of true and estimated abrupt Sequential sensor faults (bias) – ASKF.

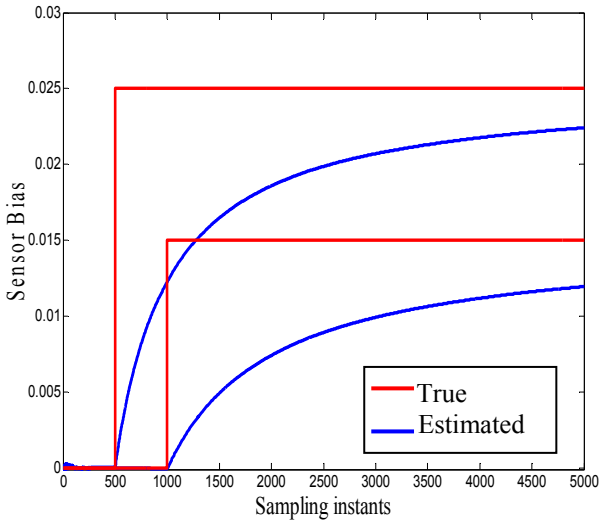

Figure 7b- Evolution of true and estimated abrupt Sequential sensor faults (bias) – TSKF.

Figure 6a shows the evolution of true (h_1, h_2, h_3) and estimated ($\hat{h}_1$, $\hat{h}_2$, $\hat{h}_3$) heights of the tanks 1, 2 and 3 in the presence of multiple abrupt sequential fault in sensors 1 and 3. The estimated states are reasonably accurate and they are unbiased. Figure 6b presents the evolution of true and estimated multiple abrupt faults in sensors 1 and 3 and the sensor biases are estimated accurately within 1500 sampling instances.

Figure 7a presents the evolution of true (h_1, h_2, h_3) and estimated ($\hat{h}_1$, $\hat{h}_2$, $\hat{h}_3$) heights of the tanks 1, 2 and 3 in the presence of multiple abrupt sequential faults in sensors 1 and 3. The estimated states are reasonably accurate and they are unbiased. Figure 7b shows the evolution of true and estimated multiple abrupt faults in sensors 1 and 3 and the algorithm cannot estimate the fault magnitudes accurately and they are biased with offsets $0.2536e^{-2}$ and $0.1528e^{-2}$ respectively even at 5000^{th} sampling instant.

3.4 Monte-Carlo simulation studies for performance Evaluation

The term Monte-Carlo simulation (MCS) means any simulation which utilizes random numbers in the simulation algorithm. Monte-Carlo simulation is also called as stochastic simulations. MCS is based on the use of random numbers and probability statistics to obtain an answer to scientific problems. Estimation does not provide a measure of uncertainty. Where as MCS allows to quantify the uncertainty in the response of several variable [14].MCS is the key technology to quantify uncertainty and consequences of making a mistake for optimal decision making.

Since the process simulations are carried out in the presence of process and measurement noises. The performance of the observer cannot be accessed based on single simulation trail because in real time the noises are random which may vary from time to time. In order to assure the accuracy of estimate ten different sets of random noise sequences using random numbers with different seed values are generated and all the simulation runs are conducted in the presence of ten different random noise sequences, for all above observer, for all type of faults namely slowly varying actuator fault, multiple abrupt simultaneous faults and multiple abrupt sequential faults. Considering the noise magnitude as 1σ the fault magnitudes are varied as 1σ, 3σ and 5σ for the state estimates. The mean $E[\hat{b}]$ and variance $\sigma[\hat{b}]$ of the fault magnitude estimates are computed for the last 100 sampling instants. The averaged values of mean and variance estimates of all trials in a run are presented in Tables 2, 3 and 4.

Table2. Mean and Variance of fault magnitude estimate (Single actuator fault)

Fault magnitude introduced	ASKF	TSKF
Actuator 1	Actuator1 $E[\hat{b}],(\sigma[\hat{b}])$	Actuator1 $E[\hat{b}],(\sigma[\hat{b}])$
1σ = 0.15e-6	1.6907e-7 (6.9753e-24)	1.2933e-7 (3.01523e-15)
3σ = 0.45e-6	4.6907e-7 (6.9753e-24)	3.8403e-7 (2.1599e-14)
5σ = 0.75e-6	7.6907e-7 (6.9753e-24)	6.3873e-7 (3.9821e-14)

Table3. Mean and Variance of fault magnitude estimate (Simultaneous and Sequential sensor faults)

Fault magnitude introduced		ASKF	
Sensor1	Sensor3	Sensor1 $E[\hat{b}],(\sigma[\hat{b}])$	Sensor3 $E[\hat{b}],(\sigma[\hat{b}])$
1σ=5e-3	1σ=3e-3	5.0658e-3 (7.6778e-18)	3.0577e-3 (1.1974e-17)
3σ=1.5e-2	3σ=9e-3	1.5065e-2 (7.2599e-18)	9.0576e-3 (1.1183e-17)
5σ=2.5e-2	5σ=1.5e-2	2.5065e-2 (7.6456e-18)	1.5057e-2 (1.0964e-17)

Table4. Mean and Variance of fault magnitude estimate (Simultaneous and Sequential sensor faults)

Fault magnitude introduced		TSKF	
Sensor1	Sensor3	Sensor1 $E[\hat{b}],(\sigma[\hat{b}])$	Sensor3 $E[\hat{b}],(\sigma[\hat{b}])$
1σ=5e-3	1σ=3e-3	4.4956e-3 (3.2187e-8)	2.61925e-3 (1.9354e-8)
3σ=1.5e-2	3σ=9e-3	1.3480e-2 (1.0095e-7)	8.0819e-3 (5.9301e-8)
5σ=2.5e-2	5σ=1.5e-2	2.2464e-2 (1.6860e-7)	1.3472e-2 (9.9134e-8)

4. Conclusion

The performance of the FDD scheme based on simultaneous state and fault parameter estimation is validated on a three-tank system for an abrupt as well as slowly varying fault. From the simulation studies on three-tank system, it is concluded that the performance of ASKF is better than TSKF for single, multiple simultaneous and sequential faults as it generates smooth estimates. The processing time is fixed for TSKF for any number of faults whereas it will vary for ASKF when the numbers of faults vary. It is observed that probability of occurrence of false and missed alarms are very low in ASKF, as compared to TSKF. The proposed ASKF based robust FDD scheme can very well be integrated with any conventional control scheme to develop a fault tolerant control scheme.

5. Acknowledgements

The authors would like to acknowledge Dr.S.P.Natarajan, Department of Electronics and Instrumentation Engineering, Annamalai University, Annamalai Nagar for granted permission to use the computer control of process laboratory.

6. References

[1] R. Isermann. Process fault detection based on Modelling and estimation Methods: A survey. Automatica, Volumn 20: 387-404,1984.

[2] M. Basseville. Detecting changes in signals and systems-A survey. Automatica 24: 309 – 326, 1988.

[3] P.M. Frank, X. Ding. Frequency domain approach to optimally robust residual generation and evaluation model based fault diagnosis. Automatica, Volumn 30(5): 789 – 804, 1994.

[4] J. Getler. Model based fault diagnosis. Control theory and Advanced Technology, Volumn 9(1): 259-285, 1993.

[5] R.J. Patton, M.Hou, Y.S.Xiong. Observing Three Tank System. IEEE Transaction on Control Systems Technology Volumn 13(3): 478-484, May 2005.

[6] Luenberger, D.G. (1964). Observing the state of a linear system. IEEE Trans Mil. Electro. MIL – 874.

[7] Efrain Alcorta Garcia and Salkvador Saucedo-Flores. Fault Detection and isolation based on Takagi_Sugeno modeling. Proc. IEEE International Symposium on Intelligent Control, Houstan, Texas, 673-678,2003.
[8] P.M.Frank, T.Marcu and L.Mirca. Neural Observer Schemes for Robust detection and isolation of process faults. UKACC International conference on control, 98 Conference Publication No.455.IEE, 958-963, 1998.
[9] L.EL.Bahir and M.Kinnaert. Fault Detection and isolation for three tank systems on a bilinear model of the supervised process. UKACC International conference on CONTROL 98 Conference Publication No.455.IEE, 1486-1491, 1998.
[10] Mohammad Abdelrahman and Malak A. Samaan. New algorithm for gyroless spacecraft angular rate estimation and its application. International conference on ACSE05 Conference Publication ACSE.
[11] B. Friedland. Treatment of bias in recursive Filtering. IEEE Transaction on Automatic Control, Volumn AC-14(4): 359 -367, 1969.
[12] Gary G.Yen and Liang Wei Ho, Online multiple-model-based fault diagnosis and accommodation. IEEE Transaction, Volumn50 (2): April 2003.
[13] E. Alcorta Garcis and P.M.Frank. Deterministic Nonlinear observer based approaches to fault diagnosis: A survey. Control Engg. Practice, volumn5 (5):663-670, 1997.
[14] N. Metropolis and S. Ulam. The Monte-Carlo Method, Journal of the American Statistical Association, volume(44), 335, 1949.

S. Abraham Lincon obtained his B.E degree is Electronics and Instrumentation Engineering in the year 1984 and received M.E. degree in Power System Engineering in 1987 and another M.E degree in Process Control and Instrumentation Engineering in 2000 from the Annamalai university, Chidambaram. Presently he is working as a professor of the Department of Instrumentation Engineering in Annamalai University. His areas of research are Process Control, Fault Detection and Diagnosis and Multivariable Control.

Dr.D.Sivakumar obtained his B.E degree is Electronics and Instrumentation Engineering in the year 1984 and further the M.E. degree in Power Systems in the year 1990 from the Annamalai University, Chidambaram. Presently he is working as a Professor in the Department of Instrumentation Engineering in Annamalai University. He is presently guiding many Ph.D research scholars in areas like Fault Detection and Diagnosis, Neural Networks and Fuzzy Logic applied to Process Control, Signal and Image Processing.

Dr. J. Prakash obtained his B.E degree in Electronics and Instrumentation Engineering in the year 1993 from Annamalai University, Chidambaram and he got his M.E degree in Control System Engineering in the year 1995 from PSG college of Technology, Coimbatore. Subsequently he received his Ph.D degree in Chemical Process Control Engineering from the prestigious institute IIT Madras, Chennai. Presently he is working as an Assistant Professor in the Department of Instrumentation Engineering, Anna University, MIT Campus, Chennai. Currently he is guiding many Ph.D and M.S scholars in the areas like Instrumentation, Process Control, Fault Talent Control, Fault detection diagnosis, Multivariable Control, Digital Signal Processing.

www.icgst.com

MRAS based Speed Control of sensorless Induction Motor Drives

S.Meziane, R.Toufouti, H.Benalla
Department of Electrical Engineering, Constantine University Aîn el bey Road Constantine Algeria
[meziane_elc, toufoutidz, Benalladz]@yahoo.fr

Abstract
Senseless induction motor drives are widely used in industry for their reliability and flexibility, particularly in hostile environment. However, the performance of many of previously developed observer based speed sensors in very low speeds of IM drives was not satisfactory. In this paper we present two types of MRAS based speed estimators, one based on the rotor flux and the other based on the back EMF. The estimated speed is used as feedback in a vector control system. The MRAS approach has the immediate advantage in that the model is simple, presents the theory, modelling and this method because eliminates the produced error in the speed adaptation, is more stable and robust. Simulation results of the proposed MRAS speed observer based sensorless field-oriented induction motor drives. The performances of both techniques are evaluated in indirect vector control system and the results are presented.

Keywords: *Sensorless induction motor, model reference adaptive system (MRAS), speed estimator.*

1. Introduction
Induction motors have been widely used in high-performance ac drives, requiring . information. Introducing a shaft speed sensor decreases system reliability, and different solutions for sensorless ac drives have been proposed. The MRAS speed estimators are the most attractive approaches [1], due to their design simplicity.
The MRAS is based on principle, in which the outputs of two models –one independent of the rotor speed (reference model) and the other dependent (adjustable model)- are used to form an error vector[1]-[7]. The error vector is driven to zero by an adaptation mechanism which yields the estimated rotor speed. Depending on the choice of output quantities that form the error vector, several MRAS structures are possible. The most common MRAS structure is that based on the rotor flux error vector [2] which provides the advantage of producing rotor flux angle estimate for the field-orientation scheme. Other MRAS structures have also been proposed recently that use the back EMF and the reactive power as the error vectors estimators. It is the intention of this paper, therefore, to present a direct comparison between two different MRAS approaches: the rotor flux based and the back EMF based MRAS [9][10]. The rotor flux based MRAS approach studied in this paper basically follows that of, while the back EMF based approach is the modified form of the one developed in. To allow for a fair comparison, no on-line parameter methods will be incorporated and same current controllers and a PWM generation technique will be used in both approaches. In order to compare the performances of the two estimators. Several performance measures are evaluated in computer simulations. The studies include the level of difficulties in tuning the adaptive gain constants and the tracking performances of both speed estimators. To obtain accurate estimation of the speed, a simple on-line identification approach has been incorporated. Based on the theory of MRAS, simultaneous estimation of rotor speed has been described in this paper. Comparing to other adaptation techniques, this method is simple and needs a low computation power and has a high speed adaptation even at zero speeds. This method because eliminates the produced error in the speed adaptation, is more stable and robust. Computer simulations results are presented to show its effectiveness.

2. Field Oriented control theory
One particular approach for the control of induction motors is the Field Oriented Control (FOC) introduced by Balaschke in [5][8]. The machine equations in the stator reference frame, written in terms of space vectors, are

$$\bar{V}_s = R_s \bar{I}_s + \frac{d\bar{\varphi}_s}{dt} \quad (1)$$

$$0 = R_r \bar{I}_r + \frac{d\bar{\varphi}_r}{dt} - j\omega m\bar{\varphi}_r \quad (2)$$

$$\bar{\varphi}_s = L_s \bar{I}_s + M\bar{I}_r \quad (3)$$

$$\bar{\varphi}_r = L_r \bar{I}_r + M\bar{I}_r \,(1) \quad (4)$$

$$\frac{d\Omega}{dt} = \frac{T - T_L}{J} \quad (5)$$

$$T = p\frac{M}{JL_r}(\varphi_{rd} i_{sq} - \varphi_{rq} i_{sd}) \quad (6)$$

This control strategy **is** based on the orientation of the flux vector along the d axis [4],[6] which can he expressed by considering:

$$\varphi_r^{d,q} = (\varphi_{rd}^2, 0)^T \quad (7)$$

Assuming a rotor flux reference frame, and developing the previous equations with respect to the axis and axis components, leads to.

$$\frac{d\varphi_{rd}}{dt} + \frac{1}{\tau_r}\varphi_{rd} = \frac{M}{\tau_r} i_{sd} \quad (8)$$

$$T = p\frac{M}{JL_r}\varphi_{rd} i_{sq} \quad (9)$$

These equations represent the basic principle of the FOC: in the rotor flux reference frame, a decoupled control of torque and rotor flux magnitude can be achieved acting on the d and q axis stator current components, respectively. A block diagram of a basic DFOC scheme is presented in Figure 1. The rotor flux estimation is carried out by.

$$\frac{d\bar{\varphi}_s}{dt} = \bar{v}_s - R_s \bar{i}_s \quad (10)$$

$$\bar{\varphi}_r = \frac{L_r}{M}(\bar{\varphi}_s - \sigma L_s \bar{i}_s) \quad (11)$$

The flux estimator has been considered to be ideal, being the effects due to parameter variations at low speed out of the major aim of this paper. The current controller has been implemented in the rotor flux reference frame using PI regulators with back emf compensation.

3. Model Reference Adaptive System

The Model Reference Adaptive Systems (MRAS) approach uses two models. The model that does not involve the quantity to be estimated (the rotor speed re in our case) is considered as the reference model. The model that has the quantity to be estimated involved is considered as the adaptive model (or adjustable model). The output of the adaptive model is compared with that of the reference model, and the difference is used to drive a suitable adaptive mechanism whose output is the quantity to be estimated (rotor speed in our case). The adaptive mechanism should be designed to assure the stability of the control system. Figure 1 illustrates the basic structure of MRAS [1]-[7],[9]. Different approaches have been developed using MRAS, such as rotor-flux-linkage estimation-based MRAS, back-EMF-based MRAS (reactive-power-based MRAS) [9].

The Overall system of the proposed sensorless control algorithm is shown in Figure 2.

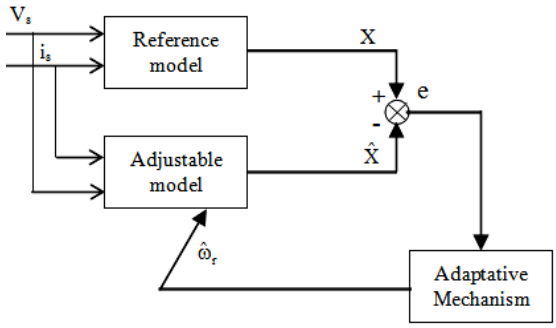

Figure 1. Block diagram of the proposed MRAS

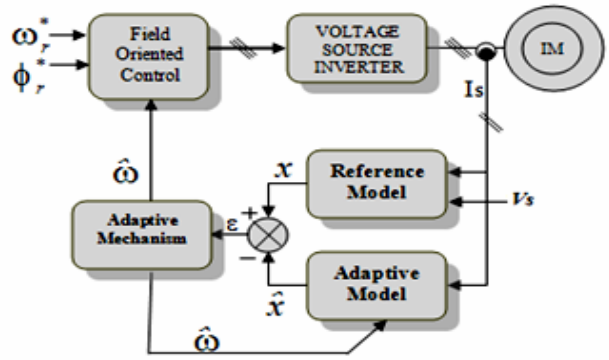

Figure 2. Configuration of overall system

3.1. MRAS based on rotor flux-linkage estimation

The proposed MRAS is using state observer model with current error feedback and rotor current model as two models for flux estimation. Figure 3 shows the block diagram of the proposed MRAS [4].

The reference model is given by:

$$\dot{\vec{\psi}}_{rd} = \frac{L_r}{L_m}\left(\int (\vec{u}_{sd} - R_s \vec{i}_{sd})dt - \sigma L_s \vec{i}_{sd}\right)$$
$$\dot{\vec{\psi}}_{rq} = \frac{L_r}{L_m}\left(\int (\vec{u}_{sq} - R_s \vec{i}_{sq})dt - \sigma L_s \vec{i}_{sq}\right) \quad (12)$$

The adjustable model is given by:

$$\dot{\hat{\psi}}_{rd} = \frac{1}{T_r}\left(L_m i_{sd} - \hat{\psi}_{rd} - \omega_r T_r \hat{\psi}_{rq}\right)$$
$$\dot{\hat{\psi}}_{rq} = \frac{1}{T_r}\left(L_m i_{sq} - \hat{\psi}_{rq} - \omega_r T_r \hat{\psi}_{rd}\right) \quad (13)$$

Where ψ_{rd}, ψ_{rq} : estimated values of rotor fluxes in state observer model

$\hat{\psi}_{rd}, \hat{\psi}_{rq}$: estimated values of rotor fluxes in rotor current model. Rotor speed is obtained from the adaptation mechanism as follows [4][9]:

$$\hat{\omega}_{re} = \left(K_p + \frac{K_i}{p}\right)\left(\psi_{rq}\hat{\psi}_{rd} - \psi_{rd}\hat{\psi}_{rq}\right) \quad (14)$$

The presence of the pure integrators brings the problems of initial conditions and drift. In [4], To reduce the effect of the derivative terms, a similar approach as that used to eliminate the pure integration problem a low pass filter was used to replace the pure integrator, but the performance in the low speed range is not satisfying, for reasons which will be explained later.

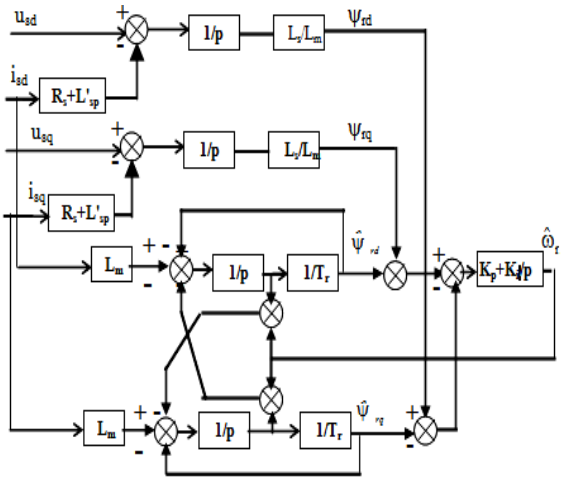

Figure 3. MRAS based on rotor Flux-linkage estimation

3.2. MRAS based on back-EMF estimation

This paper proposes a novel sensorless control algorithm based on the MRAS for the speed sensorless control of a induction motor. The proposed MRAS is using the state observer model of (15) and (16) and the magnet flux model of and as two models for the back-EMF estimation. The rotor speed is generated from the adaptation mechanism using the error between the estimated quantities obtained by the two models as follows in Figure.4, [8], [9].

The reference model is given by:

$$\begin{aligned} e_d &= u_{sd} - R_s i_{sd} - L'_s \dot{i}_{sd} \\ e_q &= u_{sq} - R_s i_{sq} - L'_s \dot{i}_{sq} \end{aligned} \qquad (15)$$

The adjustable model is given by:

$$\begin{aligned} \hat{e}_d &= \frac{L_m}{L_r}\frac{L_m i_{sd} - \hat{\psi}_{rd} - \omega_r T_r \hat{\psi}_{rq}}{T_r} \\ \hat{e}_q &= \frac{L_m}{L_r}\frac{L_m i_{sq} - \hat{\psi}_{rq} - \omega_r T_r \hat{\psi}_{rd}}{T_r} \end{aligned} \qquad (16)$$

The adaptive mechanism is given by [3, 9]:

$$\hat{\omega}_{re} = K_p\left(\hat{e}_{\beta s}\tilde{e}_{\alpha s} - \hat{e}_{\alpha s}\tilde{e}_{\beta s}\right) + K_i\int\left(\hat{e}_{\beta s}\tilde{e}_{\alpha s} - \hat{e}_{\alpha s}\tilde{e}_{\beta s}\right)dt \qquad (17)$$

Where K_i, and K_p, are the gain constants, i, and p are the estimated values of back-EMF in the state observer model, [4]. Are the estimated values of back- EMF in the magnet flux model.

Figure 4 shows the block diagram of the proposed MRAS algorithm has a robust performance through combining the state observer model and the magnet flux model [4].

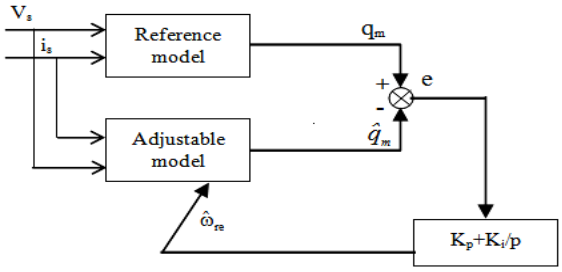

Figure 4. The MRAS speed observer;

This scheme does not have pure integrators in the reference model.

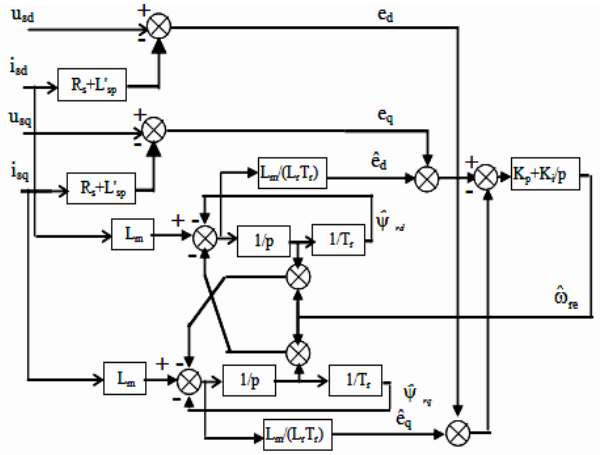

Figure 5. MRAS based on back -EMF

4. Interpretation results

To validate the performances of the proposed controller, we provide a series of simulations and a comparative study between the performances of the proposed control strategy. A 1.5kW induction motor with controller is simulated using the nonlinear controller and the following motor parameters: Pn＝1.5kW, Un＝230V, Rs＝2.89Ω, Rr＝2.39Ω, Ls＝0.225H Lr＝0.225H, Lm＝0.214H,

4.1. Tuning the adaptive gain constants

Simulation studies have been performed to compare the level of difficulty in tuning the adaptive gain constants for the two speed estimators. Figure.6 shows the simulation results of the speed sensorless vector control using the rotor flux based MRAS speed estimator for different adaptation gain constants. It can be seen that low values of adaptation gains do not yield in convergence of the speed or the fluxes see Figure 6.a increasing the gains yield in better convergence of the estimations as shown in Figure 6.b and 6.c.

Figure.7 shows simulation results of the back EMF based MRAS for different adaptation gain constants. It was found that the relationship between the adaptation gain constants and the tracking performance is not as simple as in the case of the rotor flux based MRAS. Increasing the gain constants in the rotor flux based MRAS in general results in a better tracking performance. In the back-EMS based MRAS, this has not always been the case. From Figure 7(a ,b) , it can be seen that increasing

K_I from 0.04 to 25 while keeping K_P at 0.001 helps to improve the tracking performance. However, when K_P is increased to 0.01 while K_I is kept at 25, the steady state error of the estimation increases as can be seen in Figure.7c. More surprising results were obtained when K_P is further increased to values greater than approximately 0.01, since the results then became unstable. The fact that the results went unstable for certain values of the adaptation gain constants had made the process of tuning them a difficult exercise [9].

4.2. Speed Estimators Tracking Performances

Simulation studies have been performed to compare the tracking performances of the two speed estimators. In these studies, the machine was operated in the indirect vector control operation using the speed sensor signal, while at the same time estimation of the speed using each of the MRAS speed estimators was performed.

Figure 8 shows the simulation results of the rotor flux base MRAS speed estimator when the machine is operated at different speed. It can be seen that at relatively high speed Figure 8a, the estimated speed tracks the actual speed reasonably well. As the speed is decreased, however, the steady state values of the estimated speed tend to deviate from those of the actual speed [9]. These deviations were most likely caused by the error in the stator resistance *Rs.* At lower speed, the stator voltages and currents vary at lower frequency. As the frequency decreases, the term ***R.i/p*** becomes relatively larger. Therefore, an error in the value of *Rs,* will seriously effect the estimated speed as the frequency approaches zero.

This error, however, is usually quite negligible at high excitation frequency [9].

Figure 9 shows the simulation results of the modified back-EMF speed estimator. From these results it can be seen that good tracking performances can still be achieved even at the speed of 85 rpm.

Unlike the rotor-flux based MRAS, here the error in the value of *Rs,* does not seriously effect the estimation at low speed

4.2. Influence of variation of both rotor resistance and load torque

Show the speed responses in case of considering the parameter variations where the rotor resistance is increased by 100% and torque load by 50% of the nominal value. The parameter variations are applied in the middle of the operation of [60 and -60] rad/sec.

The simulation results show that the two proposed methods sensorless control algorithm has good speed responses. for two proposed methods shown Figure (10a,10b), but the rotor flux for rotor flux based MRAS presented of the ripple in steady state compared whit rotor-flux based MRAS method as it is to show on Figure (11a, 11b);it could be expected that the stator current in rotor flux based MRAS has more harmonic distortion because the effects caused by flux drooping is more evident as show in Figure (12a,12b).

5. Conclusion

This paper proposed a novel speed sensorless control algorithm of induction motor. The proposed control algorithm is based on MRAS using state observer model with the rotor flux based MRAS technique and the back EMF based MRAS technique, comparing to other adaptation techniques, this method is simple and needs a low computation power and has a high speed adaptation even at zero speeds. These important features are very well shown in the obtained results who indicate that the proposed algorithm shows good speed responses in the low and high speeds in the rotor flux based MRAS and the back EMF based MRAS speed estimators. It was shown that although the low speed performance of the back EMF MRAS speed estimator is better than the rotor flux based MRAS, the back EMF MRAS estimator is more difficult to design due to the non-linear effect of the adaptation gain constants.

6. References

[1] Y. Hori C. Ta, T. Uchida. MRAS-based speed sensorless control for induction motor drives using instantaneous reactive power. IECON, 1417{1422, Nov. /Dec. 1991.

[2] J. Holtz, "Methods for speed sensorless control of ac drives," in *Sensorless Control of AC Motors,* K. Rajashekara, Ed. Piscataway, NJ: IEEE Press, 1996.

[3] F. Peng and T. Fukuo. Robust speed identification for speed- sensorless vector control of induction motors. IEEE Transactions of Industrial Applications, 30:1234{ 1240, Sept./Oct. 1994.

[4] Mohammad N.Marwali and Ali Keyhani''A Comparative Study of Rotor Flux Based MRAS and Back EMF Based MRAS Speed Estimators for Speed Sensorless Vector Control of Induction Machines'' IEEE Industry Applications Society Annual Meeting New Orleans, Louisiana, October 5-9,1997

[5] F. BLASCHKE, "The Principle Of Field Oriented As Applied To The New Tran Vector Closed-Loop Control System For Rotating Machine", Siemens Review, 1972, vol.39, N°4, pp.217-220,1972

[6] R. Blasco-Gimenez., G.M. Asher, M. Sumner, and K. J. Bradley, "Dynamic Performance Limitations for MRAS based sensorless induction motor drives. Part 2: Online parameter tuning and dynamic performance studies", IEE Proc. Elect. Power Appl., 1996, Vol. 143, (2), pp. 123-134.

[7] D.W. Jin Y.A. Kwon. A novel mras based speed sensorless control of induction motor. IECON, 2:933{938, Nov./Dec. 1999.

[8] R.Toufouti S.Meziane ,H. Benalla, "Direct Torque Control for Induction Motor Using Fuzzy Logic" *ICGST Trans. on ACSE*, Vol.6, Issue 2, pp. 17-24, June, 2006.

[9] S.Lassaâd and M.Ben Hamed "An MRAS - based full Order Luenberger Observer for Sensorless DRFOC of Induction Motors" ICGST-ACSE Journal, Volume 7, Issue 1, May 2007

[10] Li Zhen, and Longya Xu, Sensorless Field Orientation Control of Induction Machines Based on a Mutual MRAS Scheme, IEEE TRANSACTIONS ON INDUSTRIAL ELECTRONICS, VOL. 45, NO. 5, OCTOBER 1998.

8. Simulation results

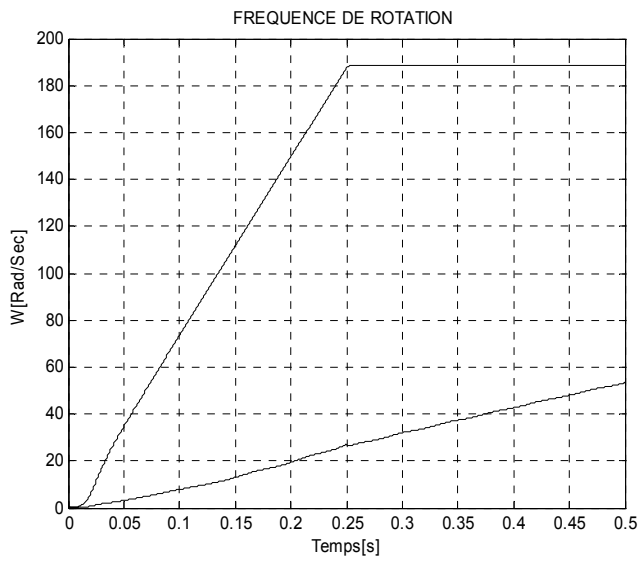

(a) K_p=0.004 K_i=0.008

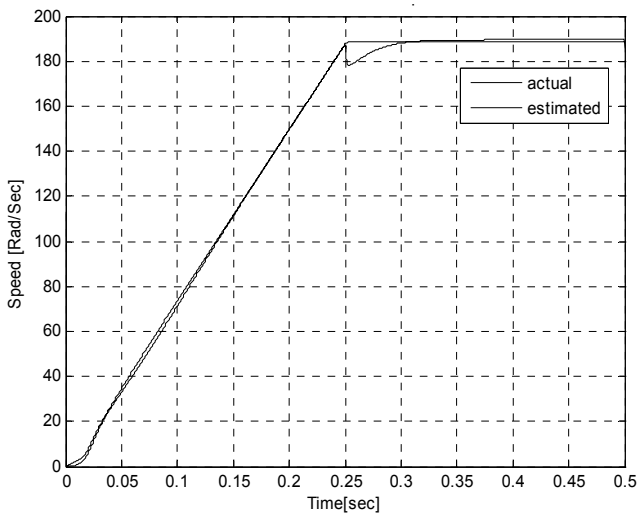

(b) K_p=0.4 K_i=4

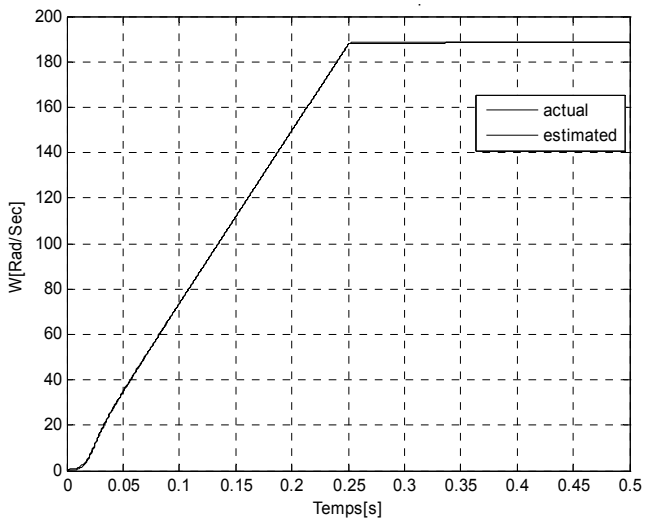

(c) K_p=0.01 K_i=20

Fig. 6. Simulation results Actual and Estimated speed : effect of different adaptation gains in the rotor flux based MRAS

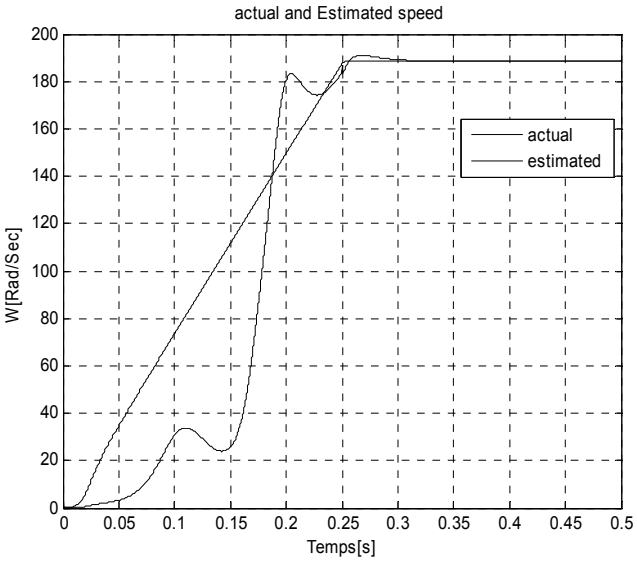

(a) K_p=0.001 K_i=0.04

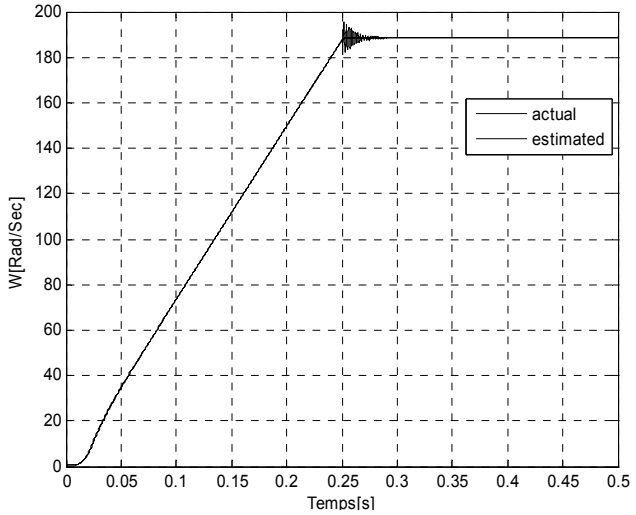

(b) K_p=0.001 K_i=25

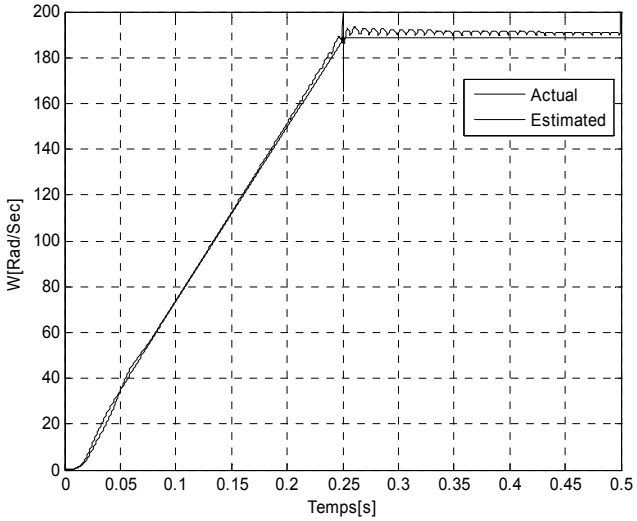

(c) K_p=0.01 K_i=25

Fig. 7. Simulation results Actual and Estimated speed: effect of different adaptation gains in the back EMF based MRAS

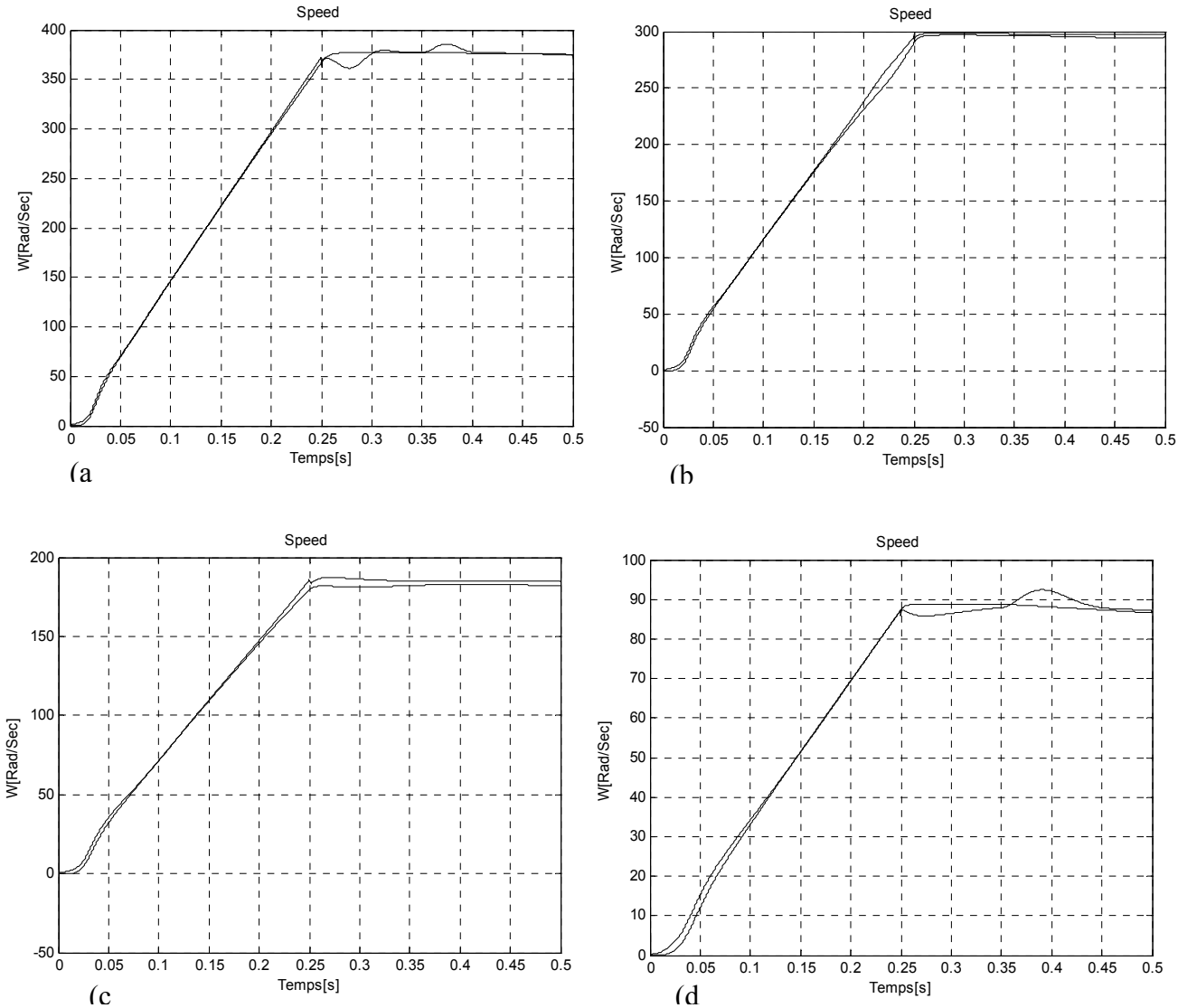

Fig. 8. Simulation results: modified rotor flux MRAS estimator for speed references at (a) 380rpm (b) 275 rpm (c) 190 rpm (d) 85 rpm

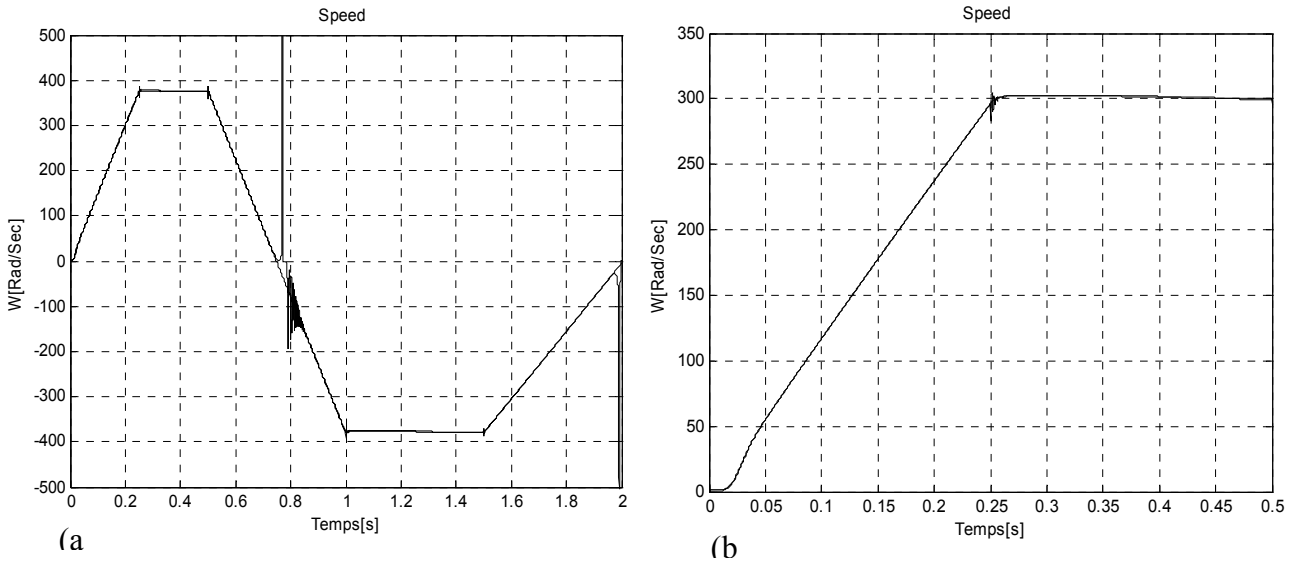

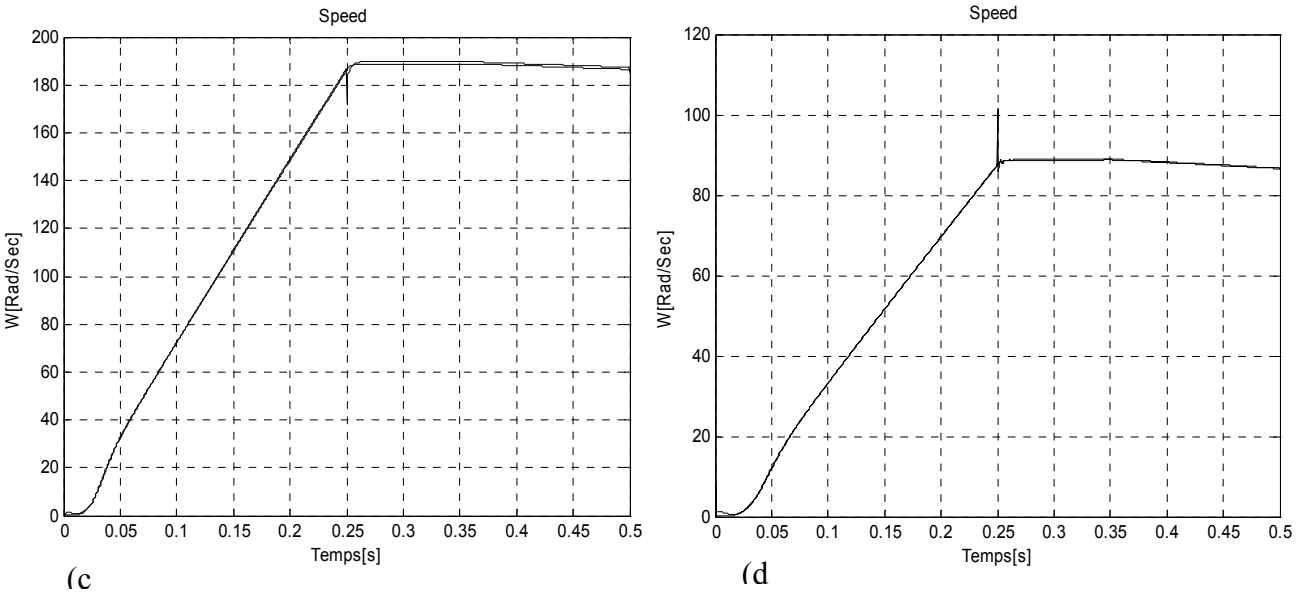

Fig. 9. Simulation results: back-emf based MRAS speed estimator (a) 380rpm (b) 275 rpm (c) 190 rpm (d) 85 rpm

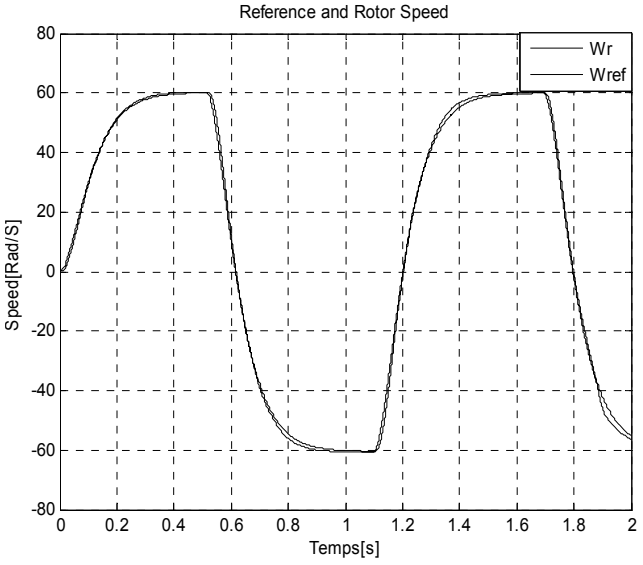

Fig. 10.a: Rotor speed

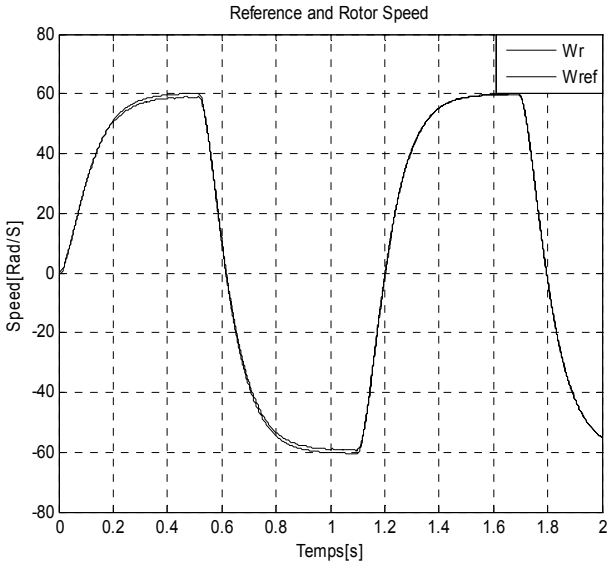

Fig. 10.b: Rotor speed

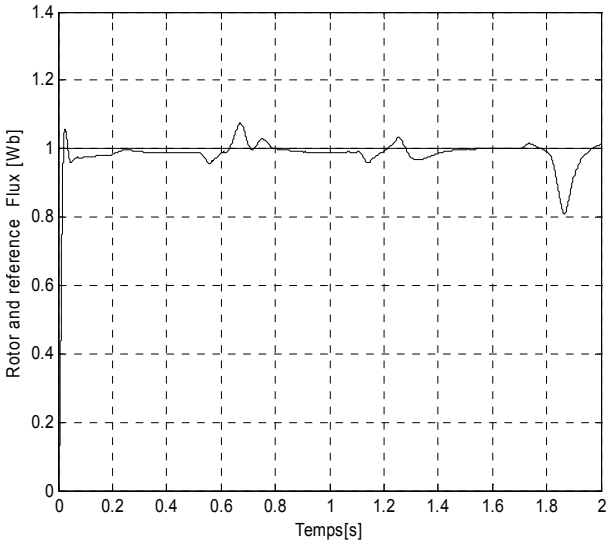

Fig.11.a: Rotor flux

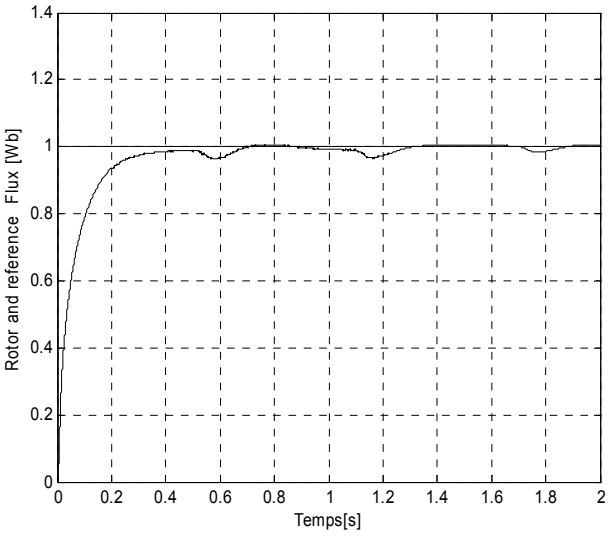

Fig.11.b: Rotor flux

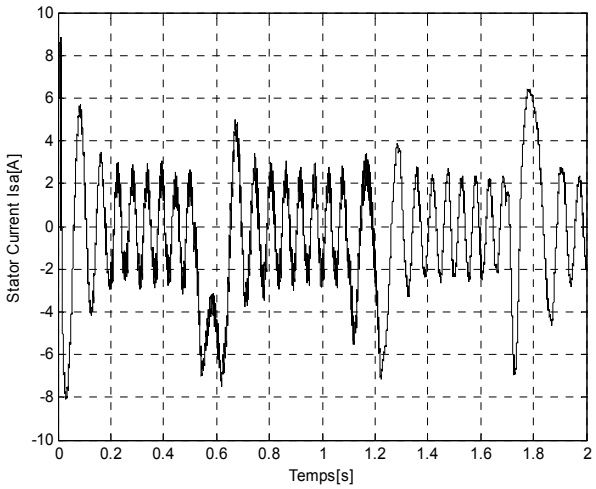

Fig. 12.a: Stator current

MRAS based on rotor flux-linkage estimation with variation of rotor resistance and load torque

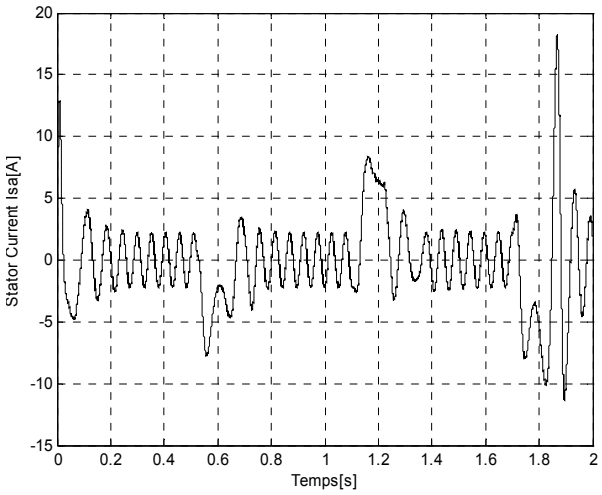

Fig. 12.b: Stator current

MRAS based on back -EMF with variation resistance and load torque

7. Biographies

Meziane Salima: was born in Oum El Bouaghi, Algeria, in 1974, in 2000 received the Engineer degree from the University of Montouri Constantine. Algeria. In 2003 received the M.S. degrees in electrical engineering, Option electrical machine. Associate teacher in Oum El Bouaghi University from October to 2003. In 2004 inscription in doctor's degree, permanent teacher from October 2004 in Souk ahras University, member for laboratory Of Electrical engineering university Constantine. Algeria.

Toufouti Riad: was born in Constantine, Algeria, in 1974, in 1999 received the Engineer degree from the university of Montouri Constantine. Algeria. In 2003 received the M.S. degrees in electrical engineering, Option electrical machine. Associate teacher in Constantine University from October 1999 to 2003. In 2003 inscription in doctor's degree, permanent teacher from January 2004 in Souk ahras University, member for laboratory Of Electrical engineering university Constantine. Algeria

Hocine Benalla: was born in Algeria in 1957. He received the D.E.A. and Doctor engineer degree in power electronics from the National Polytechnic Institute of Toulouse, France, in 1981 , and. 1984, respectively. In 1995, he received the Ph.D. degrees in electrical engineering from University of Jussieu -Paris 6, France. He is currently an Assistant Professor at University of Constantine Algeria. His current research interests include electric machines, ac drives and active filter.

www.icgst.com

Mixed H_2/H_∞ based Course-following Control for a Small Low Cost Autonomous Boat

Zhenyu Yu, Xinping Bao, Kenzo Nonami
Graduate School of Engineering, Chiba University
1-33 Yayoi-cho, Inage-ku, Chiba, Japan
[yzy, xinping_bao]@graduate.chiba-u.jp, nonami@faculty.chiba-u.jp
http://mec2.tm.chiba-u.jp/~nonami/

Abstract
This paper presents the design of course-following controller for an autonomous boat with low-cost sensors by applying H_2/H_∞ robust control approach. At first a mathematical model for the under actuated boat is derived which captures the dynamics between rudder deflection and the boat's horizontal motion. The resulted model could be seen as an extension to the Nomoto's model. Despite of its simplicity, the model offers the advantage that no compass is required for control, which promotes integrated steering and guidance at low cost. Based on the model, mixed H_2/H_∞ control approach is applied to provide robust stability in the presence of model uncertainty and environmental disturbance while maximizing the performance in the sense of H_2 norm. The proposed modeling and control strategies are tested on a small autonomous boat whose length is about 1 meter. A low-cost GPS receiver and a gyroscope are used for navigation and control. The course-following performance has been demonstrated at sea trials. The standard deviation of the cross track error is 2.3 m which is a good result for the small boat with such low cost sensors.

Keywords: *Autonomous boat, Course-following control, Mixed* H_2/H_∞*, Modeling, Low cost.*

1. Introduction
Autonomous vehicles have been of great research interest in recent years as they are promising means to remove or reduce human labors' workload. Different kinds of autonomous vehicles are developed or under development. A broad classification would include UAV (Unmanned Aerial Vehicle), UGV (Unmanned Ground Vehicle), AUV (Autonomous Underwater Vehicle) and ASC (Autonomous Surface Craft). While state-of-the-art technologies are applied to pursue good performance, the cost-effectiveness has been becoming another focus for practical applications. High cost will inevitably hinder the application. "Low cost" has turned to be one key word in recent studies [1- 4]. In this paper, we study the design of course-following control for a small low-cost boat by using mixed H_2/H_∞ approach. The autonomous boat is expected to be applied for seabed survey, mapping and aquatic environment monitoring. The performance and cost issue should be considered and balanced.

The vehicle under study is a small boat which is 1060 mm long with a mass of 12 kg. To our knowledge, it is the smallest one among those reported in the literature. The small dimension and low weight cause it be easily affected by environmental disturbances such as wind, and waves, which is one challenge for the control. The fact that the boat is driven by DC motors poses another challenging problem in installing a low cost magnetic compass to measure the yaw angle which is normally required by many existing control strategies.[5,6,7] The compact space makes it hard to compensate or isolate the magnetic disturbance from DC motors. Although gyrocompass could be used, the additional cost is not preferred. This motivates our study on control and navigation of an autonomous boat without using a compass. Instead we use GPS for its near global coverage and ease of use for positioning.

Although the marine vehicle control problem has been widely studied since the first automatic ship steering mechanism was constructed by Elmer Sperry in 1911[8]. To control a boat without using a compass is less addressed. Some recently reported autonomous surface vehicles include a wind-propelled marine vehicle from Stanford University[9], an autonomous surface platform for research in cooperative autonomy by MIT[10], a robotic boat for microbial observation by University of Southern California[11], and the DELFIM autonomous surface craft developed at Institute for systems and robotics, Portugal for data acquisition and communication relay [12]. These autonomous systems all utilize compass for yaw angle measurement.

To realize the control strategy with a GPS, the dynamic relationship should be investigated. We have developed a simple dynamic model describing the boat's maneuver with measurement from GPS. It could be seen as an extension to the Nomoto's first order model by introducing the relationship between the boat's heading

and its moving direction. This model keeps the simplicity of Nomoto's model. In addition, it enables the course-following control of a boat in the absence of a compass. We have designed and implemented a course-following controller using H_2/H_∞ robust control technique based on the developed model. The control approach is applied to optimize the performance in the sense of H_2 norm while maintaining robust stability in the presence of ignored dynamics and environmental disturbances.

The choice of H_2/H_∞ control method is because that the method offers a systematic way in designing linear controller, unlike other control schemes such as adaptive control, fuzzy control, or neural networks which actually synthesize nonlinear controller even if the plant is linear. In implementation, linear controllers are usually less complicated than nonlinear controllers. What's more, these control methods lacks such systematic way as H_2/H_∞. In H_2/H_∞ controller design the stability and performance requirements can be enforced by choosing frequency dependent weighting functions properly.

The performance of the controller has been verified through sea tests. The standard deviation of cross track error is 2.3m. This performance is achieved by using low cost sensors: a GPS receiver and a gyroscope. The total costs are below $100.

In the following text, we will describe the mathematical model in Section (2) and discuss the controller design in Section (3). We will give a brief introduction of the boat platform in Section (4). In section (5), we will present the experimental results. And finally, in section (6), we will give concluding remarks and summarize this study.

2. Mathematical model

The mathematical model of a boat can be obtained by applying Newtonian or Lagranigian theory. With this approach, the force and torque must be modeled explicitly. It involves modeling the complicated hydrodynamic effects through wave-hull interaction. This is usually done by approximating the effect with hydrodynamic derivatives. However, these parameters rely mostly on experiments such as tests by tow tank, by rotating arm device, and by planar motion mechanism for identification, which suggests a costly and maybe time-consuming process before a meaningful model can be obtained. Some simplified models, on the other hand, do not require such detailed modeling which catches the dominant dynamics only. Nomoto's model [13] is one of the simplified models. It describes the yaw motion of a boat. The simplicity of Nomoto's model is attractive for control law design. In literature, many ship autopilots are based on this model such as [6,23,24]. With the desire to get a simple model, we start with the Nomoto's model and extend it to include the motion in horizontal plane. In this section, we will first review the Nomoto's model and then develop the extension for modeling the horizontal motion.

2.1. Nomoto's Model

In 1957 Nomoto proposed two transfer functions based models for steering simulation and control [14], namely the second order Nomoto model and the first order Nomoto model. The second order Nomoto model is shown in Equation (1).

$$\frac{r(s)}{\delta(s)} = \frac{k_0(s\tau_3 + 1)}{(s\tau_1 + 1)(s\tau_2 + 1)} \tag{1}$$

This model shows the dynamic effect of rudder deflection angle δ on yaw rate r. It is noticed that one of the poles in Equation (1) is nearly cancelled by its zero [14]. With this fact, Equation (1) is further simplified into Equation (2). It is called the first order Nomoto model.

$$\frac{r(s)}{\delta(s)} = \frac{k_0}{(s\tau + 1)} \tag{2}$$

where $\tau = \tau_1 + \tau_2 - \tau_3$.

The Nomoto's model is valid on the assumption that the boat moves at constant forward velocity, the propelling thrust is constant and the rudder angle is small. Given that the conditions are satisfied, the Nomoto model gives a reasonably accurate description of the course-keeping behavior [14].

In Equation (2) the rudder actuator model is absent; we need model steering machine which actuates the rudder to get the model from steering machine command δ_m to the yaw rate. Suppose the steering machine can be modeled linearly as Equation (3),

$$\frac{\delta(s)}{\delta_m(s)} = G(s) \tag{3}$$

we obtain the yaw model with actuator considered by substituting Equation (3) into Equation (2).

$$\frac{r(s)}{\delta_m(s)} = \frac{k_0}{(s\tau + 1)} \cdot G(s) \tag{4}$$

In this study, the rudder actuator of the boat under investigation is a DC servo motor. The response of the servo motor is much faster than yaw response of the boat. By time scale separation principle, the actuator can be modeled as a constant gain k_1. Then we get the model from servo motor command to the yaw rate as shown in Equation (5).

$$\frac{r(s)}{\delta_m(s)} = \frac{k}{(s\tau + 1)} \tag{5}$$

where $k = k_0 \cdot k_1$.

The boat's yaw motion is modeled in the form of Equation (5) with the two parameters k and τ identified through experiments. A comparison of the model output and the boat's response is shown in Figure 1.

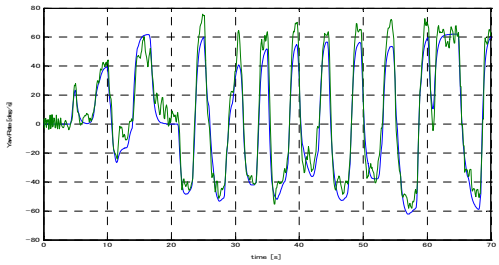

Figure 1. Validation of yaw model: the blue line shows the simulated output from the model; and the green line shows the actual output of the boat

2.2. Translational Model

It is not enough to only maintain the boat's heading if we want it to follow a straight line course especially for the small boat. Since its speed is slow and is of low inertia, it is easy to be disturbed and deviates from the course faster than full scale ship. The translational model under discussion is limited to be on the horizontal plane which is illustrated in Figure 2. We use symbols shown in Table 1 to describe the motion of the boat.

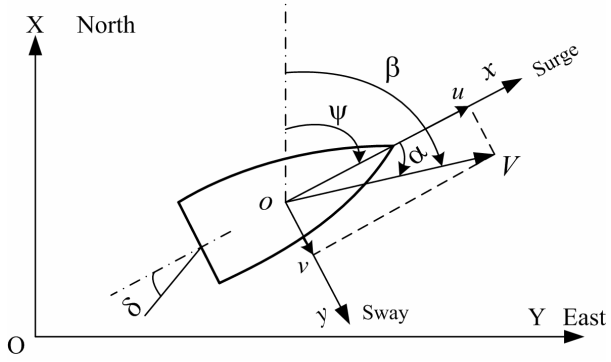

Figure 2. Description of boat's motion in horizontal plane

Table 1. Nomenclature

Symbol	Definition
ψ	Yaw angle (heading angle)
r	Yaw rate
α	Side slip angle between boat's heading and its moving direction
β	The boat's moving direction (velocity angle)
V	Velocity vector
u	Surge velocity
v	Sway velocity
δ	Rudder deflection angle

We make similar assumptions as Nomoto model did that the boat is driven by constant thrust; the boat runs at constant speed; and the boat may experience small yaw perturbation. In perturbation free condition, the boat runs along straight line at constant speed. The forces acting on the boat reach balanced state that the thrust denoted by T equals to the total drag denoted by D. Also there is no side slip between the boat's heading and its moving direction. The equilibrium state is described by Equation (6).

$$\begin{cases} T = D \\ \alpha = \beta - \psi = 0 \end{cases} \tag{6}$$

When the boat's heading undergoes a small perturbation, the side slip angle is no longer zero. This results in unbalance between the thrust and drag due to the nonzero incident angle between the forces' directions as illustrated in Figure 3. The boat will be accelerated till another equilibrium state as depicted in Equation (6) is reached. We assume the velocity loss in the process is negligible. Then the magnitude of velocity can be treated as unchanged. This condition is described by Equation (7).

$$\frac{d}{dt}|V| = 0 \tag{7}$$

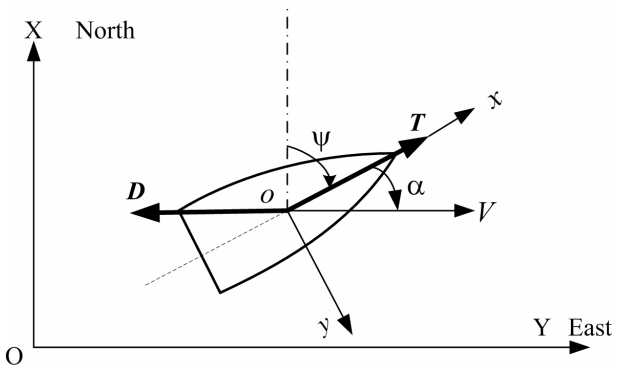

Figure 3. Simplified view of forces acting on the boat under small yaw perturbation

Since the drag is proportional to the square of boat's velocity, it will be constant under the assumption of Equation (7). The drag's direction is opposite to the direction of the velocity. The equation of motion of the boat under small yaw perturbation can be expressed by Equations (8) and (9).

$$m(\dot{u} - \dot{\psi}v) = T - D \cdot \cos\alpha \tag{8}$$

$$m(\dot{v} + \dot{\psi}u) = -D \cdot \sin\alpha \tag{9}$$

The m terms include the added mass effect. The added mass reflects the build-up of kinetic energy of the fluid as the hull moves through it which results the boat moves with equivalent additional mass in effect [15].

With the assumption of Equation (7), we can express the boat's velocity in the body coordinate as:

$$\begin{cases} u = |V| \cdot \cos\alpha \\ v = |V| \cdot \sin\alpha \end{cases} \tag{10}$$

Substituting Equation (10) into Equation (9), we obtain Equation (11).

$$\dot{\alpha} = -\frac{D}{m|V|} \cdot \tan\alpha - \dot{\psi} \tag{11}$$

When the side slip angle α is small, Equation (11) can be linearized as:

$$\dot{\alpha} = -\frac{1}{\lambda}\alpha - \dot{\psi} \tag{12}$$

where $\lambda = m|V|/D$.

With the definition of side slip angle indicated in Equation (6), we obtain Equation (13).

$$\lambda\dot{\beta} + \beta = \psi \tag{13}$$

Take Laplace transform on Equation (13) and combine Equation (5); we obtain the transfer function from rudder servo command to the boat's moving direction.

$$\frac{\beta(s)}{\delta_m(s)} = \frac{k}{s(\lambda s + 1)(s\tau + 1)} \tag{14}$$

This equation expresses the dynamics in the case that ideal sensor is available for velocity angle measurement. In fact, we use a low cost GPS for this purpose. The update rate of the GPS is only 1Hz. Our tests show that the measurement delay of the GPS is around 2-3 seconds, which can not be ignored. We explicitly model the delay T_d to obtain the transfer function from servo command to the GPS measured velocity angle β_d.

$$\frac{\beta_d(s)}{\delta_m(s)} = e^{-sT_d} \cdot \frac{k}{s(\lambda s+1)(s\tau+1)} \tag{15}$$

The simulated model output and the boat's actual response are shown in Figure 4, where blue line indicates the model output and the green line represents the actual velocity angle measured by GPS.

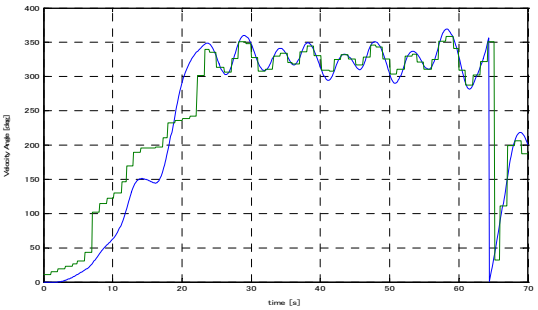

Figure 4. Validation of the translational model

2.3. Course-following Model

In application, a boat usually moves along a straight line course in most cases. The boat is considered to be on the track if it moves in the direction of the line, and at the same time the perpendicular distance to the line is around zero. Let us consider the case that the boat is commanded to move from starting point *A* to the goal point *B* along a straight line as illustrated in Figure 5. Without loss of generality, we take the starting point *A* as origin of the reference frame.

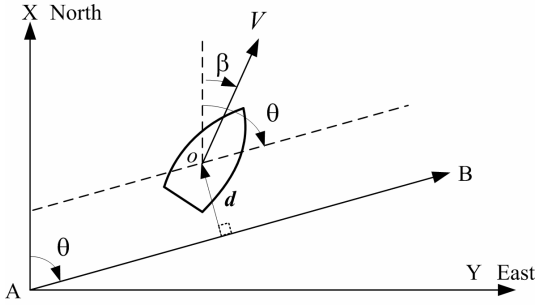

Figure 5. Line tracking configuration

The off track *d* is defined in Equation (16) which shows how far the boat deviates from the specified course.

$$d = \frac{\overrightarrow{AB} \times \overrightarrow{Ao}}{\overrightarrow{AB}} \tag{16}$$

Let γ be the difference between the boat's moving direction β and the course direction θ. The unit for angle expression is degree.

$$\gamma = \beta - \theta \tag{17}$$

Then the off track distance *d* satisfies Equation (18).

$$\dot{d} = |V| \cdot \sin\gamma \tag{18}$$

Under the condition of small variations around the line, Equation (18) can be approximated by Equation (19).

$$\dot{d} = |V| \cdot \pi/180 \cdot \gamma \tag{19}$$

The off course distance is calculated based on the position measured by GPS. Due to the delay in GPS measurement, the calculated off course distance is a delayed version. We use the same symbol to represent the measured off course distance as is shown in Figure 6.

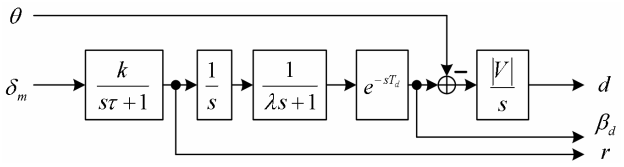

Figure 6. Block diagram of the plant model

Since the delay is infinite in dimension, we use its first order Padé approximation to get finite order model.

$$e^{-sT_d} \approx \frac{1 - s(T_d/2)}{1 + s(T_d/2)} \tag{20}$$

Its state space representation is described in Equation (21).

$$\begin{cases} \dot{\mathbf{x}} = \mathbf{A}\mathbf{x} + \mathbf{B}\delta_m + \mathbf{F}\theta \\ \mathbf{y} = \mathbf{C}\mathbf{x} \end{cases} \tag{21}$$

where

$$\mathbf{x} = \begin{bmatrix} r & \psi & \beta & \beta_d & d \end{bmatrix}^T$$

$$\mathbf{A} = \begin{bmatrix} -1/\tau & 0 & 0 & 0 & 0 \\ 1 & 0 & 0 & 0 & 0 \\ 0 & 1/\lambda & -1/\lambda & 0 & 0 \\ 0 & -1/\lambda & 1/\lambda + 2/T_d & -2/T_d & 0 \\ 0 & 0 & 0 & |V| \cdot \pi/180 & 0 \end{bmatrix}$$

$$\mathbf{B} = \begin{bmatrix} k/\tau & 0 & 0 & 0 & 0 \end{bmatrix}^T$$

$$\mathbf{C} = \begin{bmatrix} 0 & 0 & 0 & 0 & 1 \\ 0 & 0 & 0 & 1 & 0 \\ 1 & 0 & 0 & 0 & 0 \end{bmatrix}$$

$$\mathbf{F} = \begin{bmatrix} 0 & 0 & 0 & 0 & -|V| \cdot \pi/180 \end{bmatrix}^T$$

The numerical values of the parameters are listed in Table 2.

Table 2 Numerical values of the parameters

Parameter	Value
k	2
τ	0.4
λ	1.32
$\|V\|$	1.1
T_d	2

The plant model is unstable since it has two poles at origin which can be observed in Figure 6.

3. Controller Synthesis

The course following controller is required for the boat to be able to follow a spatially specified path which is studied as the path following or trajectory following problem. In [16], a line of sight guidance control for following straight line and circle trajectories is presented. More general trajectory following cases are discussed in [17,18]. In general, these approaches first parameterize the tracking error in a proper way and then construct a nonlinear control law to force the tracking error to

approach zero asymptotically. Numerical simulation results have demonstrated good tracking performance. However, it is not clear on the performance in real sea condition.

We design the controller to follow straight line segmented course which is specified by waypoints. It is believed that this is the most used application mode. The controller design will be based on the mathematical model developed in last section. The model keeps a simple form under the condition of several assumptions. However, the discrepancy between the reality and the assumptions exists, which is one source causing model error. For example, we assume that the boat's speed does not vary in the course of yaw change which in fact does decrease. Another source of model error comes from the ignored dynamics such as the effect of waves. The model error can be mitigated by refinement, i.e. using nonlinear model. This option will increase model accuracy, but may lead to complexity in controller, which is not desirable. Instead of trying to improve the model, we apply robust control theory to design controller in the presence of model error.

H_∞ optimal control is one popular scheme in robust control theory. It is formulated under the small gain theorem and can guarantee robust stability with norm-bounded model uncertainty [19]. While the small gain stability condition can be directly expressed by using H_∞ norm, yet there are cases where H_∞ norm can not best interpret the performance specifications. Mixed H_2/H_∞ approach is one method that addresses the performance objectives in both H_2 norm and H_∞ norm [20]. The mixed $H2/H_\infty$ method has been successfully applied in applications such as vibration control of flexible structures [21], robust fault detection [22] and so on.

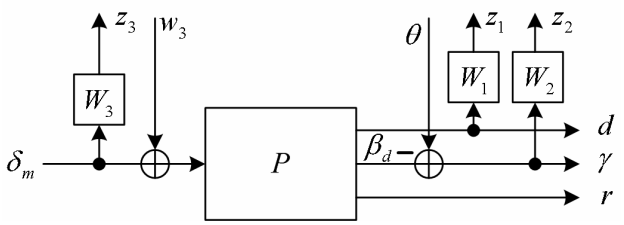

Figure 7. The generalized plant for controller design

In the course following control, the objective is to keep the boat's moving direction error γ and the off track distance d both be small. These can be seen as variations around the reference course when influenced by random disturbances. The variance should be kept to be small in order to follow the course. This performance requirement is naturally translated into H_2 control problem. The ignored disturbance and unmodeled dynamics are treated as input multiplicative model uncertainty on the fact that both wind and wave disturbance can be regarded as external inputs to the boat. In Figure 7 we show the generalized plant for controller synthesis. The plant model as depicted in Figure 6 has one control input: the rudder command and three measured outputs: the off track distance, the moving direction and the yaw rate. The input θ is the reference course angle which can not be manipulated for control. The controller will manipulate the rudder command to achieve course following goal.

The block P in Figure 7 refers to plant model as described by Equation (21).

Let J_2 and J_∞ be defined as follows:

$$J_2 = \left\| G_{\begin{bmatrix}\theta \\ w_3\end{bmatrix}\to\begin{bmatrix}z_1 \\ z_2\end{bmatrix}} \right\|_2 \tag{22}$$

$$J_\infty = \left\| R_{\begin{bmatrix}\theta \\ w_3\end{bmatrix}\to[z_3]} \right\|_\infty \tag{23}$$

where G and R represent the corresponding closed loop transfer functions between the inputs and outputs as stated in Equations (22) and (23) respectively, then the design objective can be concisely described as: subject to the constraint $J_\infty < 1$, find controller K which minimize J_2.

The weighting functions W_1 and W_2 are chosen to balance the performance of direction keeping and track following. Due to the boat's nonholonomic motion, actions trying to minimize one performance index will likely worsen the other. When large emphasis is placed on direction keeping, the boat becomes difficult to turn. On the other hand, if too much emphasis is placed on the off track error, the boat will be too aggressive to return back to the course and may oscillate to progress slowly in the direction of the reference course. The weighting functions used in this design are shown in Figure 8 which has been verified in our experimental investigation. When the synthesis problem is well formulated, the controller can be found by LMI solver efficiently. We use the MATLAB toolbox to complete the design.

The robust stability is verified in evaluating the H_∞ norm of the system R in Equation (23). We show its singular value plot in Figure 9 which show that the robust stability condition $J_\infty < 1$ is satisfied.

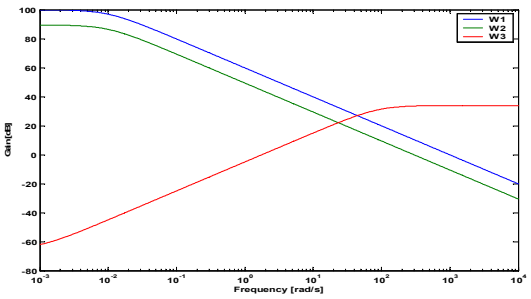

Figure 8. Gain plot of weighting functions

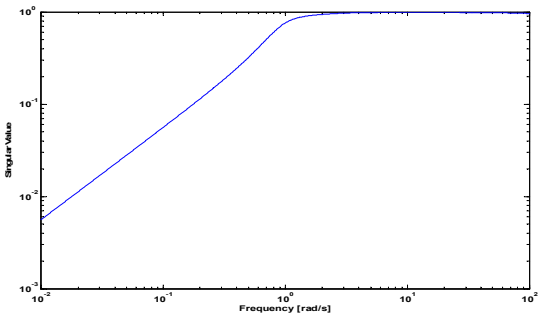

Figure 9. Singular value plot of system R

4. Testbed Description

The boat under study is a product of Coden company. Its picture is shown in Figure 10. The screw is propelled by two DC motors and the rudder is actuated by a servo motor. The boat is remotely controlled through IEEE 802.11 wireless LAN. GPS and sonar sensor are standard equipment available on the boat. We installed another gyroscope to measure yaw rate. The GPS and the gyroscope are the necessary sensors for the purpose of control. We show the specifications of the boat and sensors in Table 3 and Table 4 respectively.

Figure 10. The boat in the sea

In implementing the control algorithm, we take advantage of the existing remote control infrastructure. The control computer takes the role of a human operator. It receives sensor data from boat, executes the control law and sends the rudder command to the boat. The computer we used is a Pentium III laptop with 256 MB RAM. The operating system is Windows XP.

Table 3 Specification of the boat

Item	Description
Length	1060 mm
Width	250 mm
Mass	12 kg
Propelling Source	DC motor
Endurance	60 minutes
Maximum Speed	1.2 m/s

Table 4 Sensor Specifications

Sensor	Specifications
GPS	• Position accuracy: 15m (2dRMS) • Velocity accuracy: 0.04 m/s in magnitude; 0.14 degree in angle • Position resolution: 0.001' (1.8 m) • Velocity resolution in magnitude: 0.1 m/s • Velocity resolution in angle: 0.1° • Update rate: 1Hz
Gyroscope	• Gyro nonlinearity: 0.2% • Gyro bias stability: 0.7°/s

5. Experimental Results

The designed controller is tested through sea trials to evaluate the performance. We present the experimental results of following straight line connected course specified by waypoints. The first case is a square course with lateral length of 100m. The boat's trajectory, its moving direction and the off course distance are shown in Figures 11, 12 and 13 respectively. Another test case is to follow a hexagon with equal side length of 50m. The corresponding results are shown in Figures 14, 15 and 16.

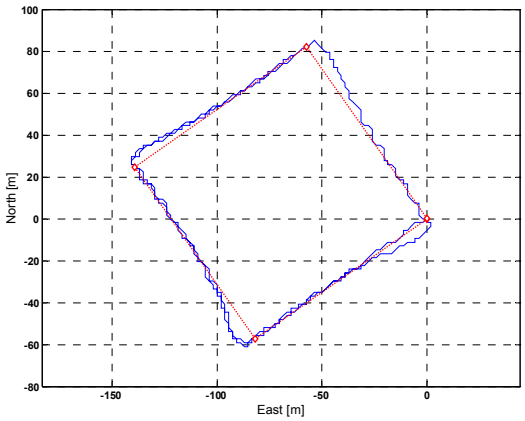

Figure 11. Trajectory of the boat following a square. The red line shows the reference trajectory and the blue line indicates the actual trajectory

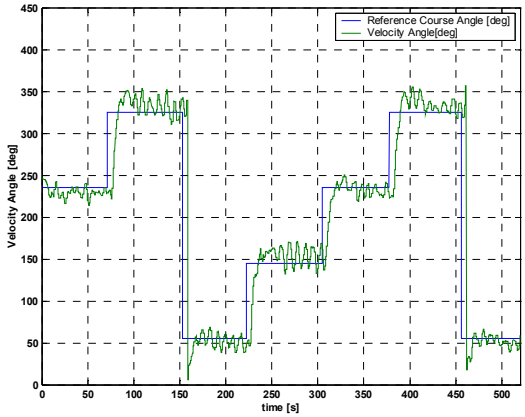

Figure 12. The boat's moving direction and the reference course angle. The blue line shows the reference course angle and the green one show the boat's actual moving direction.

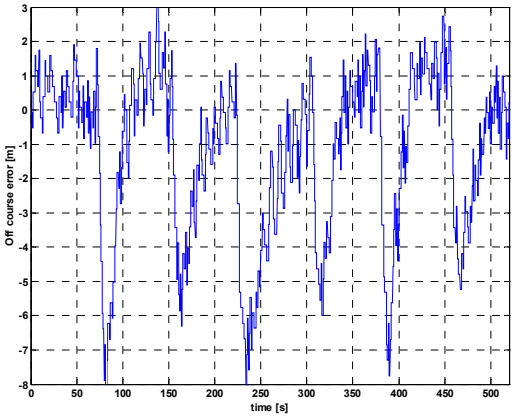

Figure 13. The off course error in the square course following case

In both cases, the boat moved in clockwise with the starting point at the origin. In Figures 11 and 14, the red line is the reference course, and the blue line is the boat's actual trajectory measured by GPS. In the square course

case, the boat travelled a 700m distance, and in the hexagon course case it went as far as 400m.

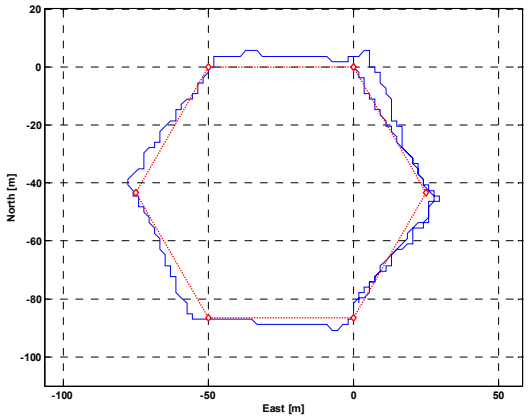

Figure 14. Trajectory of the boat following a hexagon. The red line shows the reference trajectory and the blue line shows the boat's actual trajectory

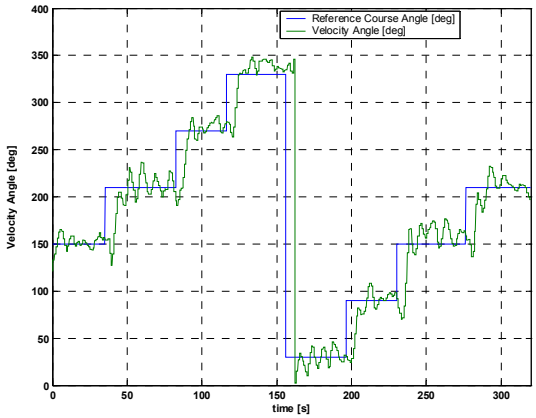

Figure 15. Reference course angle and the boat's moving direction in hexagon course case. The reference angle is indicated by blue line and the acutal moving direction by green one.

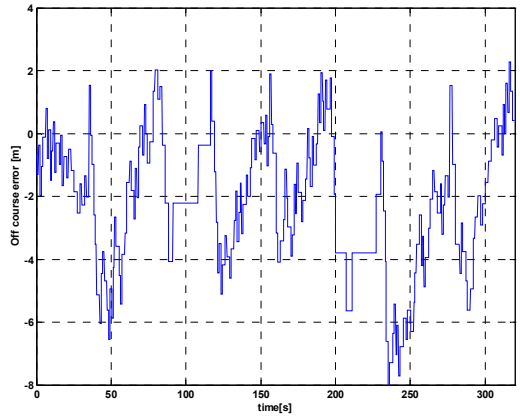

Figure 16. Off course error in hexagon course following case

The direction following performance is indicated in Figures 12 and 15. We can see that the boat move around the reference direction to steer the boat to go on the course as near as possible. The off course errors are shown in Figure 13 and Figure 16. Except for the time of turning, the off course error is less than 2 meters which is the least distance that the GPS we used can measure. After turning, the off course error decreases as the boat approaches to the reference course. The GPS resolution issue is evident by the jumps in the data as shown in Figures 13 and 16. In Figure 16, the data frozen occurred around 100s and 220s may be caused by GPS degradation, yet the exact reason is not clear.

In Figure 17, we show the distribution of off course error. This is done on all data including both the square and hexagon course cases. It shows that in most of the time, the track error lies in between ± 4 meters in the total travel of 1.1km. The overall standard deviation of the off course error is 2.3m. If we exclude the turning portion, the standard deviation is 1.4m. The negative tracking error is due to the fact that the boat is following courses with clockwise turns. The off course error builds up negatively when the boat initiates a clockwise turn. The experiments were done in the sea with the wave height of about 0.5m.

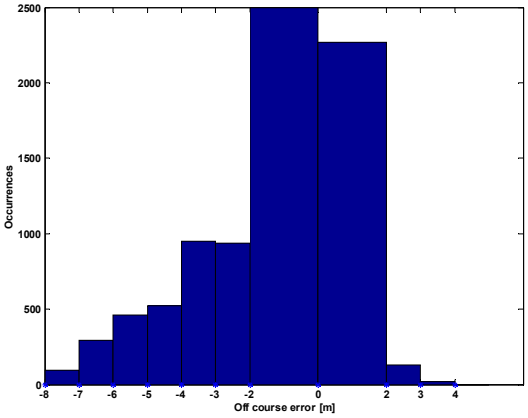

Figure 17. Distribution of the off course errors

In evaluating the performance, we made a rough comparison with previous research where experimental data were provided. In Table 5 we show the data reported in [6, 12, 24].

Table 5 A comparison of course keeping performance

Platform	Mass	Position By	Max. Error	Std. Error
Catamaran[12]	320kg	DGPS	1.5m	*
Ferry ship [24]	*	DGPS	5m	3m
Model boat [6]	*	RTK GPS	1m	*
The boat in this study	12kg	Low cost Standalone GPS	2m	1.4m

The '*' marks mean that the data are not available in the sources. DGPS refers Differential GPS and RTK GPS means Real Time Kinematic GPS.

The rough comparison indicates the good performance achieved by the proposed approach despite of its light weight and less accurate GPS. The performance can be improved if we use more expensive GPS with better accuracy and faster update rate such as DGPS or RTK GPS.

6. Conclusion

In this work, we have designed and verified a course following controller for a small boat with low-cost GPS and gyroscope. The total sensor cost is less than $100. We have derived a simple mathematical model to express the dominant dynamics of a boat for course following. This model enables us to design controllers without using a compass. The model error and environmental disturbance are handled by applying robust control theory. We use mixed H_2/H_∞ approach to optimize the course following performance measured in H_2 norm while maintaining the robust stability in the measure of H_∞ norm. The performance of the designed controller has been proved by our sea tests. The overall standard deviation of course following error is 2.3m in the total 1.1 km sea tests. The standard deviation of the course keeping error is 1.4m. The experimental data show that the integrated modeling and control approach for the course following control of the small autonomous boat with low cost sensors is robust and effective.

7. Acknowledgements

This study is carried out in the joint research project between Chiba University and Coden. Co, Ltd.

8. References

[1] P. Ridao, M. Carreras, J. Batlle and J. Amat. O2CA2: A new hybrid control architecture of a low cost AUV. IFAC conference CAMS'2001, Glasgow, Scotland, U.K., 18-20 July, 2001.

[2] J.M. Roberts, P.I. Corke and G. Buskey. Low-Cost Flight Control System for a Small Autonomous Helicopter. In Proc. 2002 Australasian Conference on Robotics and Automation, 2002.

[3] W. Pisano, D. Lawrence, and S. Palo. Low-cost UAV Avionics for Autonomous Antenna Calibration. Infotech@Aerospace, Arlington, Virginia, 26-29 September, 2005.

[4] G. Beidler and R. Wall. Low Cost Distributed Control for Autonomous Vehicles. In Proceedings of Oceans'06 Asia Pacific IEEE, Singapore, 16-19 May, 2006.

[5] T. I. Fossen and J. P. Strand. Passive nonlinear observer design for ships using Lyapunov methods: full-scale experiments with a supply vessel. Automatica, Vol. 35, pp. 3-16, 1999.

[6] S. D. Lee and C. Y. Tzeng. A study on model ship track-keeping autopilot design and experiment. International Marine Simulation Forum, Belgium, 13-17 September, 2004.

[7] T. A. Bean, A. Okamoto, J. R. Canning and D. B. Edwards. A nonlinear fuzzy logic controller developed for an autonomous surface boat. In Proceedings of IDETC/CIE 2005, Long Beach, California, USA, 24-28 September, 2005.

[8] T.I. Fossen. A Survey on Nonlinear Ship Control: from theory to practice. In Proc. IFAC MCMC'2000, Aalborg, Denmark, 2000.

[9] G. Elkaim and R. Kelbley. Control Architecture for Segmented Trajectory Following of a Wind-Propelled Autonomous Catamaran. In Proceedings of the AIAA Guidance, Navigation, and Control Conference, 24-26 August, 2006.

[10] J. Curcio, J. Leonard and A. Patrikalakis. SCOUT – a low cost autonomous surface platform for research in cooperative autonomy. In Proceedings of MTSI/IEEE, 2005.

[11] B. Zhang and G.S. Sukhatme. Adaptive Sampling for Estimating a Scalar Field using a Robotic Boat and a Sensor Network. In Proceedings 2007 IEEE International Conference on Robotics and Automation, 2007.

[12] J. Alves, P. Oliveira, R. Oliveira, A. Pascoal, M. Rufino, L. Sebastião and C. Silvestre. Vehicle and Mission Control of the DELFIM Autonomous Surface Craft. In Proc. MED2006 – 14th Mediterranean Conference on Control and Automation, Ancona, Italy, 2006.

[13] K. Nomoto, K. Taugchi, K. Honda and S. Hirano. On the steering qualities of ships. International Shipbuilding Progress. Vol. 4, pp.354-370, 1957.

[14] J. V. Amerongen. Adaptive steering of ships: a model reference approach to improved manuvering and economical course keeping. PhD thesis, Delft University of Technology, 1982.

[15] P. Tristan and B. Mogens. Mathematical Ship Modeling for Control Applications. Technical Report, Technical University of Denmark, 2002.

[16] M. Breivik and T.I. Fossen. Path Following of Straight Lines and Circles For Marine Surface Vessels. In Proc. of the IFAC CAMS'04, Ancona, Italy, 2004.

[17] K.D. Do, Z.P. Jiang and J. Pan. Robust adaptive path following of underactuated ships. Automatica, Vol. 40, pp. 929-944, 2004.

[18] P. Encarnação and A. Pascoal. Combined Trajectory Tracking and Path Following for Marine Vehicles. In Proc. 9th Mediterranean Conference on Control and Automation. Dubrovnik, Croatia, 2001

[19] K. Zhou, J.C. Doyle and K. Glover. Robust and Optimal Control. Prentice-Hall, Inc, 1996.

[20] C. Scherer, and S. Weiland. Linear Matrix Inequalities in Control. Lecture Notes, 2005.

[21] M.S. Whorton. High performance, robust control of flexible space structures. PhD thesis, Georgia Institute of Technology, 1997.

[22] A. Ríos-Bolívar and G. Garcia. Robust fault detection based-on H_2-H_∞ control for discrete-time linear systems. ICGST ACSE 05 Conference, 19-21 December 2005, CICC, Cairo, Egypt.

[23] C.Y. Tzeng, G.C. Goodwin and S. Crisafulli. Feedback linearization design of a ship steering autopilot with saturating and slew rate limiting actuator. Int. J. Adapt. Control Signal Process.

[24] T. Holzhuter. LQG approach for the high-precision track control of ships. IEE Proc. – Control theory and Applications. Vol. 144, Issue 2, pp.121-127, 1997.

Zhenyu Yu received his BS degree in Electronics and Communication Engineering from Beijing Information Technology Institute, China, in 1997, and his M.S.E degree in Electronics and Mechanical Engineering from Chiba University, Japan, in 2005. He is currently on his PhD course study in Chiba University. His research interests include robotics, autonomous vehicles, robust control theory and applications.

Xinping Bao was born in Shandong, China. He received the Master degree in Mechanical Manufacture and Automation from XIDIAN University, China, in 2004. Currently, he is in his first year PhD study in graduate school of engineering at Chiba University, Japan. His research interests include hydrodynamics, nonlinear control, and intelligent control.

Dr. Kenzo Nonami received MS degree and Ph.D. degree in Mechanical Engineering in 1976 and 1979 respectively, from Tokyo Metropolitan University. He joined Chiba University in 1979 as a Research Associate, Associate Professor from 1988 to 1994. Since 1994, he has been a full professor in Department of Mechanical Engineering and Department of Electronics and Mechanical Engineering at Chiba University. In 2004, Dr. Kenzo Nonami was a vice dean of faculty of engineering. Also, he has carried out a research in NASA in USA during two years from 1985 to 1988. His recent research interests are Land mine detection robots with multi-functional arm, Walking machines, Master slave manipulator and hand systems, Fully autonomous unmanned small-scale helicopter, Micro air vehicle, Quad tilt wing unmanned aerial vehicle, Unmanned autonomous boats, Energy storage flywheel by Active magnetic bearing system, Robust and nonlinear control, Control applications.

www.icgst.com

A Combined Framework on Fuzzy Based Call Admission Control and Optimized Bandwidth Allocation Technique in Cellular Mobile Networks

N.K. Karthikeyan*, P. Narayanasamy**
* *CSE Department, Sri Krishna College of Engg & Technology,* Coimbatore 641 008, Tamil Nadu, India
**CSE Department, Anna University, Chennai 600 02, Tamil Nadu, India
E-mail: karthiaish@rediffmail.com, sam@annauniv.edu

Abstract

Present mobile multimedia networks have different Quality of Service (QoS) requirements for diverse applications starting from voice to Multi Media Services (MMS) with major objectives such as better admission control, effective bandwidth utilization, support for real-time and non- real time applications content transfer, mobility etc. So the network aims at satisfying their demands without much degradation of quality in terms of delay call dropping and call blocking. It is possible by admission control algorithms and by optimizing the existing resources in an effective way. It improves the overall performance of the network system.

This paper addresses different Quality of Service (QoS) requirements of the users of a cellular network with a focus on fuzzy based Call Admission Control Scheme (CAC) and optimized bandwidth allocation using Linear Programming (LP) analytical model. For comparison, Meta heuristic technique- Simulated Annealing (SA) is also used. We propose a novel combined framework model to address resource allocation problem. This problem can be dealt with two critical issues in a cellular mobile multimedia networks namely Admission control and Transmission control. The admission control – the decision to admit or reject the calls based on fuzzy logic concepts. Transmission control – Bandwidth allocation using LP technique and SA method. We demonstrate the efficiency of the proposed framework model by combining fuzzy based admission control scheme and optimized techniques in bandwidth allocation, which provide better QoS differentiation and efficient usage of scarce radio resource such as bandwidth in multimedia cellular networks.

Keywords: *Call admission control, fuzzy logic, bandwidth allocation, linear programming, QoS, simulated annealing.*

1. Introduction

The tremendous growth of mobile network technology has increased the need for better admission control strategies and efficient utilization of resources such as bandwidth, to provide a better Quality of Service (QoS). In particular, QoS provisioning in Third Generation (3G) and Fourth Generation (4G) mobile networks is a challenging problem due to the scarcity of wireless resources and different QoS service class requirements.[1-2]. CAC is a fundamental mechanism used for QoS provisioning in networks. In literature most of the admission control algorithms have been dealt with Asynchronous Transfer Mode (ATM) networks [3] which are not applicable to mobile networks due to its limitations such as scarce radio resources, power control etc. The admission control for mobile networks based on thresholds were addressed in papers [4-5]. Here different admission policies are applied to different regions and threshold values separate the regions. But determining the values for the thresholds that separate those regions is a critical problem. Another AC method by the authors of [6] use a decision-theoretic approach based on Markov Decision Process (MDP). But large number of states in Markov model makes it unsuitable for real-life problems. This can be eliminated by a fuzzy logic based admission control method that is less computationally intense and it also allows embedding initial knowledge about the system behavior by means of its membership function (MF), antecedents and consequence of fuzzy rule. Paper [7] focuses on fuzzy CAC that estimates the effective bandwidth of call request from mobile station and its mobility information and makes a decision to accept or reject connection request based on estimation and resource availability. In paper [8] the authors addresses the optimal number of guard channels in a base station to make an effective use of resources. In the recent paper [9] the authors compare their algorithm with Shadow Cluster Concept with better accepted connections.

Providing better resource utilization [bandwidth, buffer, power] and ensuring QoS `guarantees to various applications are important objectives in next generation 4G cellular networks. Because it targeted at supporting various applications like voice, data, image with enhanced data rate, QoS, security, location awareness etc., a number

of bandwidth adaptation techniques exist in the literature. The papers [10-12] deal with the bandwidth estimation for multimedia networks in distributed network environment. Levine et al [13] proposed predictive resource allocation, which deals shadow cluster concept. The major limitation of this method is its large overhead. Priority based AC was proposed in [14]. The better utilization of network bandwidth using measurements based methodology is dealt in [15]. In [16], bandwidth reservation method was suggested but it has the drawback of unfair bandwidth utilization. Papers [17-19] mainly deal with a much complex mathematical model with only minimum improvement in the overall performance of cellular mobile and adhoc networks. The paper [20] uses a proportional fairness in bandwidth allocation so as to tolerate transient fluctuations using bandwidth-borrowing concept. The paper [23] deals with Linear Programming [LP] based resource reduction.

All the schemes used above deals either with CAC based on fuzzy concept or Bandwidth optimization in a mobile multimedia networks as a separate issue. But we address the two critical issues in cellular networks – Fuzzy Classification based Admission Control (AC) – Decision to admit or reject calls based on fuzzy rules and resource – bandwidth allocation in optimized way by admitting more number of applications using LP and SA techniques in a novel single framework model.

We organize the rest of the paper as follows. Section 2 presents the system and network model of a typical cellular system. In section 3 a new combined framework for CAC and optimized bandwidth allocation is proposed. Section 4 presents optimization using LP method. Section 5 addresses SA scheme and Section 6 addresses fuzzy AC scheme results. In section 7 the results of optimization using LP and SA are obtained. Section 8 concludes the paper.

2. Systems and Network Model

Figure 1 shows a typical multimedia wireless cellular network system with hexagonal shaped cells. Each cell has a base station (BS), which allocates and reserves bandwidth for mobile stations (MS). The MS communicate with their home BSs via the air interface and a number of BSs are connected to Base Station Controllers and finally to a Mobile Switching Center (MSC), which in turn is connected to the backbone wire line networks. The bandwidth can be shared for 03 types of applications namely Running, Hand-off and New applications**.** [23]

Already scheduled applications of any type are called as running applications, while the calls that move from adjacent cell to the reference cell are called as hand off applications. The new calls from the same reference target cell are known as new applications. The design of effective CAC should admit calls based on two QoS classes: hand off calls and new calls. Here the admission is based on real-time or non-real time applications with real-time as the higher priority.

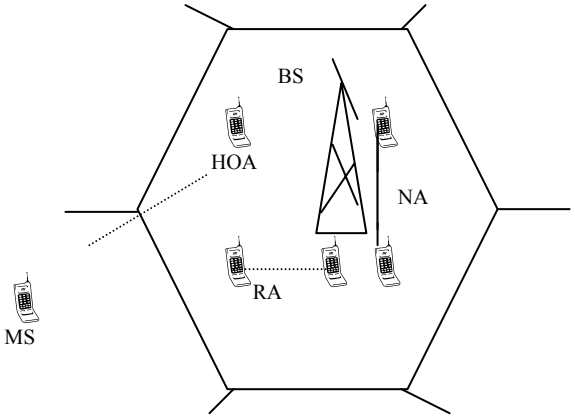

MS: Mobile Station
BS: Base Station
RA: Running Application
NA: New Application
OA: Hand-off application

Figure 1.Cell Network Model

3. Proposed framework for CAC and Bandwidth Allocation:

The proposed work involves two main modules as shown in figure 1: Fuzzy based admission control and Transmission control using optimized bandwidth Allocation. AC schemes using threshold's based on network load were proposed in [21-22]. The major problem of these schemes is the determination of the threshold values that divide the bandwidth regions. We attempt to define parameter like network load as fuzzy linguistic variable with the term low, medium and high. The transition from small to medium or from medium to high is a region associated with network load. So In the first module the inputs are network load and precedence. The fuzzy inference- process of composition between facts and rules is used. There are nine fuzzy rules defined to relate premises and conclusion to make the admission decision. Here admission control is used to admit many mobile networks with delay as one of the QoS performance requirement. Weighted Round Robin (WRR) is used since it is a good approximation of the Fluid Fair Queuing (FFQ) model and widely used in wireless networks.

The second module focuses on bandwidth allocation for various admitted applications with various QoS service classes, namely Hand-off real time, new real time, hand-off non-real time and new non real time applications. Without any optimization scheme, maximum bandwidth is allocated to each running or scheduled application. But using optimization schemes, bandwidth reduction without violating minimum QoS is obtained. The optimized output facilitates admission of more number of hand-off and new QoS applications into the cell. For comparison LP and SA based optimization schemes were used.


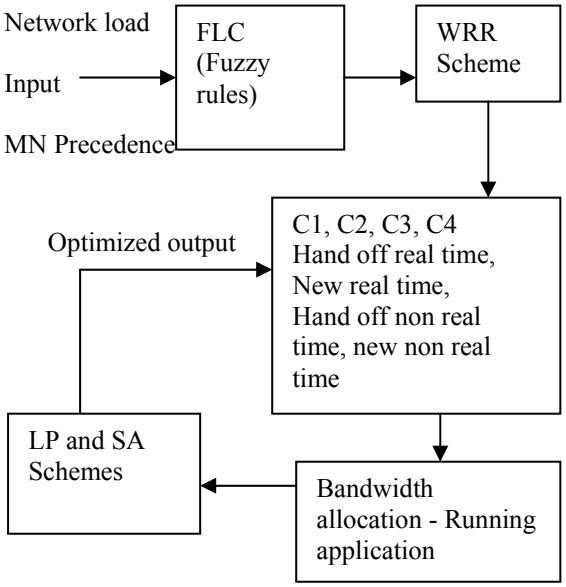

Figure 2. Proposed Framework of AC and Bandwidth Optimization

3.1. Fuzzy logic System

In set theory, if an object is an element of a set then its characteristic function is 1. Otherwise, its characteristic function is 0. It does not allow for partial membership called crisp set.

$$\text{Input } H(x)= \begin{cases} 1 & x \in A \\ 0 & x \notin A \end{cases}$$

The degree of membership in a fuzzy set, an object may belong partially to a set. In a fuzzy set the degree of membership is measured by generalization of the characteristic function called the membership function [24]. The basic building block of of a typical fuzzy system is shown in figure 3.

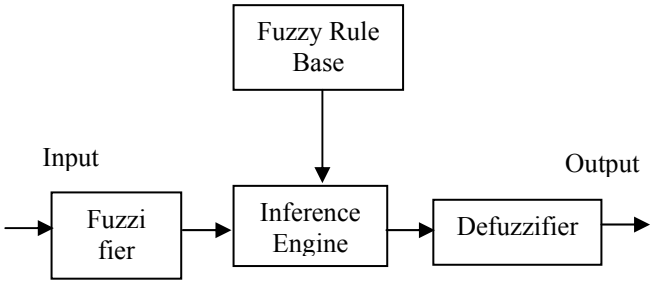

Figure.3 Block Diagram of fuzzy system

$\mu_A(x): X \rightarrow [0,1]$

A fuzzy rule can be expressed in the form "if *premise* then *conclusion*", where the premise can be simple or composed, If composed, it can be expressed in the form of

$$\text{Premise} = \text{premise}_1 \text{ AND premise2 OR} \ldots \text{Premise}_n,$$

Where the logical operators AND, OR, NOT can be used for composition [25]. In our case, we use AND operators.

3.2. Weighted Round Robin – Time delay

For Call Admission Control, Fuzzy Logic Controller is used. It is based on papers [25-26]. The linguistic variables in premises are network load and mobile nodes precedence. Network load is defined as the number of active nodes at a time period in a cell. Mobile node request precedence is weight or priorities given based on the type of request.[24-25] For example, handoff requests are given more priorities than new call request since dropping of a call during handoff is more vulnerable than blocking of new call. Both network load and precedence are having the terms low (L), medium (M) and high (H), while linguistic variable in conclusion is admission decision, with the term defined by Strong Accept (SA), Weak Accept (WA), Strong Reject (SR) and Weak Reject (WR). The delay for each QoS class is proportional to network load. The QoS requirement of the mobile nodes is met with Weighted Round Robin (WRR) scheme [26].

In the routers having multiple queues for each output line, (one for each source), When a line becomes idle the router scans the queue in a round robin fashion. It gives all hosts the same priority. But in many situations in multimedia networks it is desirable to give different QoS. For this WRR is chosen, since it is a very good approximation of fair queuing. The sending delay experienced by Mobile Node (MN_i) is given by following expression.

$$\text{Sending delay} = FL\ \Sigma_i (K_i W_i) / B_{avr}.W_i \quad \text{cntr-cycle}$$

$$\text{Network load} = \Sigma\ K_i.W_i / B_{avr}$$

Where sending delay is the time necessary to transfer a file of length FL, from a MN_j belonging to the QoS class i. While W_i is the weight assigned to a MN from class i. The sum is obtained from all MNs that are active. B_{avr} is the average number of channels allocated for mobile networks and center cycle is 20ms. The WRR algorithm with sending delay experienced by MN *j* for our problem is given below:

```
// Calculation of sending delay in sending a file length
belonging to specified class//

for {each connection}
  {
    min =   findSmallestNormalizedWeight();
    load[i] = number of active mobilei].weight of the
call[i]/min
     SendingDelay[i]=
FileLength.sum(load[i]/AvgNoChannels;
    i++
   }
for {each connection}
    sending delay < QoS TimeLimit
    acccept call
 else
     reject call
// call dropping and call blocking are determined by the
type of call request //
```

The following table I shows the nine rules used to implement fuzzy AC algorithm. In the Fuzzy Logic Controller, as discussed previously, the network load and

the mobile node precedence are used as inputs and output is the admission decision for the new user. Figure 4 shows linguistic terms Low, Medium and High in premises with m=63. Figure 5 shows the parameters b1, b2, b3 and b4, having the value as b1=8 (SR), b2=24(WR), b3=40(WA) and b4=56(SA). For an FLC output of less than m/2 the user will be rejected and greater than m/2 the user will be admitted. The FLC used in this paper is based on [25].

Table 1. The fuzzy rules

		MNs precedence		
		L	M	H
Network Load	L	WA	SA	SA
	M	WR	WA	SA
	H	SR	WR	WA

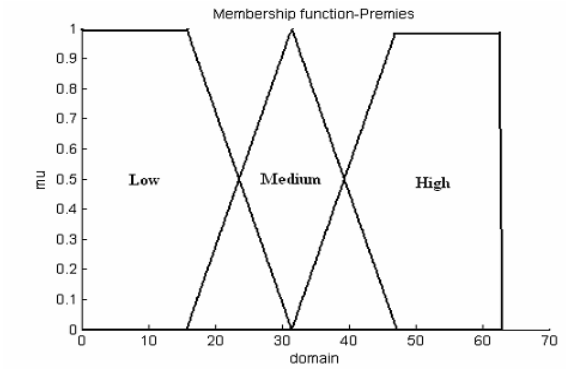

Figure 4: The Fuzzy terms in premises (Network load and MNS precedence)

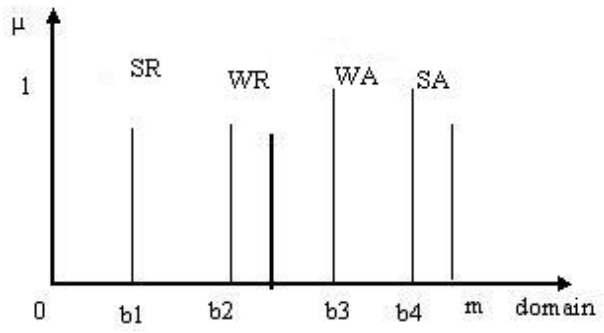

Figure 5.Fuzzy conclusion (Admission decision)

In our fuzzy approach the purpose of AC scheme is to admit many mobile nodes with varying QoS classes.

CLASS 1 (Hand-off real time Applications) – C1

This traffic class deals with calls arrival from neighboring cells in real-time. It includes Voice Service, Audio Phone, Video Phone, and Video Conference. These are Constant Bit Rate (CBR) services. A very high value of weights is assigned.

CLASS 2 (New real time Applications) – C2

This traffic class is calls arrival within the target cell in real-time. It also includes Audio Phone Video Conference services. Moderate value of weights is assigned.

CLASS 3 (Hand-off non- real time Applications) – C3

This traffic class deals with calls arrival from neighboring cells in non real-time. It includes Email, Paging, Fax and File Transfer. These are unspecified Bit rare (UBR) services of large bandwidth requirement.

CLASS 4 (New non- real time Applications) – C4

This traffic class are calls arrival within the target cell in non real-time. The weights assigned are little less than Class 3 since handoff calls are given higher priority than new incoming calls into the cell.

4. Results – Fuzzy AC Scheme

The results that are presented here demonstrate the capability of fuzzy AC algorithm to maintain the network load close to a target value and maintain the transfer delays close to a target value for each QoS class. Also comparison between fuzzy AC and Non-fuzzy based on fixed thresholds is applied.

The simulation using MATLAB 7.0 for comparison of sending delay for 04 classes were shown in figure 6 to 9. In simulation the weights used for the QoS classes are as follows. For Class 1 it is 1, for class 2 it is 0.7, for class 3 it is 0.3 and for class 4 it is 0.The simulation environment is composed of hexagonal cell with six neighboring cells. Each cell is allocated with eight channels. The number of active mobile nodes is randomly distributed**.** The time delay required for each class of service is calculated using WRR queuing model. The sending delay is calculated from WRR. And the same is plotted for four service classes by comparing it with non-fuzzy model. The fuzzy based admission control need not rely on assumptions concerning probability density functions of the parameters. The sending delay limit for real time traffic class and non real time traffic class for both hand-off and real time calls are plotted as shown in figures 6 to 9. Figure 10 represents *Sending Average Delay* for four traffic classes {handoff real time, new real time, handoff non real time, new non real time}.

Class 1: Hand-off real time calls:

It is a constant bit rate services with very high QoS in terms of minimum delay. It includes audio, video services. The sending delay is restricted to 400 ms for real-time call requests. The file length assumed for interactive audio and video services are 1-10Kbps.

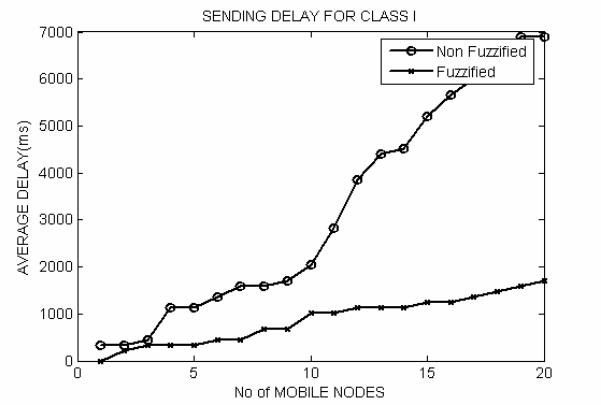

Figure 7: Sending delay of class 1

Class 2: New real time calls:

It is a constant bit rate service with very high QoS in terms of minimum delay. It includes audio and video services. The sending delay is 450 ms and file length is 1-10 Kbps.

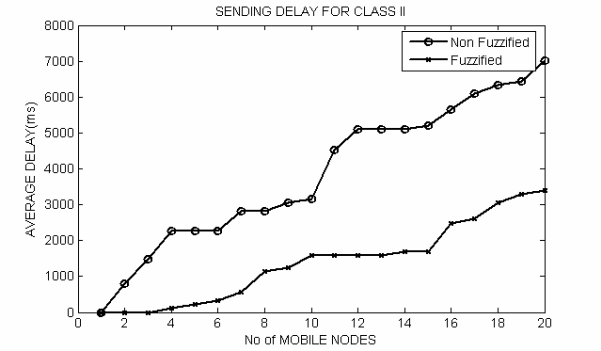

Figure 8: Sending delay of class 2

Class 3: Hand-off non real time calls:

It is an unspecified bit rate service with dedicated reactive flow supports for streaming applications. It includes file transfer, audio/video down load services and adaptive video. The sending delay is restricted to 4 seconds for non real time call requests. The file length assumed for non real time services are 1-10 Mbps.

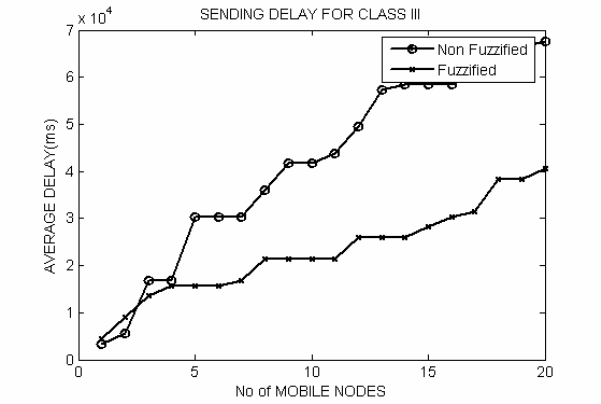

Figure 9: Sending delay of class 3

Class 4: New non real time calls:

It is unspecified bit rate services with dedicated reactive flow and includes file video/video download services and adaptive video. The sending delay is restricted to 6 seconds for non real time call requests. The file length assumed for non real time services are 1-10 Mbps.

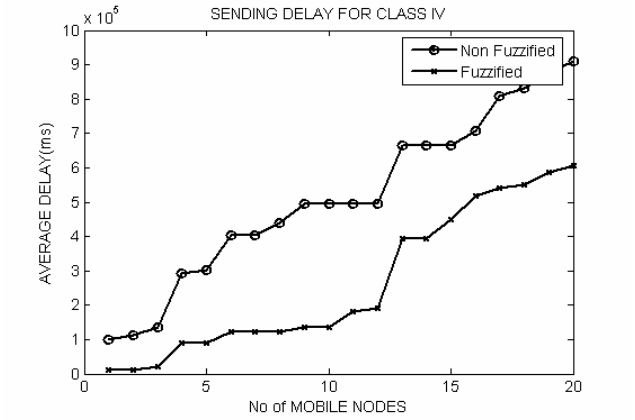

Figure 10: Sending delay of class 4

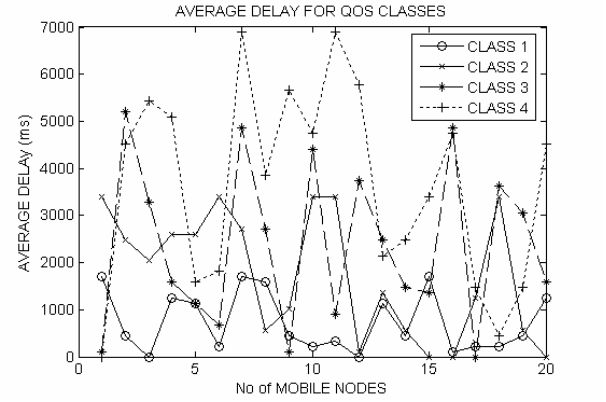

Figure 11: Average delay of QoS classes

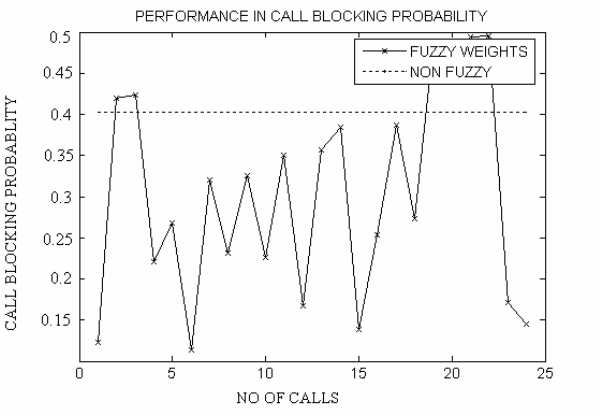

Figure 12: Performance in Call Blocking Probability using Fuzzy Logic

The performance of fuzzy AC algorithm is compared with non fuzzy AC algorithm based on threshold. The results show that in non fuzzy the call blocking probability is approximately 0.4 and using fuzzy logic by assigning different weights defined according to the traffic classes reduces the Call Dropping Probability to 0.23. The

simulation result using fuzzy and non fuzzy approach is shown in figure 12 above.

5. Optimization using LP

In our problem bandwidth is used as a constraint for optimum resource allocation for multimedia mobile networks. The optimization algorithm deals with formulation of optimization problem and then identifying important design variables that can be changed in a design. The next task is to formulate objective function with minimum or maximum function. The final task is to identify some bounding limits for design variables [27].
Effective and efficient resource allocation is essential for cellular mobile network system that supports various applications. The objective of resource allocation is to decide how to allocate resources such as bandwidth, meeting the QoS requirements for all the applications. In general, multimedia connection has several service classes, each of which presets a range of feasible QoS levels (e.g., data rates).

The principle used here is mainly devoted to admission control by maintaining QoS guarantee to existing applications and to increase the percentage of admission to real time and non-real time application, using LP based resource reduction method. The LP-Resource Reduction minimizes the allocated bandwidth of already scheduled applications without degradation in QoS. It is helpful in obtaining a large quantity of available resources for scheduling the remaining hand-off and new applications. The LP method [18] for given problem is given as below.

$$\text{Maximize} \quad \sum_{i=1}^{r} C_i R_i \tag{1}$$

$$\text{Subject to} \sum_{i=1}^{r} R_i \le (1-\Omega)(P-\Theta) \tag{2}$$

$$R_i^{\min} \le R_i \le R_i^{alloc} \tag{3}$$

$$R_i \ge 0, \forall i \in [1, r] \tag{4}$$

Where R_i is the decision variable to be solved to provide new bandwidth for running applications on solving above problem. C_i Is the weight function defined as $C_i = (R_i^{max} - R_i^{alloc}) / (R_i^{max} - R_i^{min})$. Ω is the reduction parameter and P is the maximum bandwidth and Θ is the remaining bandwidth. Note that each running application has different bandwidth requirements. The optimized Bandwidth requirement of each application is calculated using LP reduction using simplex algorithm.
To illustrate the proposed approach, the following problem is solved for typical running application r=5.

Where P=300 Kbps, Ω =0.1 and Θ = Remaining bandwidth after allocation. This can be explained with the following case study using LP.

Find $(R_1, R_2, R_3, R_4, R_5)$ so as to maximize
$f_1 = (C_1 R_1, C_2 R_2, C_3 R_3, C_4 R_4, C_5 R_5)$.

Subject to constraints as in equation 3 and 4 above.
The software TORA is used to solve the problem. The individual optimal solution of the 05 running applications are $(R_1, R_2, R_3, R_4, R_5)$ = (40 kbps,24.5 kbps,45 kbps,35 kbps,40 kbps)
Without optimization for 5 running application the total bandwidth used is 205 kbps. Using LP based bandwidth reduction total bandwidth is 184.5 kbps only. This is shown in Figure 13. The bandwidth saving of 20.5kbps is used for hand-off and new applications with the priority as explained above.

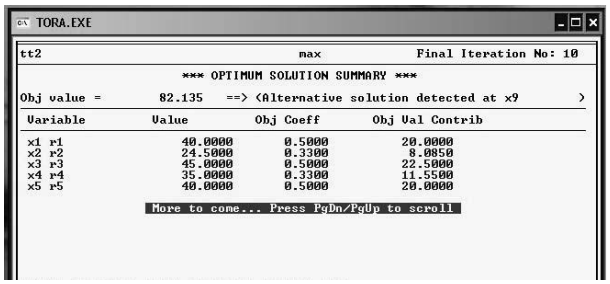

Figure 13: Bandwidth allocation for the typical five applications in LP

6. Optimization using SA Scheme

The major limitation of LP method is with its optimization for local minima only. The intelligent optimization methods will provide better optimal solutions than complex mathematical model for a mobile wireless networks in a real time environment. But the quality of solution in comparison to classical optimization technique is often a trade off against computation time and it is possible to reach a near optimal solution within bounded computation time. Hence we propose an algorithm based on SA. The algorithm takes the available constraints resources etc and finds an optimal or near optimal solution for resource allocation in mobile multimedia networks.
The fundamental concepts of SA [28] as a solution methodology for combinatorial optimization problem are considered here.
The design aspect of SA fundamental has the following elements namely,

a. Set of allowed configuration.
b. Cost function.
c. Feasibility (Perturbation mechanism)
d. Cooling schedule.
e. Acceptance criterion

In our optimization problem, the feasible solution is resource allocation (bandwidth) within bounded values.
The proposed SA based solution algorithm for our problem and results refer author's paper [29]. The proposed SA based solution algorithm for our problem is described as below.

Step 1:

Choose an initial point $x^{(0)}$. (Initial values are calculated as the average of $(R^{\min}, R^{alloc})$

In SA temperature T decides the freedom of making sufficient number of random moves. Set T a sufficiently high value (same for all the applications), number of iterations to be performed at a particular T as n, and set $t = 0$. $\{t$ Varies from 0 to $n\}$ .To simulate cooling schedule we decrease the value of T after n iterations.

Step 2:

At each iteration a neighboring point of the current solution is chosen.

Let $x^{(t)}$ denote the current feasible solution.

A few feasible solutions in the neighborhood of $x^{(t)}$ are chosen and are denoted as $x^{(t+1)}$, where the range of the neighborhood is determined by the parameter T.

Step 3:

Using Metropolis algorithm we find out whether the new feasible solution is better than the current feasible solution. If so we accept the new feasible solution as the current feasible solution.

If $\Delta E = E(X^{(t+1)}) - E(X^{(t)}) < 0$

Set $t = t + 1$; (accept the values)

Else create a random number (r) in range $(0,1)$

If $r \le \exp(-\Delta E / T)$ set $t = t + 1$;

(accept the values)

Else go to step 2.

Step 4:

If T is very small terminate

Else if $(t == n)$ then lower T by a factor of 2

Then go to step 2

Else go to step 2

7. Results – Optimization using LP and SA

Platform used for experiments are linux and windows with PIII processor. For the objective function and constraints for various applications LP method is used.

The same is done using SA technique. The experiments are repeated for different input applications and the comparison is made. The optimized bandwidth obtained using these techniques are again utilized for the hand -off and new applications as explained in figure 2. From figure 14 and 15 it is observed that better results are obtained using SA than LP and without LP.

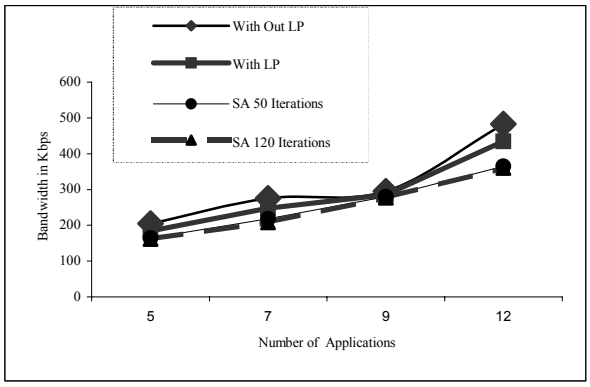

Figure 14: Bandwidth allocation with and without LP

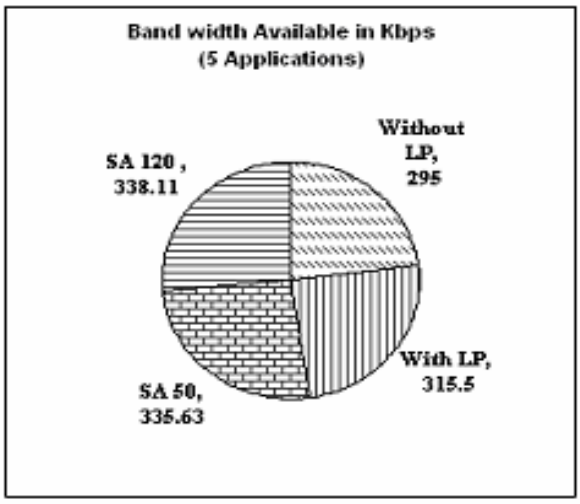

Figure 15: Optimized Bandwidth with and without LP and SA

8. Conclusion and Future Work

The admission Control Algorithm and Bandwidth Allocation for a cellular mobile network using Fuzzy logic Controller, LP and SA scheme have been proposed respectively. The fuzzy rule based classifier performance is good in improving service class classification and enhances QoS in admitting calls. The result of the comparison between fuzzy and non fuzzy shows that the call blocking probability is reduced by 17%. Also the resource allocation i.e. bandwidth allocation is efficient in LP method when compared to that of the scheme without LP. It facilitates more number of applications with better QoS in mobile multi media networks. For comparison semi heuristic technique-SA also proposed. Further improvement is witnessed in this scheme.

The better AC and resource allocation can be possible using computationally efficient and robust tool. For AC mobility prediction concepts in terms of Interference Guard Margin and for resource optimization heuristic based techniques such as Genetic Algorithm (GA) and Particle Swarm Optimization(PSO) will be considered in future for better solutions.

Acknowledgements

The first author gratefully acknowledges the support of the SKCET management and Principal Dr. S. Subramanian. He also wished to thank students Ms. S. Rudhiny and G. Subhameena for their support.

References

[1] MAJID GHADERI, RAOUF BOUTABA, Call admission control in mobile cellular networks: A, comprehensive survey, Wireless communications and Mobile computing, vol 6 No 1, pp-69-93, Feb 2006.

[2] DAPENG WU, QoS provisioning in wireless networks, Wireless communications and Mobile computing, pp-957-969, 2005: 5.

[3] PERROS .H. AND KIM, Call admission control schemes: A review, IEEE Communications magazine vol 34, no 11, pp 82-91, Nov 1996.

[4] KIM.S., KWON.T. AND CHOI.Y. Call admission control for prioritized adaptive multimedia services in wireless mobile networks, Proceedings of IEEE Vehicular technology conference Spring Tokyo, Japan 2000

[5] STUCKMANN.P. , QoS management in GPRS based radio access networks, Telecommunication systems, Vol 19:3, 4, pp 515-546, 2002.

[6] HAAS .Z. HALPERN .C, LI...L AND WICHER. S., A decision theoretic approach to resource allocation in wireless multimedia networks, proceedings of 4th International workshop on discrete algorithms and methods for mobile computing and communication 2000

[7] JUN YE, XUEVURIN SHEN, MARK J.W. CAC in Wideband CDMA cellular Networks by using fuzzy logic, IEEE Transcations on Mobile computing vol 4, Issue 2, pp 129-141, Mar- Apr, 2005.

[8] YU FENG MA,XIULIN HU,YUM YU ZHANG ., Intelligent CAC using fuzzy logic in wireless networks, Proceedings of American Control conference Vol:6,Issue 8-10, pp 3981-3985 June 2005.

[9] LEONARD BAROLLI, FATOS XHAFA,ARJAN DURRESI,AKIO KOYAMA, A Fuzzy based CAC system for wireless cellular networks, International Conference on Distributed Computing Workshops pp 38-40, ICDCSW 07, 2007.

[10] RAPPAPORT, S.S... The multiple-call handoff problem in high capacity cellular communication system, IEEE Trans.on Vehicular Technology 40(3), pp 546-557, 1991

[11] NAGHSHINEK. M and ACAMPORA A.S., QoS provisioning in microcellular networks supporting multimedia traffic, proceedings of IEEE INFOCOM, pp1075-1084, 1995.

[12] NAGHSHINEK. M and SCHWARTZ M., Distributed CAC in mobile wireless Networks, IEEE JSAC, Vol; 14, pp 711-717, 1996.

[13] LEVINE D.A, AKYILDIZ I.F AND M.NAGHSHINEK, A resource estimation and CAC algorithm for wireless multimedia networks using the shadow cluster concept, IEEE/ACM Trans.on Networking 5(1), pp 01-12, 1997.

[14] AYYAGARI.D AND ANTHONY EPHERMIDES, Admission Control with Priorities: Approaches for multirate wireless systems, Mobile Networks and Applications vol; 4, pp; 209-218, 1999.

[15] ANUP.K.TALUKDAR, BADRINATH. B.R. and ARUP ACHARYA, on accommodating mobile hosts in an integrated services packet networks, IEEE INFOCOM pp.1046-1053, 1997.

[16] OLIVERIA C., KIM. J.B. and SUDA. T, An Adaptive bandwidth reservation scheme for high-speed multimedia wireless networks, IEEE JSAC, Vol16, no6, pp.858-874, 1998.

[17] CHAO. C.C and CHEN. W., Connection Admission control for mobile multiple class personal communication networks, IEEE JSAC Vol 15, pp1618-1626, 1997.

[18] CHEN. S. and NAHRSTEDT, K. Distributed QoS routing in Ad-hoc networks, IEEE JSAC , Vol 17, 1999,1488-1505.

[19] CHIN. M. And BASSIOURI, M.A, Predictive scheme for hand-off prioritization in cellular networks based on mobile positioning , IEEE JSAC, Vol 18, pp 510-522, 2000.

[20] EL-KADI, OLARIU.S and ABDUL WAHAB.H.,A rate based borrowing scheme for QoS provisioning in multimedia wireless networks, proceedings of IFIP sixth international conference on Intelligent in networks Sep, pp.237-252, 2000.

[21] S.KIM,T.KWON and Y.CHIO, "Call admission control for prioritized adaptive multimedia services in wireless/mobile networks", Proceedings of IEEE Vehicular technology Conference(VTC'00 spring), Tokyo, Japan 2000.

[22] J.R.MOOORMAN,J.R.LOCKWOOD and S.N.KANG, "Real time prioritized call admission control in a base station scheduler", Proceedings of ACM Wowmom , PP 28-37, Boston, MA,USA, 2000.

[23] VIJAY KUMAR. B.P and VENKATARAM. P., LP based admission control using ANN for integrated services in mobile networks, Wireless Personal Communications, Kluwer Academic publishers, pp.219-236, 2002.

[24] ZIMMERMANN. H.J, Fuzzy set theory and its application", 2nd Edition, Kluwer Academic Press. 1991

[25] PATYRA M.J., Design considerations of digital fuzzy logic counselors in Fuzzy Logic – Implementation and Applications, 1996 P 143-176, edited by Patyra. M.J and Mlynek D.M., Wiley and Teubuer

[26] DORU TODINCA etc, Fuzzy logia based admission control for GPRS / EGPRS networks, Computer Science, Vol. 49 (63). 2004

[27] DEB, K. Optimization for engineering design: Algorithms and examples, Prentice-Hall 1995

[28] VAN LAARHOVEN P.J.M and EHL ARTS, Simulated Annealing theory and applications, Kluwer Academic Publishers, London 1987.

[29] KARTHIKEYAN. N.K and NARAYANASAMY. P., Bandwidth Allocation Scheme for Multimedia Mobile Networks using Optimization Techniques Proceedings of IEEE International Conference on Cybernetics and Intelligent system CIS 2006 , PP 312-316, 2006.

Biography

P. Narayanasamy acquired his B.E. Degree in Electrical and Electronics Engineering from Coimbatore Institute of Technology, Coimbatore in the year 1980.He obtained his Master's Degree in the year 1982 from Anna University, Chennai and his PhD in the year 1990 from Anna University Chennai. He is at present professor and Head of the Department of Computer Science and Engineering Anna University Chennai. He has wide area of interest and his research interest focuses on wireless communication and computer networks. He has published more than ten papers in the International and Nation journals and presented more than twenty one papers in international and national conference. His presentation also includes IEEE Conferences. He holds additional charge as a coordinator for both Information Security Education and Awareness Project sponsored by ministry of communication and Information Technology India and value added services in Regional Language on hand held devices sponsored by Tamil Virtual University.

N.K.Karthikeyan completed his B.E. Degree in Electronics and Communication in Engineering in Kongu Engineering College, Bharathiar University Coimbatore in year 1988. He obtained his Master's Degree in Computer Science and Engineering from Anna University, Chennai. He is at present working as Assoc.Professor, Computer Science Department at Sri Krishna College of Engineering. His research interest focuses on Wireless Communication, Mobile Computing, Soft Computing and Optimization. He has published more than five papers both in International and National journals and has presented more than fifteen papers both in International and National conferences. His project proposal titled "Resourse Allocation in Multimedia Cellular Networks using optimizing Techniques" has been sanctioned by Computer Society of India under CSI RnD Project for the year 2006-2007.

www.icgst.com

Validation Study of Maghrab Europe Electric Power Interconnect

C.BOUCHOUCHA [1], S. CHEBBI [2], S.MEJRI [3] and M. ANNABI[4]

[1] *Engineer STEG, National Dispatching,* bouchoucha_chokri05@yahoo.fr
[2] *Teaching – researcher at l'ESSTT Tunis,* , chebbisouad@yahoo.fr
[3] STEG, Head of division Technical Studies in the Dispatching, Radès Tunis;
[4] *Professor at the ESSTT, Tunis,* mohamedannabi@.esstt.rnu.tn

Abstract:
In this paper we propose the validation of the electric models of the Maghreb system inter-connected to Europe by the simulation of the real cases of incidents, in order to obtain results in conformity with the observations made at the time of the defects recorded in this system. In order to achieve this objective the study was based on two parts. A first relates to the theoretical validation in open loop of the models suggested and a second part based on digital simulations for a practical validation.
The first part of the study which relates to the theoretical validation of modeling in open loop is based to dynamic measures of performances which are the first tests of the electric model validation. These tests which it is necessary to apply to a system of control (voltage regulator, speed regulator…), to translate the characteristics of the system giving an image on its effectiveness opposite to stability in a electric system. The elementary system of production made up of the alternator and the associated regulators (speed and voltage) are subjected to an excitation by level. Its answer is evaluated according to time in order to conclude on its stability in loop open (disconnected from the whole of the electric system). It is a question individually of testing in this stage each generator with its regulators isolated from it in order to make sure that the associated regulators are not at the origin of instability in closed loop.
With regard to the second part of the validation study, we proceeded to a treaty of sensitivity in order to determine the most influential factors during the transient state (prim mover) which takes place following the loss of a production. Then we checked the validity of the conclusions drawn from the treaty of sensitivity on real incidents (which the data are available), the most influential factors are adjusted in order to approach the maximum of the real recordings.

Key words: voltage regulator, speed regulator, validation, dynamic performance, recordings.

1 - Theoretical validation of modeling

1.1- Unit System of production

The production of electrical energy, of mechanical origin is based mainly on the primary energy conversion in calorific form (boiler, turbine) for the steam turbines and potential for the hydraulic turbines. The control of the electric request is done by the adjustment of the primary energy through the principal valves of admission in the turbine, see figure 1.

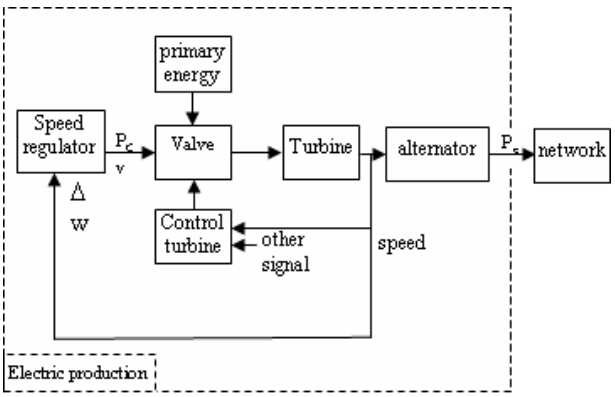

Figure 1 Functional Diagram of generation and control in production unit

The energy required by the consumers must be delivered according to a certain quality defined by the tension and the frequency for the electric power, the pressure and the temperature for calorific energy. These various factors characterizing the various forms of energy are regulated and maintained in the beaches agreed by suitable closed loops. The generators must produce a wave of tension whose frequency and amplitude are inside certain tolerances. The maintenance of the frequency is ensured by a balance of active power whereas the maintenance of the amplitude is ensured by a balance of reactive power. In network as in local load, if the generation of active power exceeds loads, then the frequency increases and if the generation of reactive power exceeds consumption, the amplitude of the tension increases. The source of active power is the driving force which is in the case of the hydroelectric generators the fall of water in the pressure pipe and the case of a steam turbine the vapor under pressure. The source of reactive power is the magnetic flux in the machine which is controlled by the operate current of the alternator.
Generally, the regulation of the voltage is considered independent of the regulation of frequency. Actually,

there is an influence crossed between the tow regulations. However, the regulators used in practice are mono-variable. Indeed, the use of the generator with vacuum implies that no current traverses rolling up of the stator and thus that the latter behave like inertia of rotation. Figure 2 presents the functional diagram of the regulation of tension (IEEE Working Group one Computer Modeling of Excitation Systems, 1981).

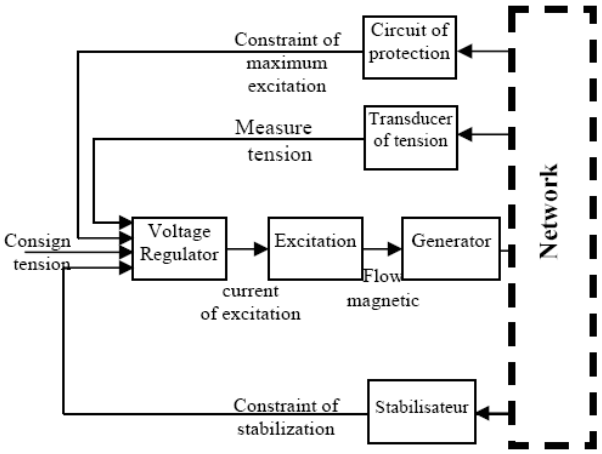

Figure 2: Functional diagram of the voltage regulator

The speed regulator acts on the driving force provided to the machine using the positioning of the principal valves of admission, which are valves making it possible to adjust the flow and the direction of flow of water for hydraulics and vapor for the power stations, to balance the active power. If the opening of the principal valves is increased, then the generator provides more power activates and the frequency increases.

Dynamic performances measurements are the first tests of the electric model validation. These tests which it is necessary to apply to a system of control (excitation and speed), to translate the characteristics of the elementary system into open loop and giving an image on its effectiveness in closed loop (answer, speed…).

1.2- Validation of the voltage regulator

Figure 3 shows a general representation of the excitation system :

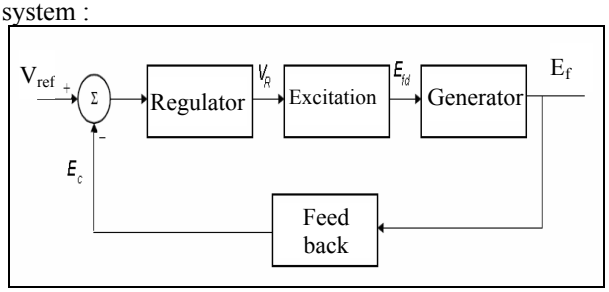

Figure 3 : General representation of the excitation system.

Being given that the model of the excitation system is generally nonlinear thus two analyses are highlighted:

- ✓ Analyze performances following great disturbances.
- ✓ Analyze performances following small disturbances.

In the first case we will preserve the non linearity of the system; but we suppose that it is linear in the other case.

1.2.1 Analyze performances following great disturbances

This analysis enables us to have an estimate on the performances of the excitation system following severe disturbances which translate the stability of the system. It consists in determining the nominal response (called response ratio in the Anglophone literature) of the excitation system which is the image of its response speed following great disturbances.

The nominal answer can be given while preceding the following stages:

- ✓ Initially, the system of excitation works in nominal load (i.e. $E_{fd} = E_{fd\ full\ load}$)
- ✓ Then we abruptly add to $V_{réf}$ a level of amplitude giving the saturation of the output voltage of the excitation system.

According to figure 4 the response ratio is calculated as follows:

$$\text{Response ratio} = \frac{cd}{(oa)(oe)}$$

oe = 0.5s

$oa = E_{fd\ full\ load}$

The point -c- is such as surface (*acd)* is equal to surface (abd), see figure 4.

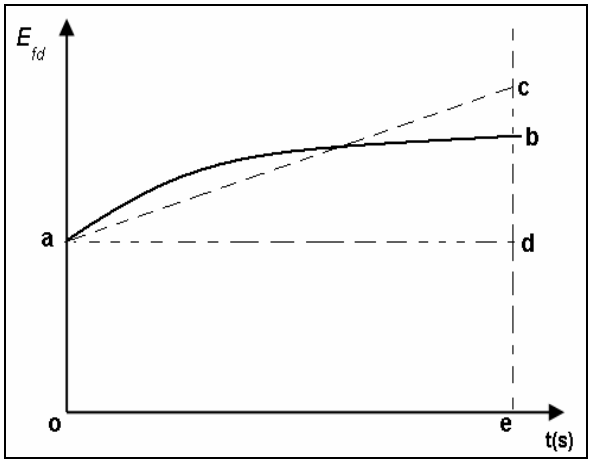

Figure 4 : Response ratio of an excitation system.

1.2.2 Analyze performances following small disturbances

In this analysis two tests are highlighted:

Test 1: Indicial response in closed loop:

A typical answer is given by figure 5 and according to can extract several parameters like time from assembled, the going beyond, value of peak etc. But among these parameters the going beyond (*overshoot*) is used the most for the validation.

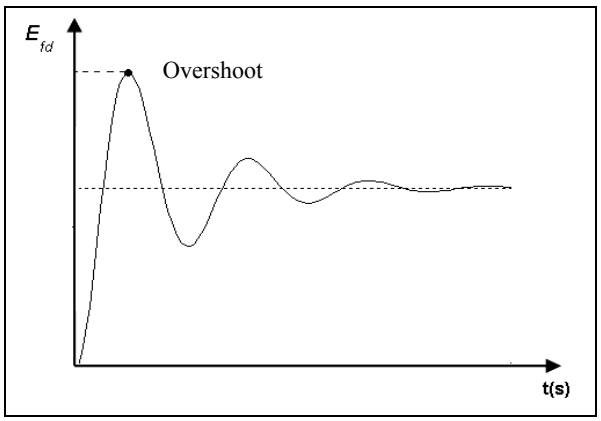

Figure 5: Indicial response of an excitation system.

Test 2: Frequencies response in open loop:
A typical frequency response of the excitation system is given by the Figure 6, and according to can extract two principal parameters which are the magnitude margin and the phase margin.

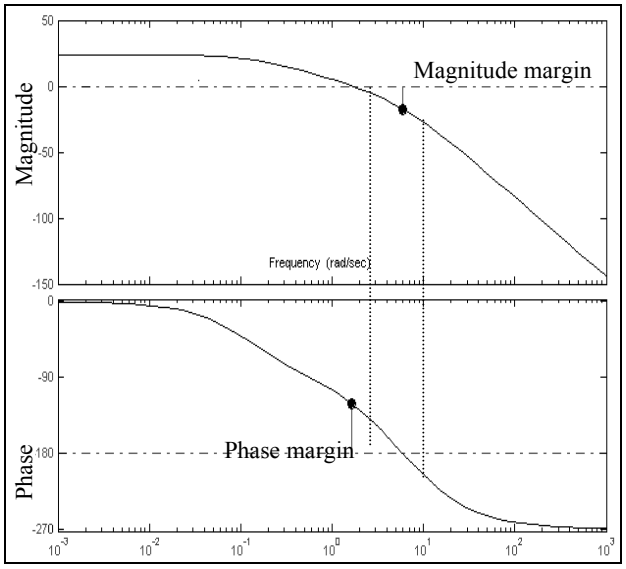

Figure 6: Typical frequencies response of the excitation system.

We note in table (1) an example of this test type, simulate on software PSSE of company PTI:

1.3- Validation of the speed regulator

The first objective of the regulation is thus to maintain the frequency of the network constant. For that, the system of regulation acts on the flow admitted in the turbine to balance the power provided by the turbine and the power absorbed by the network.

Thus, the regulation must order a machine part able either to control the flow of principal admission valve entering the turbine, or to control the energy transferred to the turbine. In addition to its role of regulation of speed, the regulator with for ambition to limit, with an acceptable value, large the variations speed which would be caused by abrupt load variation, and whose amplitude can sometimes be very large.

Table 1: Calculation of the response ratio :

N°	BUS NAME	Id	FULL LOAD EFD	RESPONSE RATIO
112	RADESV2 15.500	1	2.72851	0.92343
113	RADESV3 15.500	1	2.89246	0.83870
114	RADESV4 15.500	1	2.89246	0.83870
115	RDSIIG1 15.500	1	2.38742	0.97318
116	RDSIICC 15.500	1	2.40752	0.95248
117	RDSIIG2 15.500	1	2.38742	0.97318
142	B.MCHERG15.500	1	2.58590	3.55710
322	KORBATG211.000	1	2.43307	2.05852
511	SOUSSEV115.500	1	2.74870	1.46704
513	SOUSSEG115.500	1	2.58590	3.55710
514	SOUSSEG215.500	1	2.58590	3.55710
515	SOUSSECC15.500	1	2.73548	0.91967
622	SFAX.TG211.000	1	2.57320	0.66264
751	KNOR.TG111.000	1	2.43307	2.05852
752	KNOR.TG211.000	1	2.43307	2.05852
811	GHANNTV112.500	1	2.98204	0.45912
813	GHANNTG25.5000	1	2.57320	0.66264
823	BOUCHEM 15.500	1	2.58590	3.55710

Figure 7 shows the response of a voltage regulator following a disturbance of 5% of the output voltage:

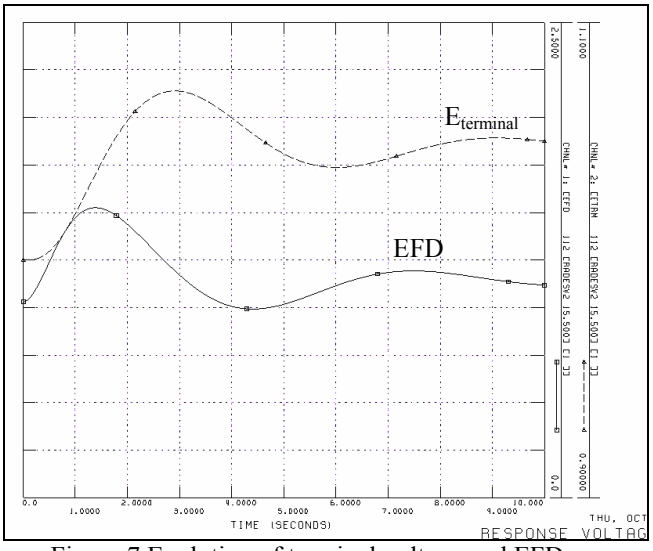

Figure 7 Evolution of terminal voltage and EFD

The regulation system of the group turbo-alternator with thus two principal functions:

- ✓ To adapt the speed of turbine to the frequency of the network, which is thus a function used in a permanent way during operation of the turbine;
- ✓ To protect the group from the abrupt load variation which have as a consequence the shortening of the equipment duration. It is however conceived that this function only very seldom is used, even exceptionally, and this, even if it is quite as significant as the first.

To test a speed regulator means to simulate the behavior of the regulator and the turbines under hypothetical conditions which consider the evolution isolated from

the unit. The parameters of the regulators are possibly adjusted in order to lead to a deadened answer. This test consists in initializing each speed regulator on a level of load indicated by the user and a power-factor unit. We simulate the response of the speed regulators for a load increment. The values recommended to simulate this test are: initialization of the regulator with 80% of load and excitation by a stage with 10% of load. This test also makes it possible to validate the compatibility between the load flow (which determines the static point of operation) and the data dynamic such as limiting device.
We notes thereafter an example of this test type, simulate on software PSSE of company PTI:

Network of reference: The network of reference considered is that of year 2006 of the countries considered. Only the network configurations relating to the levels of tensions equal to or higher than 90KV were considered. The 400KV is introduced on the level of the interconnection Spain –Morocco. The parameters taken into account are:

- Topology of the network in normal diagram (all works available).
- Plan of production of each system.
- Electric characteristics of the lines of transport and the transformers.
- Data relating to the types and levels of compensation.
- Active and reactive nodal loads.
- Limits of production of active power and reactivates generating groups.
- Dynamic data relating to the manufacturing units and the regulators associated.

Assumptions of load: The study of the operation of the network inter-connected maghrébin was carried out for the situation of point of the year 2006. The respective levels of loads are those indicated in table (2):

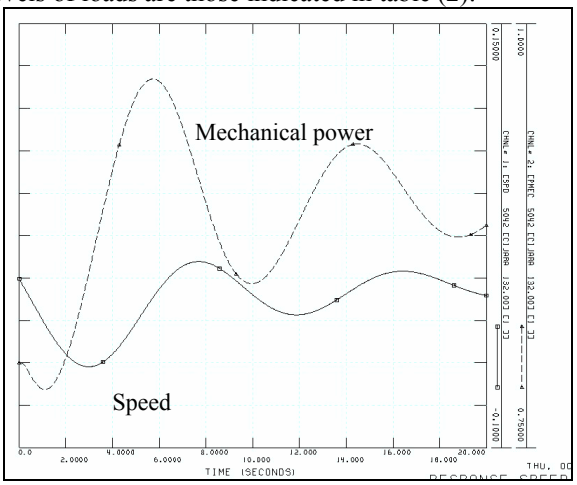

Figure 8 Evolution of mechanical power and speed

2 - Validation practices modeling

2. 1 Data of studied electric system

The studied electric system is that of the Maghreb (Tunisia, Algeria and Morocco) inter-connected in Europe (Spain) via the cable under sailor Morocco-Spain. It is characterized by several blocks connect between them by lines of relatively long interconnections and a connection with a very powerful network, the European network (UCTE), as shows it the following figure.

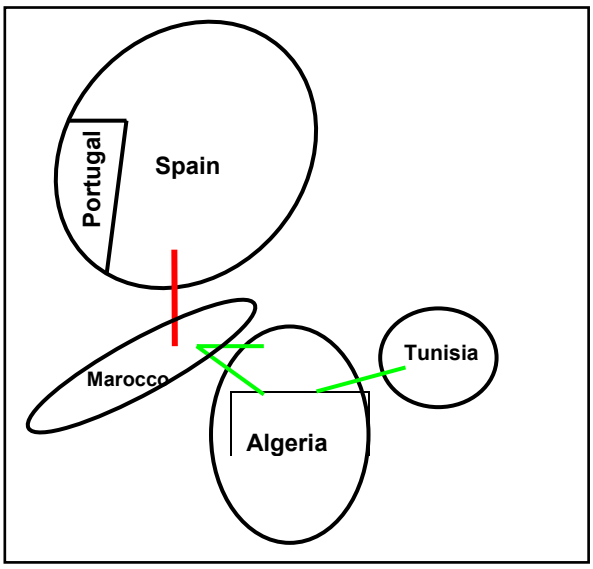

Figure 9 Studied electric system

Table 2: The respective levels of loads

Country	Load in MW
ALGERIA	*4756*
TUNISIA	*2475*
MAROCOO	*2774*
TOTAL	10005

Exchanges on the interconnections: The study takes account of a null exchange on the interconnections of the system inter-connected maghrébin and of an importation of Spain towards the Moroccan network of 150MW.

2. 2 Strategy of practical study

The approach adopted for this study of practical validation passed by the three following slaps:

1. To analyze the history of the incidents in order to draw from the real facts of the lesson being able to allow to explain the variations observed between reality and theory;
2. To make a study of sensitivity allowing to determine the most influential sizes following the loss of a production in an inter-connected system
3. To check on real incidents (which the data are available) validity of the conclusions drawn before. At the time of this third phase, the most influential parameters are adjusted until obtaining results nearest possible recordings. From the various simulated incidents, it is then a question of drawing the most adequate models with the maghreb electric system.

The choice the incident to be simulated for the reconstitution was based on the following criteria:

- To have a maximum of information relating to this incident (of 0 sec until 20 sec)
- most recent possible
- Reliability of information (stepping to be made between the various sources).

Information which was considered to be necessary is as follows:
- Plan of starting before the incident of the three maghreb countries (Algeria, Marocco and Tunisia)
- Exchanges of power before the incident
- Power called in each maghreb country before the incident
- revolving Reserve of each maghreb system
- Plan of tension on the level of the maghreb network
- Load for each node
- Recordings of the transient state rose following the loss of the production on the various maghreb interconnections.

The comparison enters the results of simulation and those provided by the real recordings doors mainly on the active transit on the interconnections Spain-Marocco, Marocco-Algeria and Tunisia-Algeria. We will be interested particularly in the following comparison criterions:
- Final value attack at the end of 20 seconds,
- Maximum Value attack during the 20 seconds,
- Shape of the curves,
- Contribution, during the loss of production, for the each country.

2. 3 Basic data

The real recordings which were regarded as reference are those consigned during the following incidents, table 3:

Table 3: The real recordings

Date	Hour (GMT)	Origin
13/04/1999	19h32	release of a TV in the Rades (Tunisia) charged with 110MW
24/03/2000	18h20	Release of the TG of Bir Mecherga (Tunisia) which is charged with 120MW
31/03/2000	19h16	Release of the n°3 group to the power station of Marsat (Algeria) which is charged to 166 MW
31/03/2000	21h21	Release of the n°1 group to the power station of Jorf-Lasfar (Morocco) which is charged to 330 MW
05/09/2003	23H14	Release of TVCC (114MW) + TV4 of Rades (100) in Tunisia
11/09/2003	15H22	Release of the TG3 Bouchemma (105MW), 2TV of Ghannouch (48MW) in Tunisia
24/05/2003	20H32	Release of the TG Hamma (300MW) in Algeria
30/10/2003	13H16	Release of the n°1 group to the power station of Jorf-Lasfar (Morocco) which is charged with 300MW
07/12/2004	19H35	Release of the TVCC with Radès II (134MW) in Tunisia
21/12/2004	11H28	Release of the ½ combined cycle of Sousse to 170MW in Tunisia

The representation of the European system was done in detail for the Southern network of Spain; an equivalent was taken into account for the rest of Europe. The consumption on the European system is equivalent for an 80 GW.

For all these reconstitutions, the initial conditions of the static case were adjusted until obtaining initial values identical to those recorded actually and this for all information available and in conformity with the reports of exploitation and the recordings carried out.

2.4- Principal results

The study described in this synthesis comprised three principal shutters:
- Analysis of the history of the real incidents,
- A treaty of sensitivity,
- A stage of incidents reconstitution.

2.4 1 Historical of the incidents

The systems Spanish and Moroccan were inter-connected for the first time in October 1997. The interconnection was maintained in service for one month to carry out the operational tests industrial necessary to the reception of the installation and was brought into service definitively on May 25, 1998 for its commercial exploitation.

To the level of the maghreb countries, these incidents are normally consigned in reports of exploitation submitted by each company and which are necessary for the reconstitution of the incident by simulation. It is a question of having access, at least, with recordings on the interconnections connecting Magreb to Europe and between the various maghreb countries.

Thus, and in the light of this history, some remarks often return at the time the analysis of these incidents:
- The contribution of Europe following the release of a production in the Maghreb, generally, quasi-total,
- The power developed during the primary regulation adjustment by the maghreb units is low and this some is the revolving reserve available to the moment of the incident,
- The evolution of the active power on the interconnections presents an irregular behavior being characterized by oscillations which are stabilized at the end of 15 seconds.

This oscillatory pace observed on the recordings available is not in conformity with the first simulations which present, generally, a regular behavior while passing from an initial value towards an end value in an ascending.

2 4.2 Treated sensitivity

The objective treated of sensitivity is to determine which the most significant sizes influencing the transient state are caused by the loss of a unit. This study related to the following sizes:
- Droop of the unit (static magnitude of the speed regulators),
- The revolving reserve (reserve available on the unit moving),
- Regulation speed (dead band),
- The inertia of the groups,
- The modeling of the load,
- The initial plan of tension,
- The electric distance.

While varying each time only one size, the other parameters being constant, we lead to the following results:

a) Droop of the groups:

The results obtained after simulation the droop variation of the unit show that the effect of this parameter is observed at the end of the period of simulation (20 seconds). The shape of the curves during the first second


and before the damping of the signal is not affected by the variation of this parameter.

It is noticed finally that more the size of the European system, on which the variation is carried out, is significant is larger the beach of variation of the end values. However, this variation is not sufficient to allow obtaining a contribution of Europe in conformity with the recordings (i.e. quasi-total contribution). It is noted indeed, that in best case this contribution of the European network does not exceed 71%.

b) The revolving reserve

In spite of the variation of this parameter, the contribution of the various systems remains constant. Indeed, this parameter influences the secondary adjustment of the zones concerned which is spread out between 30sec to 15min, and does not have a direct influence on the transient state.

c) Regulation speed

The inhibition of the action of the speed regulators due to an operation of these regulators inside their dead band was simulated for several assumptions. These assumptions, in particular, consisted of the suppression of the whole of the Maghreb regulators or in one or two countries in Maghreb. The first observation to make show that starting from a certain rate of absence of speed regulators (estimated with half of the started machines) the shape of the curves represent the evolution of the active power becomes similar to that actually recorded.

This pace translates an oscillatory behavior characterized by maximum amplitude (raised in general at the end of 4 seconds) higher than the end value (at the end of 20 seconds).

The variation of this parameter influences the maximum power especially during the first oscillations. Concerning the final transit, the beach of variation is about 3.5% between the two extreme cases.

d) The inertia of the groups:

While varying the inertia of the maghreb groups the simple one with the double, we obtain a temporal shift of the curves relating to the active transit on the interconnections.

e) The modeling of the load:

In transient state, the constant load not to be regarded more as in static mode. Indeed the variations of the tension and the frequency affect the power called. In order to better model the load of the network, we carried out several tests of simulation to obtain a simple modeling allowing to better approach reality.

The modeling of the load in the electrical supply networks leads to two representations; one static and other dynamics. A static head is an algebraic function (generally polynomial) of the tension and frequency. For a fast variation of the tension, the static model does not reflect the dynamic behavior of the load; it characterizes only the final state of the load. For fast phenomena and the studies of stability of tension, it is recommended to use the dynamic model of the load. In fact especially the engines represent the most significant share of the dynamic aspect of the characteristics of the load.

The modeling of the load by static models is justified for weak variations of the amplitude of the tension and frequency. This type of model is appropriate in the studies of stability of long-term tension. The studies relating to the interregional oscillations or fast collapse of the tension required a modeling of the load by a dynamic model.

The model of static head represents its characteristics, at every moment, like an algebraic function of the module of the tension and frequency in the node considered. The component activates P and the component reactivates Q are considered by the following exponential model:

$$P = P_0\left(\frac{V}{V_0}\right)^a \left(\frac{f}{f_0}\right)^c \quad \& \quad Q = Q_0\left(\frac{V}{V_0}\right)^b \left(\frac{f}{f_0}\right)^d$$

Where P and Q are the components active and reactive load when the module of the tension is V. The index 0 indicates the value of the variables to the initial conditions. The parameters of this model are the components a, b, c and d. the exhibitors a and b of this model are equal to 0, 1 or 2 in order to represent the characteristics of the load, respectively at constant power, constant current or constant impedance. For a system having a composed load, exposing a is between 0.5 and 1.8; the exhibitor b is typically between 1.5 and 6. A significant characteristic of the exhibitor b is variable according to a nonlinear function of the tension. This is caused by magnetic saturation in the transformers of distribution and the motors.

Consequently, it is convenient to represent the consumers by groups, either according to the topology of the consuming departures (cities, areas), or according to their natures (metal foundries, industries, cement factories, chemical industries, craft industry, equipment domestic, lighting, etc....).

To this end, we considered the various cases of the characteristic of the following load. We simulated the behavior of these models following the loss of production.

- **Characteristic I,Z** : the active power is represented by a constant current and the reactive power by a constant impedance
- **Characteristic I,I** : the active power is represented by a constant and of the same current for the reactive power
- **Characteristic Z,Z** : the active power and reactivates are represented by a constant impedance
- **Characteristic Z,I** : the active power is represented by a constant impedance and the reactive power by a constant current.

The results obtained after simulation of the various assumptions relating to the modeling of the load lead to the following remarks:

- ✓ The influence of the modeling of the load is not exerted on the shape of the curves relating to the evolution of the active transit on the Maghreb interconnection which presents a similar behavior, ascending or descendant.
- ✓ The model of the load influences primarily the permanent value of the active transit all the interconnections in a uniform way.
- ✓ Model (**I,Z)** gives place to a final transit which is most significant on the Maghreb interconnections whereas a representation by a characteristic **(Z,I)** gives place to the weakest transit.
- ✓ The model of the load more adapted for the Maghreb network is characteristic I,Z


f) The initial plan of tension:
While varying the initial plan of tension, we upwards obtains a light shift or to the bottom of the curve representing the evolution of the active transit on the interconnections what generates a change of the maximum and final values.

g) The electric distance:
To study the influence of this factor on the transitory behavior of the groups, two releases were simulated; in the substation of Radès in Tunisia and the other in the Mohammedia in Morocco. The power being losses is the same for the two cases. The curves of the first disturbance on the level of Radès have oscillations which diminish after 20 seconds approximately. These oscillations are not observed for the case of the release of the TV Mohammedia. This was explained by the propagation of the disturbance.

2.4.3 Synthesis of sensitivity treated
In the light of what precedes, it proves that the most influential parameters are:

- The dead band of the speed regulators,
- The modeling of the load

Indeed, a dead band regulated on an interval which includes the variation of the frequency on the inter-connected network cancels the action of the speed regulators. The absence of regulation speed in the Maghreb influences especially the shape of the curves representing the evolution of the active power on which one observes an irregular behavior showing of the significant oscillations which are also observed actually. We raises also a light rise of the end value of the active transit on the interconnections.
Concerning the modeling of the load on all the system inter-connected by a characteristic I,Z (constant current for the active power and constant impedance for the reactive power) we notes that it makes it possible to raise the contribution of Europe up to a value of 94% (for characteristic Z,Z; it is 68% is a rise of 26%). If we combines the absence of regulation speed in the Maghreb with a modeling of the load by a characteristic I,Z on all the system Euro-maghreb, we obtain a contribution of Europe exceeding the 100% at the end of 20 seconds. Table 4 presents a summary indicating the beach of variation of the end value of the active transit on the interconnections according to each studied parameter.

Table 4: Transit active (End value)

Studied parameter	End value of the active transit (MW)			
	Spain-Morocco	Morocco-Algeria	Algeria-Tunisia	Contribution Europe (%)
Droop	185,6→197,7	98,5→107,4	66,7→68,4	60→71
Revolving reserve	194,1	104,1	68,1	67,3
Regulation speed	194→200,8	104,1→110,2	68,1→69,1	67,3→81,6
Modeling of the load	189,3→224,2	100,5→125,5	67,6→73,2	63,4→94
Regulation speed charges I,Z	194,1→232,4	104,1→124,9	68,1→73,8	67,3→102,5

2.4.4 Reconstitution of real incidents
To validate and specify still the results of the study of sensitivity and on the basis of the result obtained by this study of sensitivity (presence of the dead band on the speed regulators and modeling of the load by a characteristic I,Z) as bases, was carried out to the reconstitution of three incidents having taken place and consistent in the loss of a group in each maghreb country. These incidents are as in table 5:

Table 5: The incidents

Date	Hour	Incident
11/09/2003	15H22	Release of the TG3 Bouchemma (105MW), 2TV of Ghannouch (48MW) in Tunisia
24/05/2003	20H32	Release of the TG Hamma (300MW) in Algeria
30/10/2003	13H16	Release of the n°1 group to the power station of Jorf-Lasfar (Morocco) which is charged with 300MW

To compare reality with the simulated incident, three criteria were selected:

- Shape of the curves,
- The maximum value of active transit on the interconnections,
- The end value of the active transit on the interconnections.

Shape of the curves:
The application of the rule draw from the study of sensitivity relating to inhibition of the action of the regulation speed to the level of the maghreb groups (presence of the dead bands) makes it possible to find the real pace recorded in the event of loss of production which is characterized by the appearance of an oscillatory mode deadened on the power forwarded on all the lines of interconnection.

Maximum and final value of the active transit:
The second and third comparison criterions between the real recordings and simulation relate to the maximum and final active power on the interconnections. It is noted that there is agreement between the real recordings and simulations for the evolution of the active power on the interconnections, where the relative error $\left(a = \frac{\Delta P_{\max}}{P_{\max}} etb = \frac{\Delta P_{finale}}{P_{finale}} \right)$ does not exceed the 20%.

With the fact, we notice that the results are all the more close to the real recordings that the interconnection considered is European side. Table 6 presents a summary of the relative error for all the reconstituted incidents:

$$(*)\ a = \frac{\Delta P_{max}}{P_{max}}(\%) \text{ and } (**)\ b = \frac{\Delta P_{finale}}{P_{finale}}(\%)$$

It should be noted that these results are in conformity with the collected recordings; however it is to be announced a difference on the distribution in active power on the interconnection Tunisia-Algeria is observed while keeping an acceptable agreement on the level of the sum of the transits on the 4 lines of interconnections. This can be explained by the situation inherent in the plan of starting on the Algerian side as well as the real topology of the Algerian network which present configuration special of exploitation at the moment of each incident.


Table 6: Error relative on the active transit

Interconnection		Loss of B.M'cherga (120 MW)		Loss of Marsat (166 MW)		Loss of Jorf Lasfar (330 MW)	
		a (*)	b (* *)	a	b	a	b
Spain-Morocco		7	1	2.6	0.7	0.7	1.1
Morocco-Algeria		09	15	1	6.2	-	-
Algeria-Tunisia	line 225Kv	15	17	-	-	-	-
	line 90Kv	12	20	-	-	-	-

3. Conclusion

This study consists in validating the model of the maghreb system inter-connected in Europe in seen to obtain results sufficiently close to the real recordings. With this intention, it was proceeded to the study of sensitivity relating to the most significant parameters:

- ✓ Offset of the groups,
- ✓ The revolving reserve,
- ✓ Regulation speed,
- ✓ The inertia of the groups,
- ✓ The modeling of the load,
- ✓ The initial plan of tension,
- ✓ The electric distance.

In the light of this study, it a rises the following conclusions:

- ✓ The influence of the regulation speed is especially observed at the first moments (pace of dynamics, maximum and minimum reach). On the other hand, the description of the load influences primarily the end value reached at the end of 20 seconds.
- ✓ To find the dynamic behavior recorded for the reconstituted incidents, it is necessary to inhibit the action of the regulation speed what amounts introducing a dead band (band inside which the speed regulator is insensitive with the variations of the frequency. It is made up of a zone adjusted voluntarily for the very weak variations of the frequency.
- ✓ To find the real contribution of the various networks, in particular a total help starting from Europe; it is necessary to model the load by a characteristic (I,Z) where the active power is described by a constant current and the reactive power by a constant impedance.

4. References

[1] Treaty of electricity of the federal polytechnic school of Lausanne published under the direction of Jacques Neirynck, Volume XII, electric Power (edition 1992).

[2] Year analysis of phenomena of voltage collapse there is transmission system Barbier C general Barret J.P. re-examined of electricity, special number; p3-21, 1980.

[3] Voltage stability evaluation of the interconnected modal Tunisian power system by the analysis technical, Said Abdellaziz, Chokri Bouchoucha, Khdija Kilani.Third IEEE International Conference one system, signals and Devices; march 2005, Tunisia.

[4] Modal voltage stability analysis of power systems modeling and application, Said Abdellaziz, Khdija Kilani. Third IEEE International Conference one system signals and Devices; march 2005, Tunisia.

[5] Power system Stability and control, R. Kundour; (Edition 1996).

[6] Simulation of the Dynamic Behaviour of Electrical Power Systems in the Shorts and Long Terms; Mr. Stubbe, A. Bihain, J.C. Baader and J Deuse; (CIGRE 1998 Session - 28th august - 3rd september - paper 38-02).

[7] "Simplified Mathematical Representations of Heavy-Duty Gas Turbines", W.I. Rowen, Oktober 1983, Newspaper of Engineering for Power.

[8] "Simplified Mathematical Representations of Single Shaft Gas Turbines in Mechanical Drive Service" W.I. Rowen, June 1992, ASME.

[9] Practical of various owners networks in the world: "Analysis and control of power system scillation", Task force 07, study committee 38, December 1996.

[10] Feasibility study of the interconnection of the electrical supply networks in 500/400 Kv of Egypt-Libya-Tunisia-Algeria-Morocco, Stains B2: Dynamic study, 2003-2004.

[11] Electric machine, J Chatelain, polytechnic school of Lausanne, Switzerland, Volume X, CH 105 Lausanne, edition 1994.

[12] IEEE transactions one power systems, JF Hauer, CJ Demeure and LL Scharf. February 1990, Flight 5 No 1 pp 80-89.

[13] "Industry Experiment with Special Portection Schemes", IEEE/CIGRE Committee Carryforward, IEEE Transactions one Power Systems, flight 11, N°3, Augsut 1996

[14] "Hydro-Quebec defense plan against extreme contingencies" G Trudel, S Bernard, G Scott, IEEE transactions one Power Systems, flight 14, n°3, August 1999.

[15] "Modelling of Out-of-Step Conditions in Power Systems", N.V. Kosterev, V.P. Yanovsky, D.N. Kosterev. IEEE Transactions one Power Systems, flight 11, N°2, May 1996.

[16] "Emergency Control in UES of Russia" A; Bondarenko, V Gerikh, IEEE Transactions one Power Systems, flight 11, N°2, May 1996.

[17] R. DUGUAN, D. SABIN, E. LEINFUSS. Electrotek Concepts. Signatures of the black out of 2003. October 6, 2003.

[18] Summary of group 39. Lessons learnt and to Be learn from the 2003 black out, Cigré WG C2.03. 2004

[19] ICF Consulting. the economic cost of the black out, year exit paper one the northeastern black out, August 14 2003.

[20] UCTE. Interim carry forward of the investigation committee one the 28 September 2003 black out in Italy.

[21] P. KUNDUR K MORISON: Practical Consideration in Voltage Stability Assessment, Electrical Power and Energy Systems, No 4, 1993.

[22] G MATUSZ, T MAJ, Z HANZELKA (university of science and technology: Poland): Voltage disps and shorts interruptions different strategies in contract for the electric power supply. CIGRE 04, C4-107 paper; August 2004.

Biographies:

Chokri BOUCHOUCHA: he obtained in 2002, his diploma of extensive studies in automation production engineering from the school of sciences and technology of Tunis (ESSTT). From that moment, he has been an engineer of networks studies, working in the Tunisian Society of Electricity and Gaz. He is also a departmental manager in network functioning and member of Maghreb committee of electricity (COMELEC)-sub-group of studies. At the moment, he is preparing a thesis on the securizing systems of electrical networks within the team ATMAC directed by Professor Mohamed Annabi

.

Souad Chebbi has obtained her mathematics university bachelor's in1975. She has continued her superior studies in high teacher level school of technical education. Her first level university studies have ended up by a master's degree in electrical engineering with good distinction in1980. Afterwards, she has obtained her diploma of extensive studies in electronics in 1981 with very good distinction (in the same school), the research theme that has been treated in order to obtained this diploma was the study of the static stability of electrical network. She has also prepared a doctorate thesis in electrical engineering which was directed by professor Ribbens-Pavella of Montefiore institute in Liege-Belgium. The research theme was related to the transitory study of the big electrical networks. The thesis has been held at the high teacher level school of technical education in Tunis in1983, with very honorable distinction. From that moment, she has been an associate professor in the same school which has changed its name to (ESSTT) high school of sciences and technology of Tunis. She is a member of the research team ATMAC at ESSTT specializing herself in energetic.